University of Alberta

Simulation of the Molecular Interactions for the Microcantilever Sensors

by

Padet Khosathit

A thesis submitted to the Faculty of Graduate Studies and Research
in partial fulfillment of the requirements for the degree of

Master of Science

Department of Mechanical Engineering

Fall 2009
Edmonton, Alberta

Examining Committee

P.-Y. Ben Jar, Mechanical Engineering

Phillip Y. K. Choi, Chemical and Materials Engineering

Andre G. McDonald, Mechanical Engineering

To Mom and Dad

Thank you for everything

Abstract

Microcantilever sensor has gained much popularity because of its high sensitivity and selectivity. It consists of a micro-sized cantilever that is usually coated on one side with chemical/biological probe agents to generate strong attraction to target molecules. The interactions between the probe and target molecules induce surface stress that bends the microcantilever.

This current work applied the molecular dynamics simulation to study the microcantilever system. Lennard-Jones potentials were used to model the target-target and target-probe interactions and bond bending potentials to model the solid cantilever beam. In addition, this work studied the effect of probe locations on the microcantilever deflection.

The simulation results suggest that both target-target and target-probe interactions as well as the probe locations affect the arrangement of the bonds; in term of the bonding number, the area containing the bonded molecules, and the distances between them. All these factors influence the microcantilever deflection.

Acknowledgements

I am particularly in dept to Dr. Ben Jar and Phillip Choi. Their insightful advice and helpful guidance have been instrumental in completing this thesis.

I would like to thank all my colleagues. Their help in setting up the computer software is greatly appreciated.

I am grateful for the financial support provided from the Natural Sciences and Engineering Research Council of Canada in the form of the Postgraduate Scholarship Master, the University of Alberta under Walter H Johns Graduate Fellowship, the University of Alberta Faculty of Graduate Studies and Research for Mary Louise Imrie Graduate Student Award, and the Graduate Students' Association of the University of Alberta for Professional Development and Travel Grant.

Throughout the thesis as well as my life, I have been blessed with many wonderful friends and families. Thank you, grandma, grandpa, mom, dad, and sis for all your love and support. To a person very dear to my heart, Ann, thank you for all the wonderful time.

Lastly, I would not be able to stand here at this point without my mom, dad, and sis. No word can describe the love, you have given me.

Table of Contents

List of Tables

List of Figures

Chapter 1

Introduction

Modern transportation has greatly improved our quality of life by swiftly moving goods and people. However, at the same time, it also provides passages for disease to spread. The recent spring 2009 outbreak of swine flu is a prominent example. Within a matter of weeks, it became a global pandemic. One of the problems lays in the current technology for the viral detection that requires a laboratory testing. A fast response and portable detector capable of detecting tiny concentration of disease would be ideal in halting this spread. One sensor, that has shown a promising sign in accomplishing these objectives, is a microcantilever sensor. The principal component of the sensor is the micro-sized cantilever which is coated on one side of the beam with the chemical or biological probe agents that bind with the target virus. These bindings create surface stress which bends the microcantilever and changes its resonance frequency. Because of its size, the microcantilever is extremely flexible, giving the sensor its high sensitivity rivaling the best commercial sensor. Its size also allows the sensor to be portable.

In addition to detecting virus, the microcantilever can also be used as a biological and chemical sensor, mass scale, temperature sensor, and micro-scaled calorimeter. These make the microcantilever sensor quite unique, capable of detecting wide varieties of properties. Furthermore, the sensor has a fast response

time and, with the proper set-up, the sensor is highly selective, capable of differentiate minor variation in target molecules.

Since the development of the microcantilever sensor is still in its infancy, many of its behaviours are unclear. In this research, a molecular dynamics simulation was used to study the basic trends of the effect of molecular interactions on the microcantilever sensor. Note that, so far, the sensor has been referred to as 'microcantilever.' However, this simulation was performed without using any real unit values. Since some of the models used were at the molecular level, its function can be at the nano-scale. The paper will refer to the sensor as 'microcantilever' or sometime 'cantilever', to keep the name consistent to that used in literatures.

1.1 Microcantilever Sensor Description

Typically the microcantilever is made of silicon-based material with the size of 50-200 μm long, 10-40 μm wide, and a few micrometer thick (Thundat, Pinnaduwage, & Lareau, 2004). Figure 1.1 shows the scanning electron microscope picture of a rectangular-shaped microcantilever and Figure 1.2 a triangular-shaped microcantilever, both are commonly used. A layer of chemical/biological probe agents that exhibit strong affiliation to target molecules are applied on one side of the microcantilever, while the other surface is usually made of non-reactive layer. Two things usually happen when the target molecules are adsorbed onto the probe layer. Firstly, the unbalanced surface stress from the two surfaces causes the microcantilever to deflect. Secondly, the adsorption increases the mass and changes the modulus property of the beam, both affecting the resonance frequency of the microcantilever. Detection of these changes is typically measured by an optical system or a piezoelectric element.

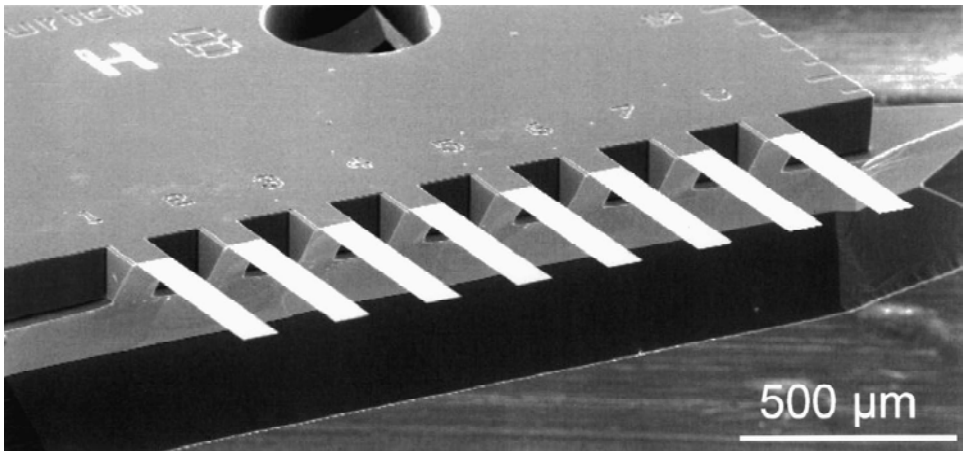

Figure 1.1 The microcantilever array image from the scanning electron microscope. (Baller et al., 2000)

Due to its size, the microcantilever sensor proves to be extremely sensitive. However, along with its high sensitivity comes the noise problem. Tiny disturbance can be picked up by the microcantilever sensor. Normally, noises originate from variations in temperature, pH, fluid flow, viscosity, and ion concentration. Many procedures were proposed to reduce the noises. The microcantilever must be allowed to equilibrate in the system, where the measurement will take place, i.e. in the same fluid environment. Moulin et al. (2000) reported a drift of deflection right away after placing the microcantilever inside the measuring liquid even before the target molecules are introduced. This is usually the case when some of the probe molecules are highly reactive, for example, gold exhibits strong attraction to many molecules. After the target molecules are introduced into the system, the system must be kept as much as possible at the same temperature, PH level, and other fluid properties. In addition to this procedure, Fritz et al. (2000) proposed a design for microcantilever array. Because the noises from thermal fluctuation and fluid flow have the same influence on every microcantilever in the array, by comparing the deflection with other microcantilevers in the array, the noise errors cancel each other.

The response time of the microcantilever sensors was reported to be ranging from extremely fast in seconds to slow shift in hours or days. The response time is mainly dependent on the types of probe and target molecules involved. Some biological molecules are large and complex, thus taking a long time to unwind, while some chemical molecules react instantly. (Baller, et al., 2000; Moulin, O'Shea, & Welland, 2000; Thundat, Pinnaduwage, & Lareau, 2004)

1.2 Detection Method

A few methods were derived to detect the deflection and resonance frequency of the microcantilever. The two most commonly used are the optical method and piezoelectric element. Both have some advantages and disadvantages. Following are discussions of these methods.

1.2.1 Optical Method

The set-up for optical detection method is similar to the atomic force microscope (AFM), which consists of a laser and optical position-sensitive sensor (see Figure 1.2). A laser beam is focused onto the microcantilever surface and reflected back to the position-sensitive detector. When the microcantilever deflects or vibrates, the laser reflects back to a different location on the position-sensitive detector. The difference in locations is used to calculate the actual deflection of the microcantilever.

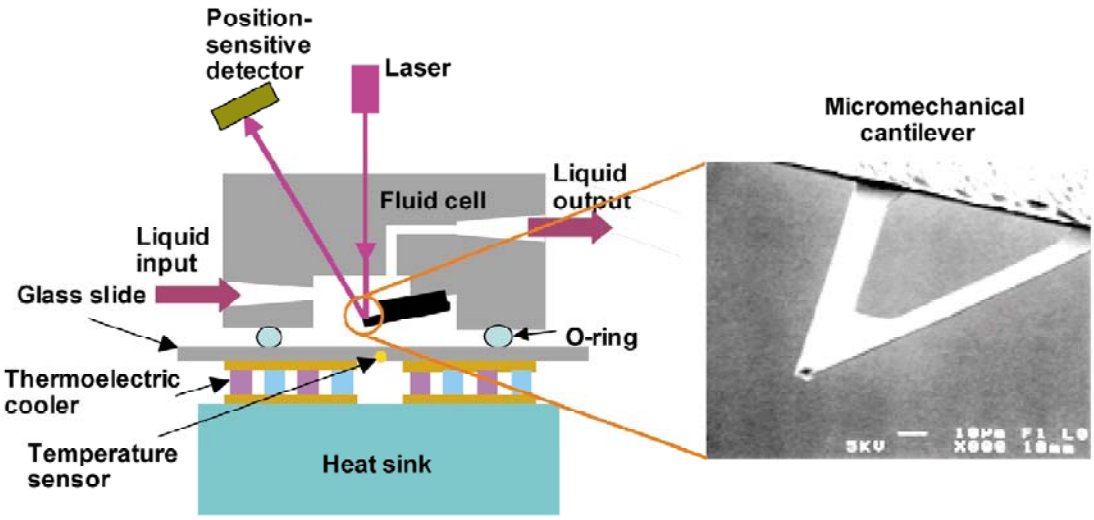

Figure 1.2 Experimental set-up using optical technique to measure the deflection of the microcantilever. (Wu, Datar, Hansen, Thundat, Cote, & Majumdar, 2001)

There were a few designs proposed to improve the sensitivity of the optical detection. Yue et al. (2004) proposed a microcantilever design shown in Figure 1.3. The intention of Yue's design is to have a very rigid tip to provide a flat area in order to reduce the error due to the reflection from a curve surface. The rigid tip was achieved by adding a square ridge to increase the tip's moment of inertia. In addition, a highly reflective gold surface was used to improve the reflection quality.

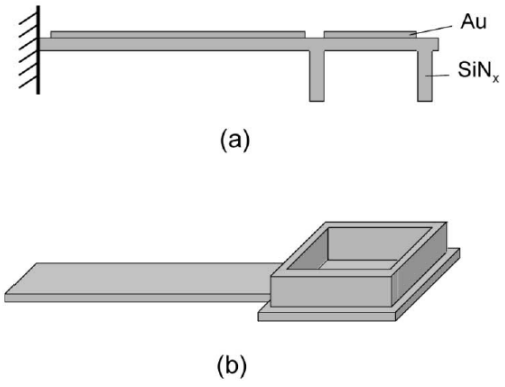

Figure 1.3 Design of the microcantilever with stiffened tip for flat reflective surface. (a) The side view. (b) Showing the rigid tip area. (Yue et al., 2004)

Another objective of the microcantilever sensors is to be able to detect many different types of target molecules at the same time. Yue proposed a design that assembles individual microcantilevers into an array as shown in Figure 1.4. Each microcantilever had its own chamber for probe functionalization with corresponding chemical/biological agents. Systems of lasers, mirrors, and cameras were used to measure the deflection.

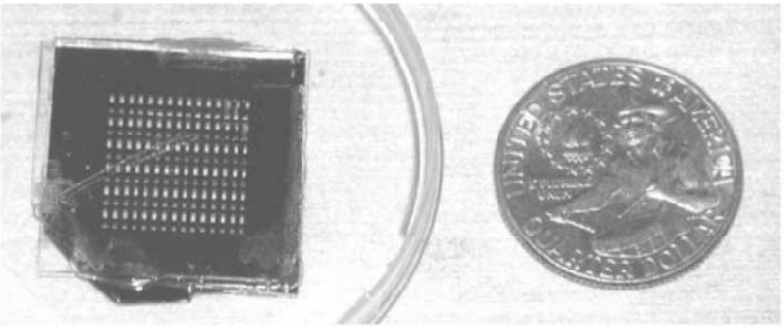

Figure 1.4 Yue's design of 2-D microcantilever array. There are 6 × 15 microcantilevers. (Yue et al., 2004)

1.2.2 Piezoelectric Element

In addition to the optical method, the deflection as well as the resonance frequency can be measured using a piezoelectric element. When under strain, the piezoelectric element gives electrical outputs. Common piezoelectric material is made from doped silicon, which is usually applied as one of the microcantilever layers. The adsorption-induced surface stress deflects the microcantilever, straining the piezoelectric element. One benefit of the piezoelectric detection over the optical one is that the piezoelectric element is cheaper compared to the complex set-up of the optical method. Moreover, without the complex optical set-up, the piezoelectric system can be very small which is important if mobility of the sensor is essential. Another advantage of the piezoelectric technique is that it can be used in opaque liquid that does not transmit light. However, one disadvantage of the piezoelectric element is that its sensitivity, reported so far, is

at least one order of magnitude lower than that of the optical technique (Yue, Majumdar, & Thundat, 2006).

1.3 Measurement Mode

As mentioned previously, two types of motions can be measured from the microcantilever: the total deflection and resonance frequency change.

1.3.1 Deflection

The adsorption of the target molecules induces surface stress, causing the microcantilever to bend. The bending of the microcantilever can be calculated from the surface stress though Stoney's equation: (Stoney, 1909)

$$Pt = \frac{1}{6}\frac{Ed^2}{r} \qquad (1.1)$$

where P is the surface stress, t the coating layer thickness, E the modulus of elasticity, d the thickness of beam, and r the radius of the curvature after thin film deposition. Stoney originally derived this equation to predict the deformation of a substrate from a coating of thin film. According to Stoney's equation, it was reported that the sensor can detect surface stress as low as 10^{-4} N/m (O'Shea, Welland, Brunt, Ramadan, & Rayment, 1996). However, accuracy of this equation is still being debated and will later be discussed in Section 1.5.4.

1.3.2 Resonance Frequency

Another detectable quantity is the change in resonance frequency. The resonance frequency, f, of a microcantilever depends on its effective mass, m, and spring constant, K, and can be expressed as: (Thundat, Oden, & Warmack, 1997)

$$f = \frac{1}{2\pi}\sqrt{\frac{K}{m}} \qquad (1.2)$$

When target molecules are absorbed, not only the effective mass, *m,* of the microcantilever increases, but the spring constant, *K,* is also changed due to the increase in beam's thickness as well as the change in surface property.

A few additional devices are required to measure the change in resonance frequency. Actuation source is needed to vibrate the microcantilever. Commonly, a piezoelectric actuator is used for this purpose in a similar manner to AFM tapping mode. The piezoelectric actuator induces mechanical motion when electrical signal is applied to vibrate the microcantilever. In addition to the actuator system, a feedback circuit is required to measure the frequency and apply appropriate excitation. (Cunningham, Jenkins, & Khalid, 1997; Han, Lindsay, & Jing, 1996; Passian et al., 2002)

The resonance measurement works well in gas. However, in liquid, the high viscosity severely dampens the vibration of the microcantilever. To improve the resonance measurement in liquid, Vidic et al. (2003) proposed a system of external magnetic or electrostatic excitation with active feedback system (see Figure 1.5). For magnetic excitation, Vidic et al. used a magnetic coil to excite the microcantilever containing a layer made of magnetic material. Vidic's design for electrostatic excitation is to utilize Coulomb force generated from capacitor plates. Both designs use electrical feedback system to actively vibrate the microcantilever.

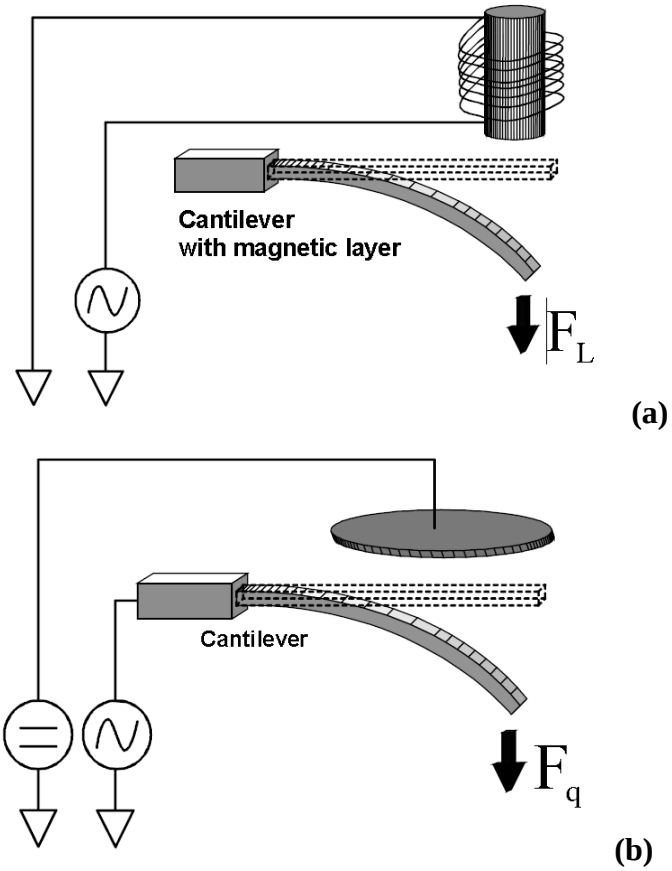

Figure 1.5 Vidic's design for magnetic (a) and electrostatic (b) excitation for resonance microcantilever sensor. (Vidic, Then, & Ziegler, 2003)

1.4 Applications

The microcantilever sensor can be configured to measure a wide variety of physical, chemical, and biological properties. As always, the underlying principle of the microcantilever sensor lies in its small size, which gives the sensor its high sensitivity. Followings are a few examples of its applications.

1.4.1 DNA Detection

One of the most basic building blocks for organic lives, DNA (deoxyribonucleic acid) is extremely important for it regulates the reproduction of cells. Many organic characteristic, such as human traits or diseases, could be traced back to

DNA, or more specifically the DNA sequence. The DNA sequence indicates how cells are reproduced and their functions. By looking at the DNA sequence, scientists can detect abnormal cells and diseases.

DNA commonly consists of 2 long strands of polymers made from unit monomers called nucleotides. A nucleotide consists of a deoxyribose (five carbon sugar), a phosphoric acid (H_3PO_4), and an organic base group (see Figure 1.6). There are 4 types of the organic base groups: Adenine (A), Thymine (T), Guanine (G), and Cytosine (C). The deoxyribose bonds with phosphoric acid to form the 'back bone' of the DNA. The base group bonds to the deoxyribose. The order of the base groups is essentially the DNA sequence. Due to the structure of the base groups, Adenine only bonds with Thymine and Guanine with Cytosine. As a result, one strand of DNA only bonds to the other strand of DNA that contains its complementary base groups. For example, a 4-mers single-stranded DNA shown in Figure 1.6 with ACTG sequence (left-hand strand) bonds to the strand with TGAC base groups (right-hand strand). (Madet, 2007; Zumdahl, 1995)

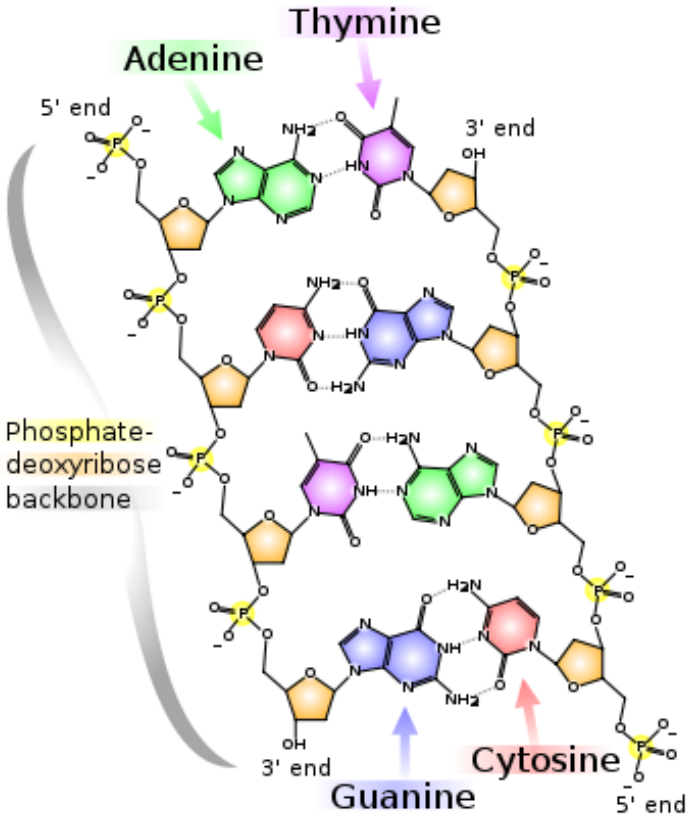

Figure 1.6 DNA structure. http://en.wikipedia.org/wiki/DNA

It is this ability to bond with complimentary base groups that is utilized by the microcantilever sensor in detection of a particular sequence of DNA. Usually, the single-stranded probe DNAs with the required base group sequence are attached to the gold layer of the microcantilever through the sulfur atoms (from the phosphoric acid). This microcantilever is "functionalized" and ready to hybridize (bond) with the complimentary single-strand target DNAs.

Fritz et al. (2000) and Wu et al. (2001) showed from their experiments that the microcantilever sensor can detect and differentiate DNA sequences. In both experiments, single-stranded probe DNAs were immobilized on the surface of the microcantilever. The target DNAs bond with the complementary probe DNAs. The hybridization process causes changes to the DNA shape, entropies, and energy. Those changes are believed to induce the surface stress that bends the

microcantilever. Fritz and Wu also tested the selectivity of the sensor using DNA strands with different base sequences. They found that the sensor did not respond to incorrect sequences. In another research, Mckendry et al. (2002) showed that the sensor can also differentiate complementary DNA strands with different tail end configurations. For example, in Mckendry's experiments, some target DNA strands had additional Adenine groups attached to their 3' tail ends (the tail ends with hydroxyl groups, see Figure 1.6), on the 5' end (the tail ends with phosphate groups), or on both ends. Mckendry found that the sensor reacted differently to those tail end configurations.

Su (2003) designed a two-step hybridization method that utilized a silver bonding at the tail ends of hybridized DNAs to improve the sensor sensitivity. Su functionalized the microcantilever with short "capture" DNAs (see Figure 1.7). Then the longer target DNAs were hybridized with the shorter capture DNAs leaving exposed end section of the target DNAs. After that, Su added the probe DNAs with gold atoms attached to their tail ends. These probe DNAs are hybridized with the exposed section of the target DNAs to complete the double strands. Then, silver particles were added to the system. These silver particles grew on the gold atoms, increasing mass to the microcantilever and thus enhancing changes to the resonance property.

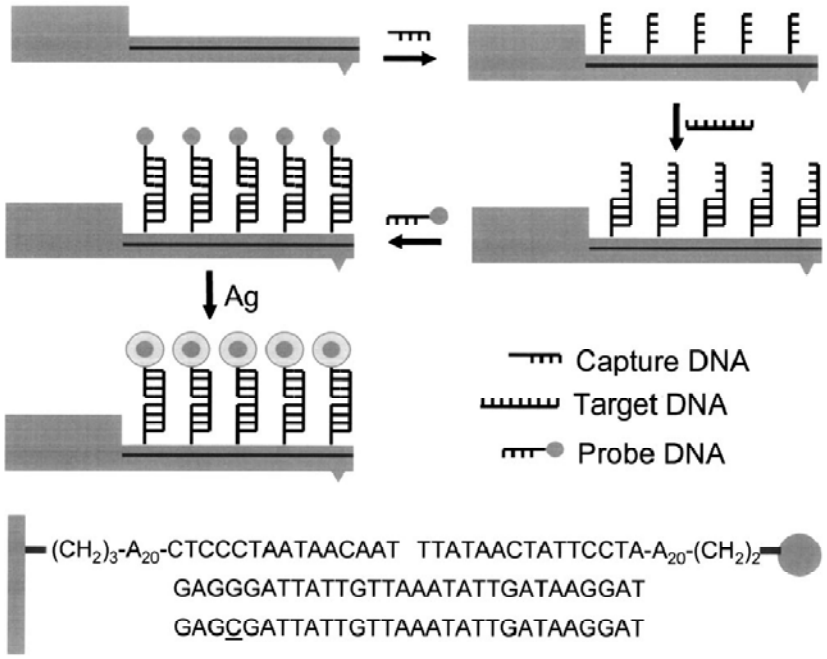

Figure 1.7 Process from Su to increase the change in resonance of the microcantilever to detect DNA. (Su, Li, & Dravid, 2003)

The DNA detection of microcantilever sensor has a few advantages over current detection method of fluorescent or radioactive tag (McKendry et al., 2002). The microcantilever sensor is a one-step method only requiring the addition of the DNAs, while the current technology requires multiple steps involving intensive labours. Furthermore, muti-microcantilever array sensors are being developed in order to detect several DNA sequences at the same time (Lang et al., 1998; Yue et al., 2004).

1.4.2 Antigen-Antibody Binding

The binding of antigen and antibody allows the body's immune system to respond to the infections of virus, bacteria and foreign materials. Diseases and abnormal cells, such as cancer cells, produce antigens. To fight against those intrusions, human body produces antibodies that attach to the antigens of the exact complementary shapes (see Figure 1.8), marking those cells for future termination.

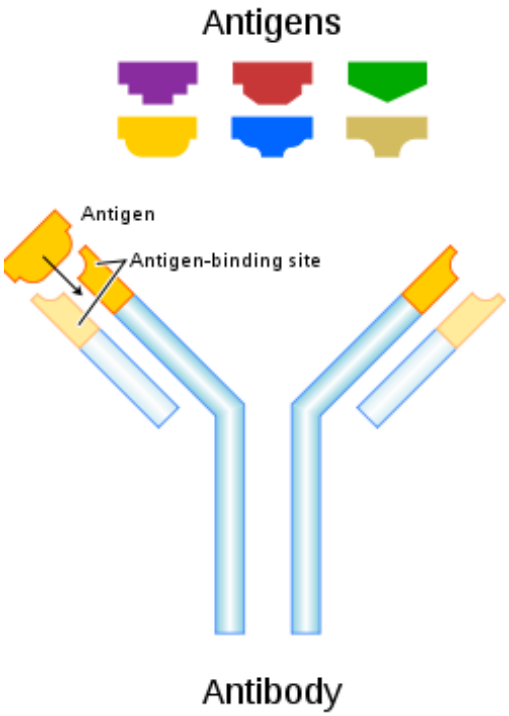

Figure 1.8 Antibody and antigen. Only certain shape antigens can bond to the complementary-shape antigens. http://en.wikipedia.org/wiki/Antibody

To detect the antigens, the selected antibodies are attached to the microcantilever usually through gold layers. Similar to the hybridization of DNAs, the bindings between the antigens and antibodies create a change in surface stress that deflects the beam as well as increases the mass of the microcantilever which changes the resonance frequency. Because antigens only bind with the antibodies with the exact complementary shape, the sensor is highly selective. Wu et al. (2001) successfully used the microcantilevers to detect prostate cancer cells by attaching the polyclonal anti prostate-specific-antigen antibodies to bind the prostate-specific antigens.

1.4.3 Chemical Detection

The ability to detect a tiny amount of chemical agents is highly beneficial in many aspects, such as the early warning of harmful gas built-up or the recognition of explosive TNT particles. The microcantilever sensor could be ideal in this role because of its sensitivity and portability. As mentioned earlier, the microcantilever sensor was found to have some of the highest sensitivity. Due to its size and the ability to function without further laboratory analysis, the microcantilever sensor can be designed for portable application. Similar to the biological agent detection, one side of the microcantilever is coated with a chemical layer that exhibits strong affiliation with the target chemical molecules. The interactions between the target molecules and the chemical layer generate surface stress that deflects the microcantilever.

Baller et al. (2000) used multiple microcantilevers as an "artificial nose" to identify different type of alcohols and natural flavours. Baller coated the microcantilever with various kinds of polymers. The alcohols and natural flavours were recognized to react with each polymer surfaces differently and at different respond rates. By analyzing the reactions, Baller identified each alcohol and the natural flavor. Baller showed that the accuracy for natural flavour detection could be as high as almost 100% with the lowest accuracy at 73%.

Other researches in chemical detection using microcantilever sensor are: the detection of dimethyl methylphosphonate, a components of sarin nerve gas, by lead zirconate titanate/stainless steel microcantilever (Zhao, Zhu, Shih, & Shih, 2006), the detection of explosive vapour using 4-mercaptobenzoic acid coated microcantilever (Thundat, Pinnaduwage, & Lareau, 2004), and the mercury detection through gold-coated microcantilever (Drelich, White, & Xu, 2008; Thundat, Wachter, Sharp, & Warmack, 1995). Thus many types of chemical agents can be detected using the microcantilever principle. Moreover, multi-

microcantilever array can be used to detect many chemical agents at the same time.

1.4.4 Mass

The microcantilever sensor can be used to measure mass because changes in mass lead to changes in resonance frequency. It was found that the resolution for mass measurement is as high as at 1 pg level (Chen,Thundat,Wachter, & Warmack, 1995; O'Shea, Welland, Brunt, Ramadan, & Rayment, 1996). The target molecules can be adsorbed over the entire length of the microcantilever or only just at the tip. In the first case, the entire-length adsorption changes the surface properties of the microcantilever, which leads to changes in both spring constant and mass. In the second case, the target molecules only adsorb onto the tip thus, only increasing the beam's mass with negligible change in the spring constant. One common experimental procedure is to use zeolites as the probe agents (Berger, Gerber, Lang, & Gimzewski, 1997). Zeolites are highly porous material with high surface to mass ratio. The pore size of zeolites can be controlled to capture only target molecules of certain size.

1.4.5 Temperature/Calorimeter

By utilizing the fact that different material expands at different rate, the microcantilever can be used to measure heat flux (Thundat, Pinnaduwage, & Lareau, 2004). For this application, the microcantilevers are commonly made of at least 2 distinct layers of different materials, one of which is usually metal because of its high thermal expansion rate. When the microcantilever is exposed to temperature changes or heat fluxes, one layer expands or contracts more than the other causing the microcantilever to bend. The magnitude of the bending can be calibrated by applying known temperature changes or heat fluxes to the system (Berger, Gerber, Lang, & Gimzewski, 1997). Because of its small mass, heat can propagate throughout the microcantilever within milliseconds giving the sensor very fast response time. The approach can be applied in calorimeter application

where small sample is burned on the microcantilever surface or the heat given off from the reaction between the target and probe molecules induces the bending. The resolution was reported to be as low as 10^{-5} K for the temperature measurement and 20 fJ (10 pW) for calorimeter application (Thundat, Oden, & Warmack, 1997).

1.5 Literature Reviews

One difficulty in developing the microcantilever sensor is that the "exact mechanism of adsorbate-induced bending on 'real surfaces' still remains to be solved" (Thundat, Pinnaduwage, & Lareau, 2004, p. 252). Many research groups are currently studying the sensor behaviour. This section provides some discussion about the previous researches, with particular emphasis on the simulation studies. The discussion also includes comparisons between the previous works and our current work.

1.5.1 Dareing and Thundat (2005)

In 2005, Dareing and Thundat presented a simulation study for a microcantilever using the minimum energy approach. They used Lennard-Jones potentials to model the target-target interactions. The target molecules are fixed on the microcantilever surface. The target-target interactions force the target molecules to move, in order to minimize the Lennard Jones potentials. However, for the target molecules to move, the beam has to bend, which increases the strain energy. The minimum of the sum of the strain energy and the Lennard-Jones potential determines the microcantilever deflection.

Taking into account the geometry, Dareing and Thundat expressed the Lennard-Jones potentials, U_s, as:

$$U_s = \frac{-A}{(b-z)^6} + \frac{B}{(b-z)^{12}} + 2\left\{\frac{-A}{\left[\frac{1}{4}(b-z)^2+a^2\right]^3} + \frac{B}{\left[\frac{1}{4}(b-z)^2+a^2\right]^6}\right\} \quad (1.3)$$

where b is the original horizontal distance between 2 target molecules (see Figure 1.9), z is the horizontal displacement of the target molecules after the microcantilever deflects ($z = \frac{b}{R}(c+a)$), a is the height of the layers between 2 neighbour target molecules, and A and B are Lennard-Jones constant.

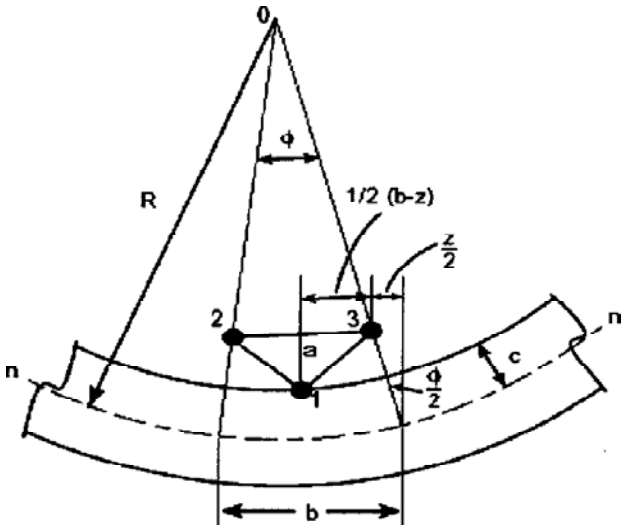

Figure 1.9 Arrangement of molecules used in Dareing and Thundat simulation (Dareing & Thundat, 2005)

From elasticity theory, the strain energy of the microcantilever, U_b, can be expressed as:

$$U_b = \frac{1}{2}EI\left(\frac{1}{R}\right)^2 b \quad (1.4)$$

Then, the deflection of the microcantilever can be calculated by minimizing the total potential energy ($U = U_s + U_b$).

Our current work uses molecular dynamics method, which is a force-based method using integration of equations of motion to find the trajectories of all molecules. Unlike Dareing and Thundat's approach that uses the combination of continuum and molecular scales, our method is entirely within the molecular scale. Another difference is that Dareing and Thundat predefined the locations of the target molecules by fixing them to the microcantilever, while our simulation allows the target molecules to move freely. The free movement of target molecules permits us to study the system in the equilibrium dynamics where target molecules can bond and de-bond. Furthermore, it allows the study of the target-probe interactions as the target molecules are not required to be fixed in certain locations and can move around to interact with the probe molecules.

1.5.2 Wu, Sun, & Wang (2007)

In 2007, Wu proposed the use of an embedded-atom-method potential to model the molecular interactions. The potential can be expressed as: (Daw & Baskes, 1984)

$$E_{tot} = \sum_i F_i(\rho_{h,i}) + \frac{1}{2}\sum_{\substack{i,j \\ i \neq j}} \emptyset_{ij}(R_{ij}) \quad (1.5)$$

where the first term is the potential due to the embedded atom and is a function of electron density , $\rho_{h,i.}$ The potential and the density function are determined through empirical experiments. The second term is the pair potential between 2 atoms.

In Wu's approach, a few target molecules were deposited into the system during each iteration. Through the embedded-atom potentials, these target molecules moved to the locations that minimize the total energy of the system. This process was repeated until the surface of the microcantilever was covered by the target molecules, and then the final deflection was determined.

In Wu's case, the target molecules were allowed to move just like our current work. However, our simulation consists of all target molecules from the beginning. Wu showed that the deflection depends on number of bonds between target and probe molecules which is similar to the behaviour observed through the current work.

1.5.3 Yu, Huang, & Liu (2009)

Yu used a very similar energy simulation approach as Dareing and Thundat, in which the target molecules are fixed relative to the microcantilever and the minimum energy state is calculated to find the deflection. In addition to this, Yu used a molecular dynamics simulation from Material Studio to confirm the results. The latter molecular dynamics method might be similar to our approach. Unfortunately, details of Yu's set-up for the molecular dynamics simulation were not given. Yu mainly studied the effect of microcantilever dimensions, such as the length and width, on the deflection for specific interactions of H_2O adsorption on Al surface. Our simulation, as presented in this work, considers diverse interaction properties by using variation of Lennard-Jones parameter pairs.

1.5.4 Other Theoretical Approaches

Previous theoretical studies usually focused on explaining the interactions between particular pair of target and probe molecules. The molecular interactions induce surface stress, which can be related to the microcantilever deflection usually through the Stoney's equation. (Berger, Gerber, Land, & Gimzewski, 1997; Chen, Thundat, Wachter, & Warmack, 1995; Moulin, O'Shea, & Welland, 2000; O'Shea, Welland, Brunt, Ramadan, & Rayment, 1996; Thundat, Pinnaduwage, & Lareau, 2004; Wu, Datar, Hansen, Thundat, Cote, & Majumdar, 2001; Yue, Majumdar, & Thundat, 2006) The Stoney's equation was originally developed to predict the deflection of thin film caused by surface stress from the thin film deposition (see Equation 1.1). Paper by Klein (2000) gives a comprehensive discussion about the errors involved in using Stoney's equation.

Klein provided a plot of error involved in using Stoney's equation which is shown in Figure 1.10.

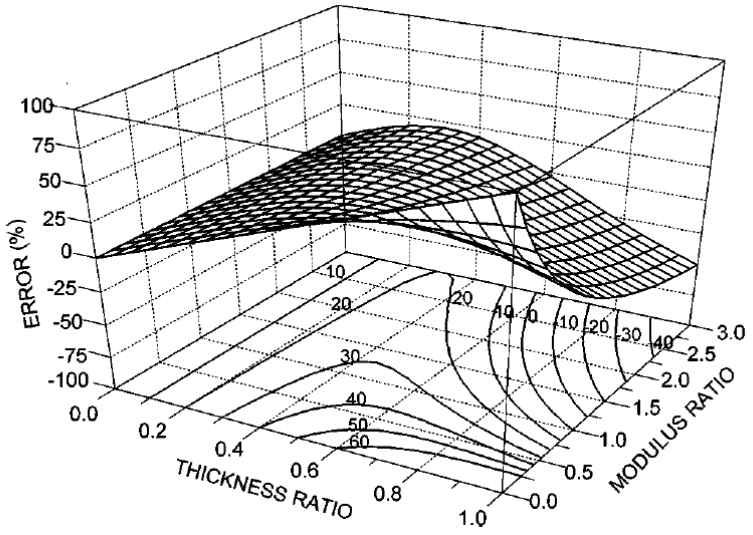

Figure 1.10 Error due to Stoney's equation. The thickness ratio is the ratio of the coating's thickness to the substrate's. The modulus ratio is the ratio of the coating's modulus to the substrate's. (Klein, 2000)

Figure 1.10 shows that the Stoney's equation is accurate over a range of thickness and modulus ratio.

Normally, each theoretical study was built upon empirical works to explain the interactions of the specific pairs of molecules observed during the experiments. However explanation for one specific system may not be suitable for the other system. One of the goals of our research is to study a general system of no specific types of molecules to find out the effect of the interaction parameters, such as the strength or interaction distance, on the microcantilever deflection.

1.6 Research Objective

Microcantilever is a unique sensor capable of measuring/detecting a wide variety of properties. For chemical/biological sensing, the interactions can be quite complex containing many different types of forces. The purpose of the current work is to study the effect of different molecular interactions on the microcantilever deflection. Therefore, we propose a molecular dynamics simulation using the Lennard-Jones potential to model interactions among the target, probe, and microcantilever molecules as well as the Lattice Spring model for the solid microcantilever beam. By varying the Lennard-Jones parameters, we can model a variety of interactions by changing the interaction distance and strength of the target and probe molecules. The molecular dynamics simulation also allows the system in a dynamics simulation that shows the movement of molecules and changing arrangements of bonds.

The research is intended to:

- compare the effect of each Lennard-Jones parameter on the deflection of the microcantilever, in order to find the basic relationships and trends between molecular interactions and microcantilever deflection
- study the design of the probe locations for a possibility of improving the sensor sensitivity

Chapter 2 will describe the construction of the molecular dynamics simulation including the explanation of the models used. Approach in collecting raw simulation data and their trends will be discussed in Chapter 3. Chapters 4 and 5 will present the results of the effect of the Lennard-Jones parameters and probe locations respectively. Chapter 6 will provide a conclusion to this work.

Chapter 2

Simulation Methodology and Models

The microcantilever system contains 3 types of molecules: target, probe, and microcantilever molecules. Each molecule behaves distinctively and thus requires a different set of governing equations. Target molecules are mostly free to move, while the microcantilever molecules have to remain closely constrained relative to each other. The probe molecules must be anchored to one surface of the microcantilever. In addition, model for the entire system must be constructed to describe what happen at the boundary. After defining the models, the trajectories of all molecules and the deflection of the microcantilever can be obtained through the simulation of the equations of motion. In this study, the simulations were performed in two-dimensional Cartesian coordinate. Following are discussions about these models and simulation methodology.

2.1 Microcantilever Model

We selected the three-body bond bending (Monetter & Anderson, 1994) to model the solid microcantilever molecule. In the first part of this section, explanations detailing the three-body bond bending model will be given. This model is one of several lattice spring models that are used in simulations of solid property. Hence,

the following section will discuss and compare the three-body bond bending model to other commonly used lattice spring models. In the last part of this section, overall model for the entire beam will be presented showing the molecule arrangement and the cantilever support.

2.1.1 Three-Body Bond Bending Model

Being a solid material, the microcantilever molecules have a very limited range of motion with restriction on their distortions with respect to their neighbouring molecules. In this simulation, the microcantilever molecules were modeled as a point mass. To restrict their movements, the microcantilever molecules were connected to each other through a network of stiff springs that resisted the change in their positions. The three-body bond bending potential was selected as the model of this spring network. The three-body bond bending potential consists of 2 components: the two-body central force and the three-body bond bending. The two-body central force represents the potential when a bond between 2 molecules is extended or compressed while the three-body bond bending can be considered as the resistance to distortion of angle formed by 3 molecules. One way to think of this model is that the central force represents 2 molecules connected with a linear spring. The compression/extension force is applied along the axis connecting the 2 centers as the spring tries to resist the change in its length. The bond bending component could be thought of as a torsional spring connecting 2 bonds that form an angle with one common vertex. When the angle between the bonds changes, the torsional spring applies the torque to resist the change. Since it is the bond bending term that distinguishes this model from other lattice models, the potential assumes the name three-body bond bending. The potential can be expressed as: (Arbabi & Sahimi, 1990; Feng, Sen, Halperin, & Lobb, 1984; Monetter & Anderson, 1994)

$$E = \frac{1}{2}k\sum_{ij}\left(|\underline{r}_{ij}| - |\underline{r}_{ij}^{o}|\right)^2 + \frac{1}{2}c\sum_{ijk}\left(\cos\theta_{ijk} - \cos\theta_o\right)^2 \quad (2.1)$$

where $\underline{r}_{ij}$ is the bond length between molecules i and j, $\underline{r}_{ij}^{o}$ the spring free length, θ_{ijk} the angle formed by bond i-j and bond i-k with i as the common vertex (see Figure 2.1), θ_o the original angle formed by bond i-j and bond i-k, and k and c are the spring constants. The first term on the right hand-side of Equation 2.1 represents the central force term and the second term the bond bending term. The spring constants should be high enough to provide the microcantilever molecules enough stiffness to produce a sufficient resistant to the deformation. However, when the values of the spring constants are too high, the system could have severe vibration and in some cases the beam would breakdown. The central force spring constant k was set to be 200 and the bond bending spring constant c to 40 (see Section 2.8 and Appendix A for explanation on the unit of the spring constant). Both values were selected by testing the simulation with various spring constants. Initial guess of the spring constants were made based on the previous works by Monetter & Anderson (1994) and Buxton et al. (2005). The values were modified to yield high enough stiffness for the microcantilever beam while still maintaining the stability of the system. If the spring constants are too low, the system might produce high deformation (usually outside the elastic strain range) and if the spring constants are too high, the system might generate strong forces that can potentially break the beam.

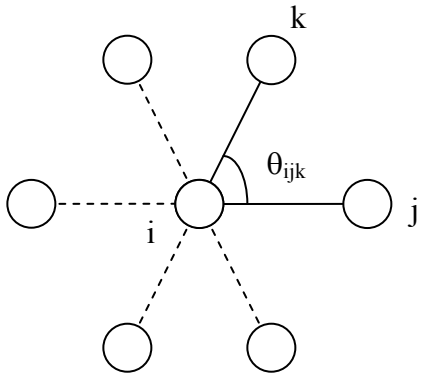

Figure 2.1 Triangular lattice. The line between molecules i and j represent bond i-j and the line between molecules i and k represent bond i-k. Angle θ_{ijk} is formed by bond i-j and bond i-k

The force can be calculated by taking the gradient of the potential with respect to the positional vector. The force on molecule i generated from bond i-j and i-k and angle ijk can be expressed as: (Monetter & Anderson, 1994)

$$\underline{F}_{ij} = \frac{\partial E}{\partial \underline{r}_{ij}} = \nabla E(r_{ij}, \theta_{ij}) \quad (2.2)$$

$$\underline{F}_{ij} = k\left(|\underline{r}_{ij}| - |\underline{r}_{ij}^{o}|\right)\underline{e}_{r_{ij}} - \frac{c}{r_{ij}}\left(\cos(\theta_{ij} - \theta_{ik}) - \cos\theta_o\right)\sin(\theta_{ij} - \theta_{ik})\,\underline{e}_{\theta_{ij}} \quad (2.3)$$

and

$$\underline{F}_{ik} = \frac{\partial E}{\partial \underline{r}_{ik}} = \nabla E(r_{ik}, \theta_{ik}) \quad (2.4)$$

$$\underline{F}_{ik} = k\left(|\underline{r}_{ik}| - |\underline{r}_{ik}^{o}|\right)\underline{e}_{r_{ik}} + \frac{c}{r_{ik}}\left(\cos(\theta_{ij} - \theta_{ik}) - \cos\theta_o\right)\sin(\theta_{ij} - \theta_{ik})\,\underline{e}_{\theta_{ik}} \quad (2.5)$$

where $\underline{r}_{ij}$ is the positional vector, r_{ij} the length scalar component of positional vector $\underline{r}_{ij}$, θ_{ij} the angular component of positional vector $\underline{r}_{ij}$, $\underline{e}_r$ the unit vector along the radial direction, and $\underline{e}_\theta$ the unit vector along the angular direction. Figure 2.2 illustrates the convention used to describe the angles and the directional vectors. Note that the positional vector $\underline{e}_{r_{ij}}$, $\underline{e}_{\theta_{ij}}$, $\underline{e}_{r_{ik}}$, and $\underline{e}_{\theta_{ik}}$ can be expressed in Cartesian coordinates through angles θ_{ij} and θ_{ik}.

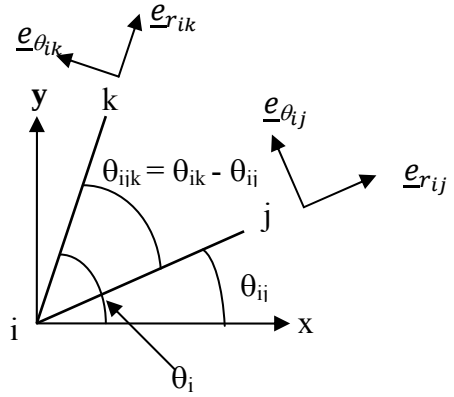

Figure 2.2 Illustration of symbols used to describe the angles and the directional vector $\underline{e}_r$ and $\underline{e}_\theta$. θ_{ij} is the angle between the i-j bond to the x-axis and θ_{ik} the angle between the i-k bond to the x-axis.

Equations 2.3 and 2.5 consist of 2 components. The first component on the right-hand side of both equations corresponds to the linear spring term (k) acting along the radius direction $\underline{e}_r$ which is parallel to the lines joining the 2 molecules' centers. The second component corresponds to the torsional spring term (c) acting along the angular direction $\underline{e}_\theta$ which is perpendicular to the bond axis formed between 2 molecules. The forces in Equations 2.3 and 2.5 are the forces generated from bonds i-j and i-k as well as angle ijk. Total forces acting on any molecule are the net of all forces from the bonds connecting to that molecule and the angles formed by the molecule.

In this simulation, criteria of r_{limit} and θ_{limit} were used to restrict the change in the spring length and angle. When $r_{ij} > r_{limit}$ the spring constant, k, was set to zero and when $\theta_{ijk} - \theta_o > \theta_{limit}$ the angular spring constant, c, was set to zero. Originally the value for r_{limit} was chosen to be 1.5 r_{ij}^o and θ_{limit} be $\pi/6$ to prevent the local bond breakage from high interaction forces. Since then, the spring model and the force calculation have been refined to reduce the chance of bond breakage. After refinement, it was found that r_{ij} and the change in angle were much lower than r_{limit} and θ_{limit}. Usually the change in total length of the microcantilever was around 1-2 %. This small spring displacement also suggested that the springs have enough stiffness. This change of around 1-2% should resemble the real material because most materials would undergo the plastic deformation if the strain is higher than 1-2% and, furthermore, the elastic spring assumption would break down. In this simulation, the value of r_{limit} and θ_{limit} were kept at 1.5 r_{ij}^o and $\pi/6$ even though these value could be in the plastic deformation region. This was to keep these values consistent with earlier simulations. However the change in total length of the microcantilever was monitored to make sure that it did not go beyond 2% of stain, the elastic deformation limit.

By using the bond bending model, the microcantilever molecules were only allowed to have relatively small movement with respect to their neighbours. The

spring constants k and c control the stiffness of the bond, while r_{limit} and θ_{limit} the distance and torsional angle above which bonds break.

2.1.2 Comparison between various Solid Lattice Spring Models

Beside the three-body bond bending model, other commonly used methods for solid modeling are the central force model and Born-spring model. All three models are widely used because of their simplicities. The following is the description and comparison between the models.

For the central force model, compression/extension spring is used to connect 2 molecules generating a force that acts along the axis connecting their centers (thus the name central force). The central force spring potential is: (Born & Huang, 1966; Buxton, Verberg, Jasnow, & Balazs, 2005; Hassold & Srolovitz, 1989)

$$U_{ij} = \frac{1}{2}k\sum_{j}\left(|\underline{r}_{ij}| - |\underline{r}_{ij}^{o}|\right)^{2} \qquad (2.6)$$

This is exactly the same as the first term on the right-hand side of Equation 2.1 for the bond bending model.

One disadvantage with this model is that the springs can rotate freely around the molecules. Hassold and Srolovitz (1989) showed that for the central force model, any transverse force causes the springs to rotate and align the springs in the direction of the applied load. Therefore, this type of spring can only apply force along its axial direction, as any force transverse to the spring axis rotates the spring freely. This model has very low resistance to bending, thus not suitable for our simulation.

The Born-spring model prevents the free rotation of the bonds by introducing the force that resists the transverse movement of the bonds. The model takes into account the original lattice spring positioning. The potential for Born-spring

model is expressed as: (Born & Huang, 1966; Feng & Sen 1984; Feng, Sen, Halperin, & Lobb 1984; Hassold & Srolovitz, 1989; Kantor & Webman, 1984)

$$E = \frac{1}{2}(k-c)\left((\underline{u}_i - \underline{u}_j)\cdot\tilde{r}\right)^2 + \frac{1}{2}c(\underline{u}_i - \underline{u}_j)^2 \quad (2.7)$$

where $\tilde{r}$ is the directional unit vector of molecules i and j in the original lattice and $\underline{u}$ is the displacement from the equilibrium. For the Born-spring model, there is a force corresponding to the spring constant *k* acting along i-j lattice direction (from the dot product with unit vector $\tilde{r}$) and another force corresponds to the *c* term acting perpendicular to the lattice direction. In other words, if any molecules are off their original lattice positions there would be forces parallel and perpendicular to their lattice directions to move those molecules back into their original lattice positions.

The Born-spring model and the three-body bond bending model are quite similar. The differences are in the direction of the spring force. The Born-spring model applies the force parallel and transverse to the original lattice position while the bond bending model applies the force parallel and transverse to the current bond direction. The actual microcantilever deforms into a curved shape. In the bond bending model, the bonds and angles deform in the manner that follow the curvature of the deflected microcantilever. Hence, forces from the bond bending model always act along with and perpendicular to the direction of the curvature. On the other hand, the Born-spring model applies the forces along its original lattice direction regardless of the deformed state of the microcantilever. Although both models resist the bending and try to restore the beam to its original positions, the bond bending model provides forces that correspond closely to the actual forces generated inside the deformed microcantilever. Therefore the bond bending model was selected for this simulation.

2.1.3 Model of the Microcantilever Beam

Figure 2.3 shows the microcantilever beam and its surrounding in their initial locations. To keep the length-to-thickness ratio similar to the actual microcantilever, the beam model contained 7 rows of 70 microcantilever molecules. Note that although the length-to-thickness ratio was kept quite close to the real microcantilever, the actual length was not the same as the real microcantilever. The left edge of the beam was restrained by fixing the microcantilever molecules' positions and velocities along the left edge to zero. Mechanically, the left edge became a fixed support capable of carrying both reaction force and moment. The rest of the beam molecules were free to move but were connected through the lattice spring network.

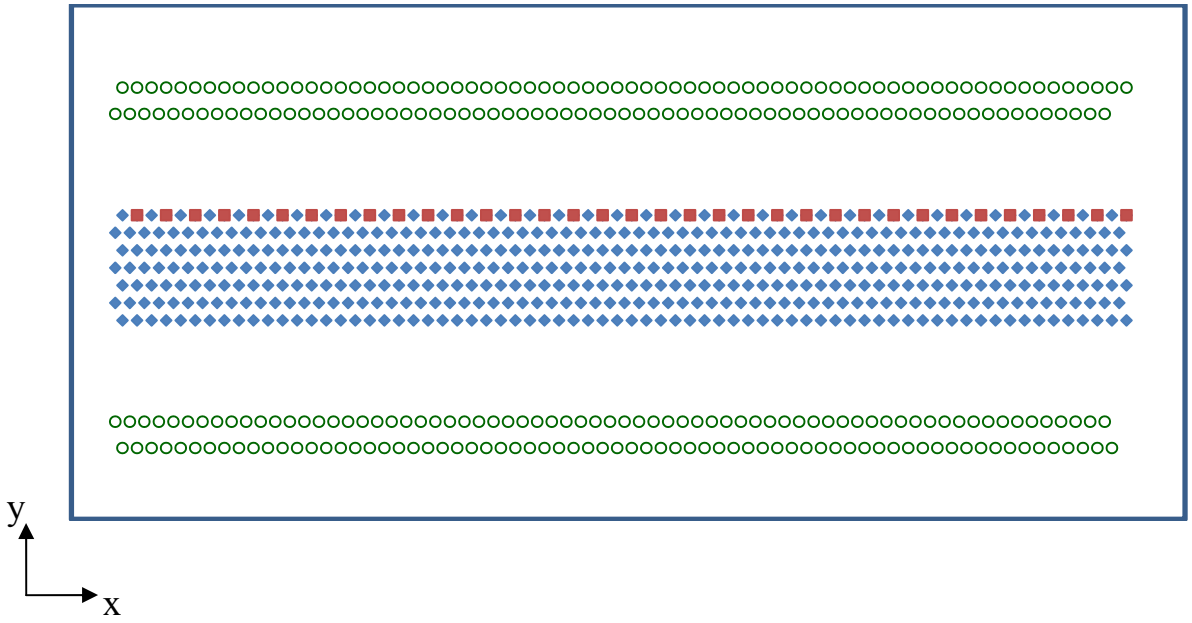

Figure 2.3 Diagram of the cantilever beam, probe and target molecules at the starting positions. The probe coverage for this cantilever is 50%. (♦) represents microcantilever molecules, (■) probe molecules and (o) target molecules. (Note that the diagram is not to scale)

Initially, the microcantilever molecules were arranged in triangular matrix (see Figure 2.3) which is a typical arrangement of molecules commonly used in modeling solid materials (Ashurst & Hoover, 1976; Beale & Srolovitz, 1988;

Curin & Scher, 1990; Feng & Sen, 1984; Garcia-Molina, Guinea, & Louis, 1988; Ladd & Kinney, 1997; Monetter & Anderson, 1994). The initial spacing between the microcantilever molecules was assigned such that the distances between microcantilever molecules were equal to the spring free length (2.0) and their angles to the equilibrium angle (60°) of the torsional spring. This was done to eliminate any initial spring forces. All microcantilever molecules were set at rest initially i.e. with no velocity.

2.2 Target Molecule Model

Normally, target molecules move around quite freely. Only when they come close to other target, probe, or microcantilever molecules, they interact. If their interactions are strong enough, the molecules bond with each other. In this simulation, the target molecules were modeled as a point mass which allowed the interaction force to be simplified so that the force acts along the line connecting both centers of mass (Haile, 1992). By using the point mass model, we ignored the rotation of the molecules. The molecular interactions were modeled using the Lennard-Jone 12-6 potential. The potential energy, U_i, for molecule i due to an interaction with molecule j can be expressed as: (Allen & Tildesley, 2007; Haile, 1992; Maitland, Rigby, Smith, & Wakeham, 1981)

$$U_i = 4\varepsilon\left(\left(\frac{r_{ij}}{\sigma}\right)^{-12} - \left(\frac{r_{ij}}{\sigma}\right)^{-6}\right) \quad (2.8)$$

With reference to Figure 2.4, ε corresponds to the minimum potential energy, σ represents the distance that the potential cross the x-axis and r_{ij} is the distance between molecule i and j.

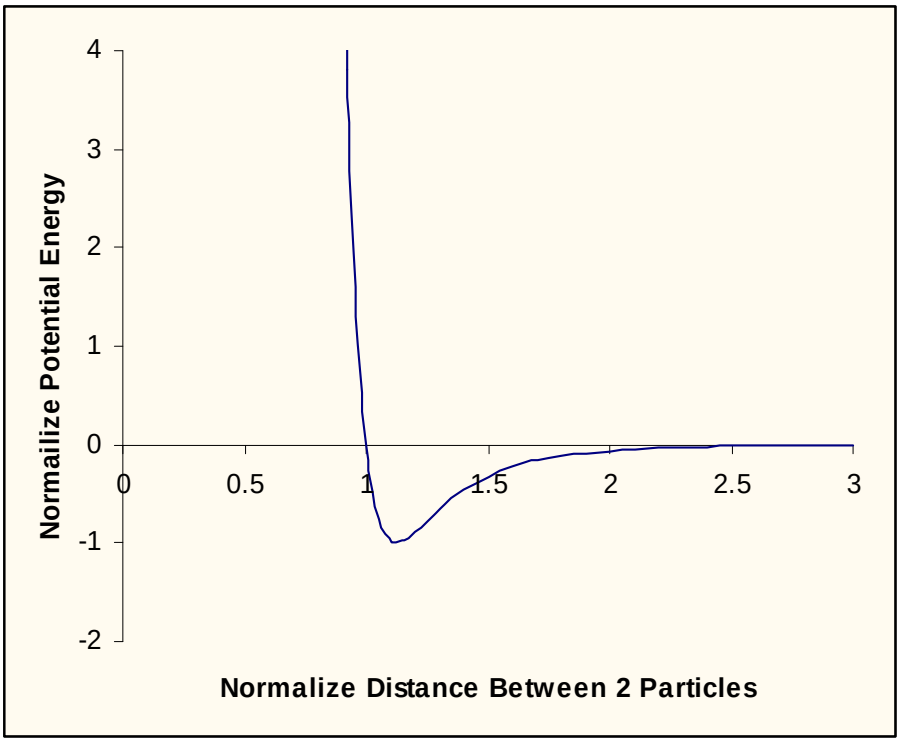

Figure 2.4 Lennard-Jones 12-6 potential

The Lennard-Jones potential was originally derived to model the attractive/repulsive interactions at a molecular level. The interaction distance represented by the value of σ is typically in a few angstroms or nanometers. Since this simulation did not use a specific unit, the results would be compared based on their relative magnitudes. In addition, the Lennard-Jones equation is being used throughout the simulation, thus other calculated properties can be expressed in term of the fundamental unit of σ and ε (more details about the unit of the system in Section 2.8 and Appendix A). σ can be thought of as the length unit of the simulation while ε as the energy unit. Therefore any properties that contain the length unit can be measured in relation to σ and those containing energy in relation to ε.

The Lennard-Jones potential is a simple model. This model is not intended to represent the real system, such as the complex DNA or antigen-antibody molecules, often used to functionalize the microcantilever sensor. The purpose of

this simulation is to understand the basic behaviour of the microcantilever sensor in a simple system thus the Lennard-Jones model was selected. With simple model of the Lennard-Jones interaction, the effect of each parameter could be compared relatively easily to each other without introducing more dependent variables and unknown complexity.

The interaction force, $\underline{F}_{ij}$, on molecule i due to an interaction with molecule j can be computed by taking the gradient of the potential, U_i, with respect to the positional vector $\underline{r}_{ij}$: (Allen & Tildesley, 2007)

$$\underline{F}_{ij} = 24\frac{\varepsilon}{r_{ij}^2}\left(2\left(\frac{r_{ij}}{\sigma}\right)^{-12} - \left(\frac{r_{ij}}{\sigma}\right)^{-6}\right)\underline{r}_{ij} \quad (2.9)$$

The molecules repel each other when their interaction distance is less than $2^{1/6}\sigma$ (negative slope in Figure 2.4). The interaction force becomes 0 at $2^{1/6}\sigma$ (the minimum point of the potential well), and turns into attractive force at the distance greater than $2^{1/6}\sigma$ (positive slope). As the interaction distance gets larger, the attraction force becomes weaker (slope approach 0). The distance of $2^{1/6}\sigma$ represents the equilibrium distance between molecules. Equation 2.9 also indicates that the interaction force is proportional to ε term. Hence, the ε term can be considered as an indication of the interaction strength. The higher the ε value, the deeper the potential well in Figure 2.4, the stronger the bonding force at a given distance. With higher ε value, the equilibrium and the bond are more stable because the molecule requires more energy to break the bond and escape the deeper potential well.

As $\boldsymbol{r}_{ij} >> \sigma$, the Lennard-Jones potential and force approach 0. However, calculating all minute interactions of all molecules in the system is not practical because it would significantly increase the computational time. Most molecular dynamics simulations ignore the interactions from molecules that are far apart by using a cut-off distance, r_c, of 2.5σ. The Lennard-Jones potential energy would be

set to 0, if the distance between the 2 molecules is longer than the cut-off distance. To account for the omitted energy when $r_{ij} > r_c$, Allen and Tildesley suggested the use of a shifted potentials U_i^S with the cut-off distance. The shifted potentials can be expressed as:

$$U_i^S(r_{ij}) = \begin{cases} U_i(r_{ij}) - U_c & r_{ij} \leq r_c \\ 0 & r_{ij} > r_c \end{cases} \qquad (2.10)$$

Where $U_c = U_i(r_c)$. Consequently, the Lennard-Jones potential shifts upward and becomes 0 at the distance greater than r_c. This shifted potential is useful in keeping track of the potential energy. When $r_{ij} > r_c$, we could ignore any interactions between molecules and still conserve the energy during the simulation. Although the energy level is shifted to a higher level, the shape of the potential remains the same, thus the interaction force is the same as the normal Lennard-Jones potential. The only thing that is changed is the reference energy level which is shifted by U_c. In this simulation, we used the shifted Lennard-Jones potential instead of the normal Lennard-Jones potential.

In this simulation, each target molecules underwent 3 Lennard-Jones interactions:

- interaction between the target molecule and probe molecule which is governed by $\sigma_{tar\text{-}probe}$ and $\varepsilon_{tar\text{-}probe}$.
- interaction between the target molecule and other target molecule governed by $\sigma_{tar\text{-}tar}$ and $\varepsilon_{tar\text{-}tar}$.
- interaction between the target molecule and microcantilever molecule governed by $\sigma_{tar\text{-}can}$ and $\varepsilon_{tar\text{-}can}$.

The Lennard-Jones parameters, $\sigma_{tar\text{-}probe}$, $\varepsilon_{tar\text{-}probe}$, $\sigma_{tar\text{-}tar}$, and $\varepsilon_{tar\text{-}tar}$, were the independent variables that were studied in the simulation. Their range was selected to produce the wide range of microcantilever motion from the downward deflection to the upward bending. In addition, the values of $\sigma_{tar\text{-}probe}$ and $\sigma_{tar\text{-}tar}$

were selected to reflect the distance between two probe molecules, set at 4.0, the distance between two microcantilever molecules, at 2.0, and the lattice spring length, at 2.0. Hence, the values of $\sigma_{tar\text{-}probe}$ and $\sigma_{tar\text{-}tar}$ were usually selected to be between 1.0 and 5.0. In the actual microcantilever sensor, the target molecules are attracted strongly to the probe molecules. To reflect this attraction, the $\varepsilon_{tar\text{-}probe}$ was assigned to have a higher value than $\varepsilon_{tar\text{-}tar}$ and $\varepsilon_{tar\text{-}can}$. The common range of $\varepsilon_{tar\text{-}probe}$ was between 5 to 50, $\varepsilon_{tar\text{-}tar}$ between 0.1 to 5, and $\varepsilon_{tar\text{-}can} = 0.05$. In some cases, the range for ε and σ values had to be modified due to the stabilities of the simulation. Some combinations of the Lennard-Jones parameters especially at the higher values of σ and ε create such a strong interaction force that could break the cantilever beam. Those values were omitted from the data analysis.

The target-cantilever interactions represented by $\sigma_{tar\text{-}can}$ and $\varepsilon_{tar\text{-}can}$ were used to prevent the target molecules from moving inside the microcantilever. This was done mainly by manipulating the $\sigma_{tar\text{-}can}$ value. The space between 2 microcantilever molecules was initially set at 2.0. If the value of $\sigma_{tar\text{-}can}$ was very low (<<1.0), target molecules could penetrate into the spring network by moving through the space in between 2 microcantilever molecules where their interactions were weak. The larger $\sigma_{tar\text{-}can}$ value yields a longer interaction length. It was found that 1.5 was an effective value of $\sigma_{tar\text{-}can}$ that prevented the penetration of target molecules. At this value, any target molecules moving too close to the microcantilever would be pushed away by the repulsive forces generated from the target-microcantilever interactions. However, the longer target-cantilever interaction distance could influence other molecular interactions by inducing a bond between the target and microcantilever molecules. This influence of the target-cantilever interactions can be minimized by reducing the value of $\varepsilon_{tar\text{-}can}$. With very low $\varepsilon_{tar\text{-}can}$, the Lennard-Jones potential well became quite shallow with very small attraction region. The microcantilever molecules would behave more like a hard surface reflecting the incoming target molecules and reducing the

chance of the target molecules from bonding with the microcantilever molecules. The value of $\varepsilon_{tar\text{-}can}$ was set to be 0.05 in our simulation.

There must be enough target molecules to bond with the probe molecules in order to produce proper interactions. In this simulation, the number of target molecules was selected to be approximately 4 times the amount of the microcantilever molecules at the top surface. In this case, there were 277 target molecules. The sufficiency of the target molecules was confirmed by the simulation results which showed that there were usually approximately 70-100 target molecules that bond with the probe molecules with no simulation having the bonding number more than half of the 277 molecules.

Only the pairwise interactions (interaction between 2 molecules) were considered. Multibody interactions (interaction between 3 or more molecules) are more accurate but require much longer simulation time. Allen and Tildesley indicated that multibody interactions account for 10% of the total interaction forces-the rest due to the pairwise interaction- while increasing the simulation time immensely.

Initially, the target molecules were assigned the positions approximately 10 simulated unit length away from the surface of the microcantilever (more on the unit in Section 2.8). Appendix B shows that different initial distances between the target and probe molecules have minimal effect on the microcantilever deflection.

Target molecules move due to the thermal excitation. At the molecular level, the target molecules' velocity profiles obey the Maxwell-Boltzmann distribution, *N(p)* which can be expressed as: (Allen & Tildesley, 2007; Haile, 1992; Hill 1986)

$$N(p) = \frac{N}{C} e^{\left(-\frac{p^2}{2m_i k_B T}\right)} \quad (2.11)$$

where k_B is the Boltzmann's constant which is equal to 1.38×10^{-23} J/K, C a normalization constant, p the momentum (= $m_i\underline{v}$), and T the temperature. The fraction of molecules having velocities between $\underline{v}$ and $\underline{v} + d\underline{v}$ can be found from:

$$f(\underline{v})d\underline{v} = \frac{1}{C} e^{\left(-\frac{m\underline{v}^2}{2k_BT}\right)} d\underline{v} \qquad (2.12)$$

The normalization constant C is found from:

$$C = \int_{-\infty}^{\infty} e^{\left(-\frac{m\underline{v}^2}{2k_BT}\right)} d\underline{v} \qquad (2.13)$$

The velocities in the x and y directions are independent from each other and $\underline{v}^2 = \underline{v}_x^2 + \underline{v}_y^2$. Therefore Equations 2.12 and 2.13 reduce to:

$$f(v_x)dv_x = \sqrt{\frac{m_i}{2\pi k_B T}} e^{\left(-\frac{m_i v_x^2}{2k_BT}\right)} dv_x \qquad (2.14a)$$

$$f(v_y)dv_y = \sqrt{\frac{m_i}{2\pi k_B T}} e^{\left(-\frac{m_i v_y^2}{2k_BT}\right)} dv_y \qquad (2.14b)$$

The exponential component is the standard deviation for the Gaussian distribution about the mean value of 0. With the same standard deviation for velocity in both x and y direction, the velocity can be expressed as: (Allen & Tildesley, 2007; Haile, 1992)

$$\text{Standard Deviation} = < v_x^2 > = < v_y^2 > = \frac{k_B T}{m_i} \qquad (2.15)$$

Equation 2.15 relates the mass and squared velocity to the temperature. In other words, the kinetic energy of the molecules is proportional to the temperature. Further discussion about the velocity unit can be found in Appendix A, especially

on how to relate the velocity and the Boltzmann's constant to the fundamental units of σ and ε.

In this simulation, the Gaussian distribution was used to assign the initial velocity value with the mean about 0. One of the problems with the Gaussian distribution is that the distribution must come from randomly independent events. At any instant, molecules can collide and interact with any nearby molecules and thus the system is dependent. However, Haile (1992) showed that the collision only takes place for a short period of time and beyond that time the molecule's velocity could be considered 'nearly' independent of that collision.

Since there was no net momentum on the system, the sum of all target molecules' momentums must be kept at zero which was done by keeping the mean velocity at 0. The initial temperature of the system was set at room temperature of 300K. After the simulation started, this temperature constraint was removed and the temperature was free to change but the system's total energy was kept constant.

2.3 Probe Molecule Model

The probe molecules are functionalized on one of the microcantilever surfaces to attract the target molecules. In this simulation, the probe molecules were created by adding the target-probe interaction properties to certain microcantilever molecules along the top surface. After the lattice spring network was constructed for the microcantilever molecules, some of those molecules on the top surface were selected to become the probe molecules, for example those molecules represented by ■ in Figure 2.3. These molecules underwent additional force calculations with target-probe parameters on top of the original spring force and interaction force calculated for the normal microcantilever molecules. Depending on the percentage of probe molecules on the microcantilever surface, different numbers for probe molecules were assigned. For example, in Figure 2.3, the

probe percentage was 50%, thus one in two microcantilever molecules along the top microcantilever surface underwent the target-probe calculation. Other physical properties of the probe molecules, such as mass, remained the same as the microcantilever molecules.

Since the probe molecules were connected to the lattice spring network the same way as the microcantilever molecules, any interaction forces generated from the target-probe interactions were transferred directly throughout the lattice network. This is similar to a method used by Buxton et al. (2005) to transfer the interaction forces produced in the liquid phase on to the solid structure. In Buxton's case, the fluid interactions created pressure force that acted on spring nodes at the interfacial between the fluid and solid.

At this point, the interactions between the probe molecules and other probe molecules were set to zero. This was done to prevent the forces generated from probe-probe interactions from bending the beam. Typically, any surface coating can induce surface stress that bend the microcantilever (Stoney, 1909). To overcome this, Fritz (2000) used a reference microcantilever, which has non-reactive surface. In an experimental study, Fritz compared the position of the active microcantilever to this reference microcantilever; thus, the initial bending of the beam would not be taken into account in the deflection measurement. Our simulation ignored the interactions between probe and probe molecules and assumed that the microcantilever was straight initially. This straight position of the microcantilever molecules was taken to be the reference point similar to the way Fritz use a reference microcantilever and the average deflection was calculated by subtracting the positions in the y-direction measured during the simulation with the straight beam reference positions.

2.4 System Mass

The mass is one of the fundamental units similar to the Lennard-Jones parameters. This means that other simulated properties can be expressed in term of the mass and the Lennard-Jones parameters σ and ε. Section 2.8 discusses more about the fundamental and simulated units and Appendix A gives formula relating the fundamental units to simulated units.

The mass of the probe and microcantilever molecules were assigned to be 10.0 while the mass of the target molecules was 0.5. The mass was selected by testing the simulation with various mass values and determining the most suitable values that reflect realistic result. For example, the mass of target molecules should not be too high so that the momentum of one target molecules could bend the beam or the microcantilever molecules should not be too massive so that the beam could not move no matter what the molecular interactions are.

2.5 System Boundary Model

The system was isolated from the surrounding by a rectangular bounce back boundary. The boundary was set at a distance of approximately 50.0σ away from the microcantilever so that the boundary did not influence the bending of the microcantilever. The bounce back boundary reverses the normal velocities of any molecules that collide with the boundary while maintaining the same tangential velocity directions and magnitudes. Mechanically, the boundary is made up of a perfectly elastic impact material (coefficient of restitution = 1) with a very heavy mass compared to the target molecules. This results in a collision that conserves the kinetic energy while the boundary remains fixed and consequently keeps the volume (in our case the area) of the system constant.

2.6 System Ensemble

With the bounce back boundary that keeps the number of molecules and volume of the system constant and no external energy flux nor external forces applied to the system, the system is considered to represent a microcanonical ensemble (NVE ensemble). The microcanonical ensemble is a representation of an isolated system where no molecule or energy can enter or leave the system. Other thermodynamic properties such as temperature, pressure, and chemical potential are free to change within the system.

2.7 System Simulation: Equations of Motion

The goal of the simulation is to calculate the deflection of the microcantilever. In this regard, equations of motion were used to find the motions of all molecules. In two-dimensional Cartesian coordinate, the general curvilinear Lagrangian motion is reduced to Newton's equation of motion which can be expressed as:

$$\underline{F_i}(t) = m_i \frac{d^2}{dt^2} \underline{r_i}(t) \quad (2.16)$$

where $\underline{F_i}$ is the force, m_i the mass, and $\underline{r_i}$ the position of the molecules. This simulation used the Velocity Verlet algorithm to integrate the equations of motion to find the trajectories of all molecules. The Velocity Verlet algorithm (Allen & Tildesley, 2007) is a finite difference method that uses an incremental change in time δt to calculate the incremental change in the molecular motions. To find the position, the Velocity Verlet algorithm approximates the position of molecule i, $\underline{r_i}(t)$ from the Taylor series as:

$$\underline{r_i}(t + \partial t) = \underline{r_i}(t) + \partial t \underline{v_i}(t) + \frac{1}{2} \partial t^2 \underline{a_i}(t) \quad (2.17)$$

The position, $\underline{r_i}$, at time $t + \delta t$ is calculated using the position, velocity and acceleration at the previous time step t. With the position at time $t + \delta t$, the interaction forces can be calculated using Lennard-Jones potential and the lattice spring potential – both depend only on the positions of molecules. Then the acceleration $\underline{a_i}$ at time $t + \delta t$, is calculated from the Lennard-Jones and spring forces. Afterward, the velocity $\underline{v_i}$ at time $t + \delta t$ is updated using the newly calculated acceleration at time $t + \delta t$ and the velocity at the previous time t.

$$\underline{v_i}(t + \partial t) = \underline{v_i}(t) + \frac{1}{2}\partial t(\underline{a_i}(t) + \underline{a_i}(t + \partial t) \quad (2.18)$$

At this point, all the necessary information about the motions of molecules (distances, velocities, and accelerations) for the time $t + \delta t$ is calculated and the calculation is repeated for the next time steps.

Proper time increment, δt, is essential in molecular dynamics simulation. Small time increment requires a large number of iterations and might generate high accumulated error due to computer round-off. Too big a time increment reduces the accuracy of the simulation due to the Taylor series truncation error. Moreover, large time increment can cause the simulation to be unstable or even yield a wrong solution. For example, if the time step is too large, it could miss the collisions and allow molecules to pass through each other unimpeded. To find a suitable time step, Allen & Tildesley suggested a comparison between the time increment and fluctuation of total energy. Table 2.1 shows this comparison. The tested simulation's total time duration was the same. The means total energy and root mean squares of the total energy fluctuation were calculated. In this particular system, as time step got larger the fluctuation in energy became bigger and eventually the system was unstable at time increment of 0.032. A good time step should balance good accuracy (smaller energy fluctuation) with simulation cost (run time).

Table 2.1 Total energy and energy fluctuation with different time step

Time Increment δt	Mean Total Energy	Root Mean Square of Total Energy Fluctuation
0.002	1398	0.013
0.004	1399	0.023
0.008	1399	0.095
0.012	1400	0.176
0.016	1401	0.357
0.032	1494	2.71

The time increment of 0.0075 was chosen for the simulation. This time increment corresponded to approximately 10^{-12} seconds based on the interaction distance (σ) unit in nanometer. See Appendix A for Equation A.6 that relates the simulated time to the actual time. This time increment should give acceptable root mean square of the energy fluctuation and seems to be small enough to capture all the change in properties of the system, especially the vibration of the microcantilever which will be discussed in Chapter 3. The total iteration was 5 million time steps which were large enough for the system to reach equilibrium.

2.8 Simulation Units and Scale of the System

As mentioned before, this simulation did not use a specific value for the units. The entire simulation depends on a few fundamental equations which are the Lennard-Jones potential that is governed by σ and ε, and equations of motion governed by the mass, m_i. All simulated properties can be expressed in term of these 'fundamental' units which consist of σ representing the length, ε the energy, and m_i the mass.

One important function of the fundamental units is that it can relate the simulated value to the actual thermodynamic or physical properties such as temperature or time. Appendix A shows how to relate these values. For example, the target

velocity was calculated from the temperature using Equation 2.15 through the Boltzmann's constant which contains the actual value of 1.38×10^{-23} J/K. The fundamental units can be used to reduce the Boltzmann's constant into the simulated value. Appendix A gives further details on how to manipulate the equation.

With all simulated properties expressed in term of the fundamental units, it is easily tempted to scale the system by assigning the value to the fundamental units. For example, the deflection and distance between any molecules can be expressed in term of σ. If the unit of σ is changed, such as from nanometer to micrometer, the interaction scale would change as well. The attempt at scaling will introduce some uncertainty because the Lennard-Jones interaction distance is applicable at the molecular level.

As all calculated values can be expressed in term of the fundamental units, the fundamental units were not assigned any actual value so it would not be confused with the actual system. Comparison of the simulated results was done based on its relative magnitude to each other and analysis of the data will be based on the trend of the results.

2.9 Programming

The simulation is based on the program by the Allen and Tildesley (2007) with some modifications, in particular, the addition of the three-body bond bending potential, boundary conditions, and calculation of molecular properties. Allen and Tildesley's program could be obtained from http://www.ccp5.ac.uk/librar.shtml. The program is in Fortran95 and the simulation can be run on typical personal computers.

Chapter 3

Simulation Data

This chapter presents the raw data obtained from the simulation, the method used to collect the simulated results, and their important trends. Analysis of these data will be done in Chapters 4 and 5. In addition to being used in the analysis, some of the data were also utilized to verify the computer programming. Three data sets were taken during the simulation: molecular positions, number of target molecules that bond with the probe molecules, and the energy.

3.1 Position Measurements

The core objective of this research is the determination of the microcantilever deflection. Therefore, position measurements of those molecules are required. Several types of position measurements were computed throughout the simulation, from the position of the microcantilever to the trajectories of the target molecules. On top of that, the average distances between selected molecules were calculated.

Positions of all molecules inside the system were recorded. Their position coordinates were used to construct the snap shot pictures such as those shown in Figure 4.4, which will be used later to help to explain the analysis in Chapters 4

and 5. Since there were many data points to collect (over 700 molecules and each with the x and y coordinates) and the limitation in data storage of the computer file, positions of all molecules were recorded once every 200,000 iterations for the duration of five millions iterations. This sampling rate should be adequate, since the data were only used in support of the analysis of microcantilever deflection.

For the analysis of microcantilever deflection, more data are required. Since the collection of all molecule positions is not practical at a high sampling rate, the average positions of 6 locations (see Figure 3.1 for the schematic illustration of the locations) equally spaced along the top of the microcantilever were used as a representation for the microcantilever deflection profile. Each of these locations contains 3 microcantilever molecules at a distance of a few molecules apart. The average position of the 3 microcantilever molecules was taken as the average position of that location. The measurement is sampled at a higher rate of one collection for every 2,000 time steps.

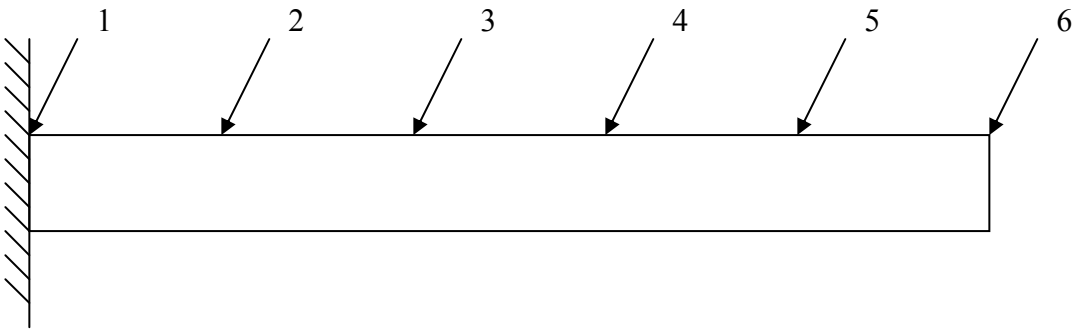

Figure 3.1 Locations of the deflection measurement.

Figures 3.2a and 3.2b show a typical average deflection of the microcantilever as function of the simulation time. Figure 3.2a shows the deflection history for the full simulation period. To give a clearer illustration and reduce the cluster of data points, Figure 3.2b only plots one in two measurement points for the simulation

time between 4,000,000 and 5,000,000 steps. As mentioned previously, the average deflections were calculated by subtracting the reference positions in the y-direction of the straight beam from the measured molecules' positions. Therefore the positive deflection value in Figure 3.2 means the upward deflection and the negative value the downward bending. Since location 6 is at the tip of the microcantilever, it has the highest deflection, while location 1, at the base of the microcantilever, barely deflects. From Figures 3.2a and 3.2b, it appears that number of data for upward deflection is more than that for downward deflection, thus, the microcantilever is deemed to have a tendency to bend upward.

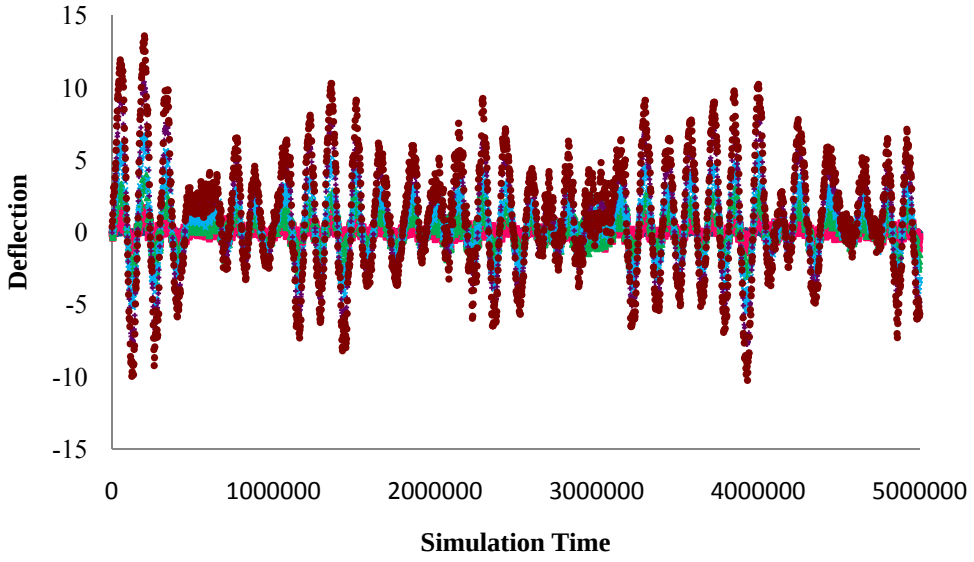

a)

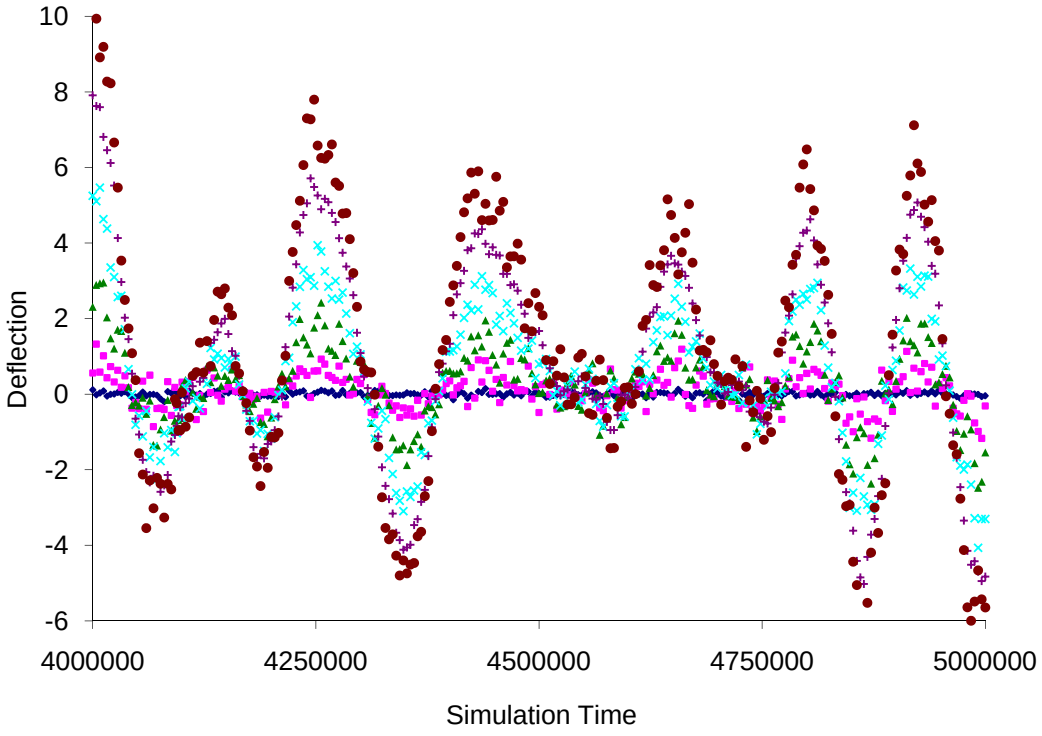

b)

Figure 3.2 Plot of microcantilever deflection as a function of time. (♦) Location 1, (■)Location 2, (▲) Location 3, (×) Location 4, (+) Location 5, (●) Location 6 of Figure 3.1. Figure 3.2a show the deflection for the full simulation time. Figure 3.2b shows only a section from 4 million to 5 million time steps and uses only one in two data points to illustrate clearly the individual data points.

Figure 3.2 suggests that the microcantilever vibrates all the time. The vibration motion was found to exist in every simulation result regardless of the value of the manipulated variables. This is probably due to the lack of a damping mechanism in the model used, thus energy is transferred between kinetic and potential energy back and forth. For example, the kinetic energy of the microcantilever motion is transformed to the potential energy, and stored in the lattice spring as the microcantilever deflects. In a real system, the actual material contains some damping and the vibration can be also damped out by the surrounding fluid. The damper was not used here because it introduces another variable of which the quantity is unknown. Moreover, the damper is a function of velocity, which means that the Velocity Verlet algorithm that only depends on the distance component cannot be applied. Subsequently, a more complicate algorithm would

be needed to include the velocity term during the integration of equations of motion which requires additional calculation steps at the expense of the simulation time. Since the purpose of this simulation is to compare the effects of Lennard-Jones parameters to find out the fundamental principle behind the microcantilever bending motion, the average values of the deflections without the damper should give good comparison data to analyze the trends of the molecular interactions and the microcantilever deflection. As mentioned previously, this simulation is not intended for the calculation of the actual deflection. Thus, the damper is ignored.

In addition to the position measurements, the analysis includes calculation of average distances between selected molecules. A few types of average distances were computed: average distance between target molecules that bond with the probe molecules and their nearby target molecules; average distance between the probe molecules and the bonding target molecules. The average distance can be resolved further into its x and y components. The sampling rate for both average distances was taken for every 2000 iterations.

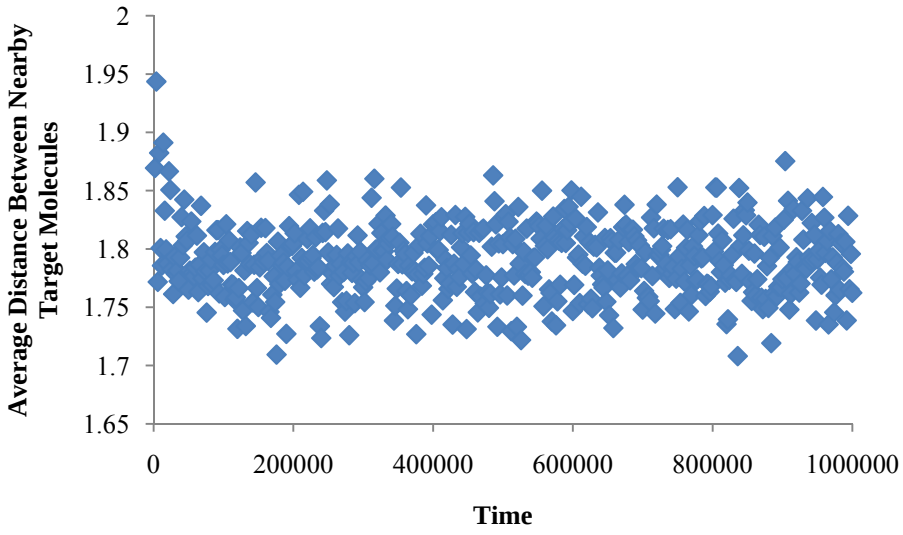

Figure 3.3 A typical plot for average distance between nearby target molecules that bond with the probe molecules. The plot only shows the first one million iterations for clarity. The trend for the average distance remains the same for the rest of 4 millions iterations.

Figure 3.3 shows the typical plot for the average distance between nearby target molecules that bond with the probe molecules for the duration of the first one million iterations (the trend stays the same for the remaining 4 millions iterations, but the data would be too cluster to be shown in one plot). The distance was computed by averaging the distance between target molecules that were within the cut-off distance ($2.5\sigma_{tar\text{-}tar}$) of each other (i.e. those target molecules that interact with each other). Note that this average distance is for the target molecules that bond with the probe molecules. There are target molecules outside the influence of the probe molecules that can interact with other target molecules but those do not interact with the probe molecules and should not have any effect on the deflection, thus they were not included in the measurements. One interesting observation here is that value for the first few data points are higher than the rest. At the start of the simulation, only a few target molecules bond with the probe molecules, thus the distances between them are larger. After a while, more target molecules come in and bond with the probe molecules, reducing these distances. Eventually, the average distance stays almost constant within a maximum/minimum range.

3.2 Number of Target Molecules that Bond with the Probe Molecules

The bonding between target and probe molecules is thought to be one of the possible reasons to induce stress that bends the microcantilever. One measurement, that can indicate bonding, is the number of the target molecules that bond with the probe molecules. Usually target molecules move around inside the system boundary. If some of them move near the probe molecules and their interactions are strong enough, the target molecules would bond with the probe molecules. These target molecules would stay within a 'bonding' area around the probe molecules. The number of these bonding target molecules was calculated by counting the number of target molecules that are within $2.5\sigma_{tar\text{-}probe}$ (cut-off distance) from the probe molecules. The number of bonding target molecules was

sampled at the same rate as the deflection measurement of once every 2,000 iterations.

Figures 3.4a and 3.4b show a typical plot for the number of bonding target molecules, with the former for the entire simulation and the latter in a shorter time duration in order to view the maximum/minimum range. The bonding number curve rises quickly and reaches equilibrium within the first few thousand iterations. After obtaining the equilibrium, the bonding number seems to stay within a range of maximum/minimum value between 70-80 molecules. This range of maximum and minimum values could be caused by bonding and de-bonding of the target molecules. At any instance, some target molecules can come inside $2.5\sigma_{tar\text{-}probe}$ and interact with the probe molecules, while others are being pushed away or having enough energy to break the bonds on their own.

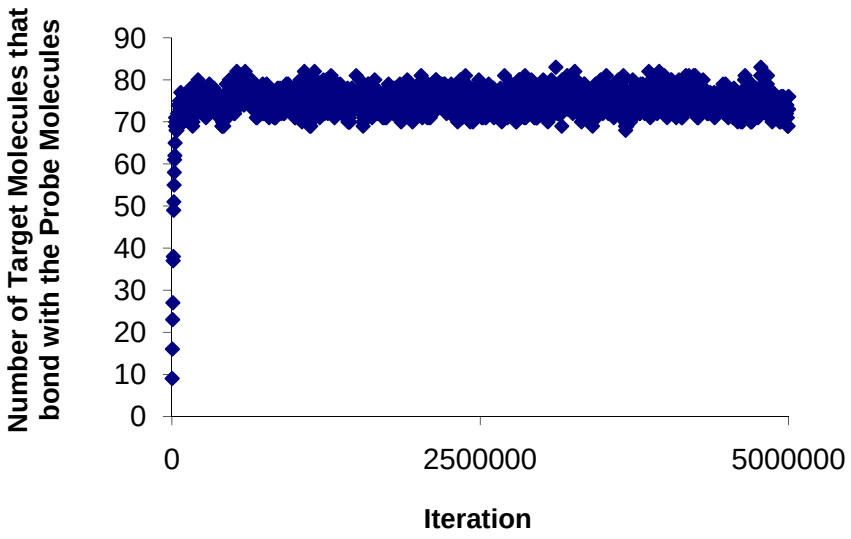

a)

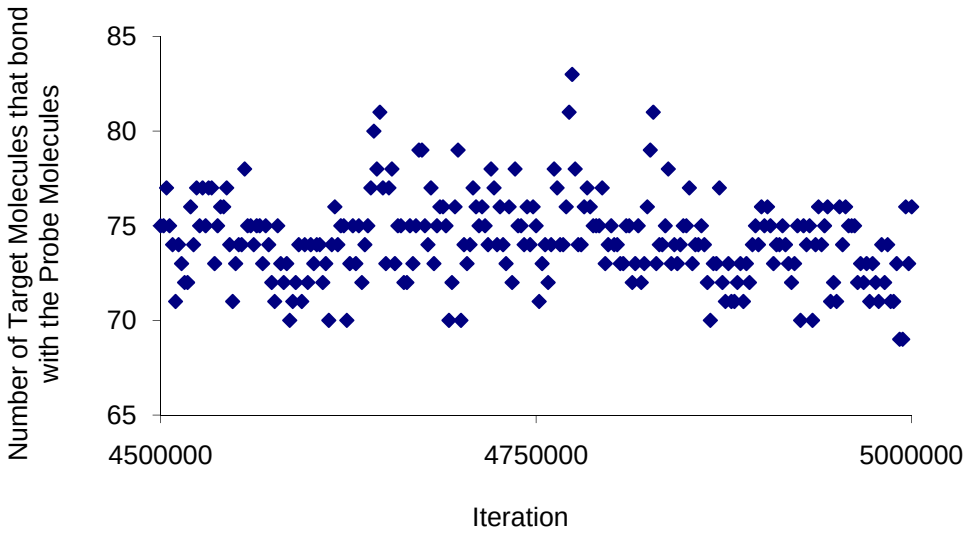

b)

Figure 3.4 Typical plot for number of target molecules that bond with the probe molecules. (a) the result for the entire simulation time, (b) the result in the last 500,000 time steps to show the range of bonding target molecules.

All simulated results have the same feature as given in Figure 3.4 in that the bonding number reaches the equilibrium state in a very short time. Since all simulations obtain equilibrium quickly, the total simulation time of 5 million iterations should be long enough to capture the behaviour of the microcantilever. Figure 3.4 also suggests that the sample rate is fast enough to capture the bonding/de-bonding process.

3.3 Energy

One important function of energy is that it reflects the stability of the simulation. For example, an exponential increase of energy could indicate the breakdown of the simulation from unrealistically high interaction forces. Several types of energy were computed during the simulation and their sum is equivalent to the total energy of the system. The total energy consists of:

- Lattice spring potential for both central force (first term on the right hand side of Equation 2.1) and bond bending term (second term on the right hand side of Equation 2.1);
- the Lennard-Jones potential (Equation 2.8) for target-target, target-probe, and target-microcantilever interactions;
- kinetic energy ($\frac{1}{2}m_i v_i^2$) for the target, probe, and microcantilever molecules (in this case, contribution from the probe and microcantilever molecules were counted together because they have the same motion and mass properties, i.e., both are in the same lattice spring network).

The energy measurements were taken at the rate of one measurement for every 2,000 iterations. Figure 3.5a presents the plot of energy over the entire simulation duration, while Figure 3.5b in a shorter time period at the beginning of the simulation to illustrate the initial energy change, and Figure 3.5c in a shorter time period at the end to show the energy oscillation after the equilibrium is reached.

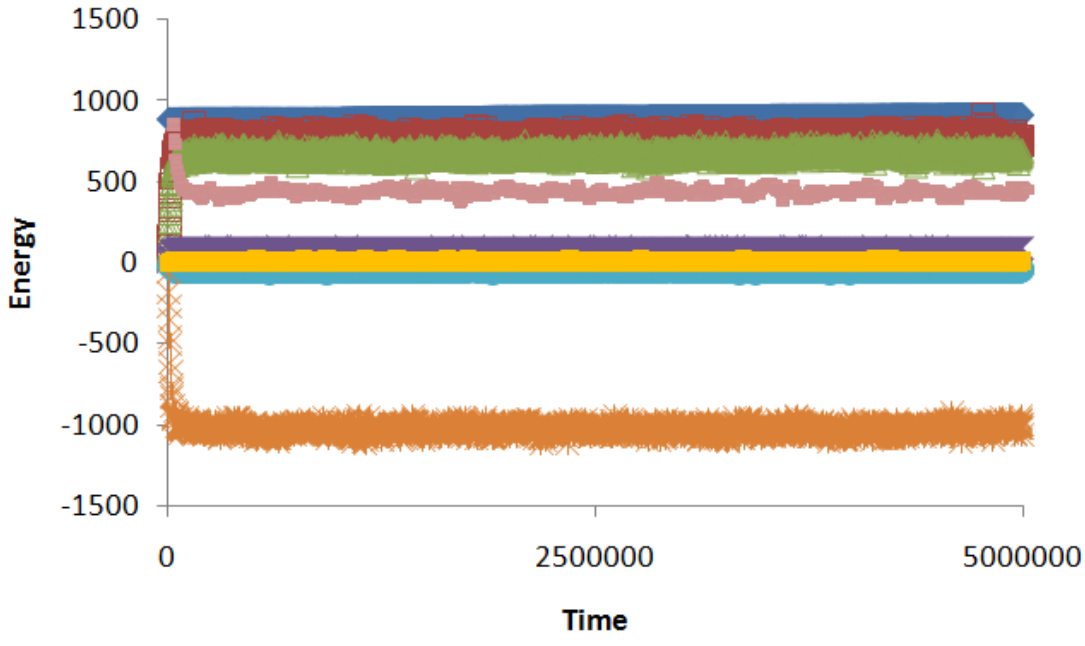

a)

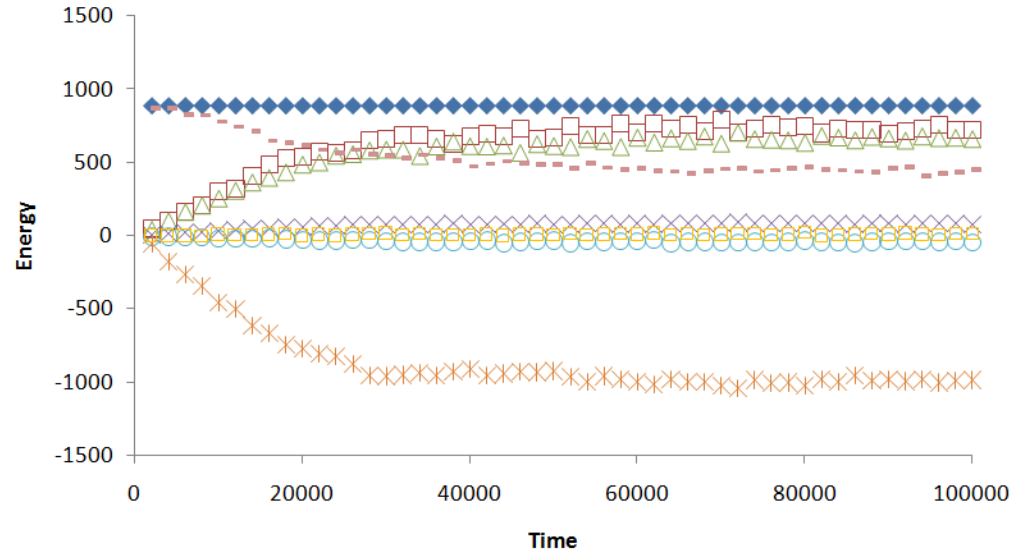

b)

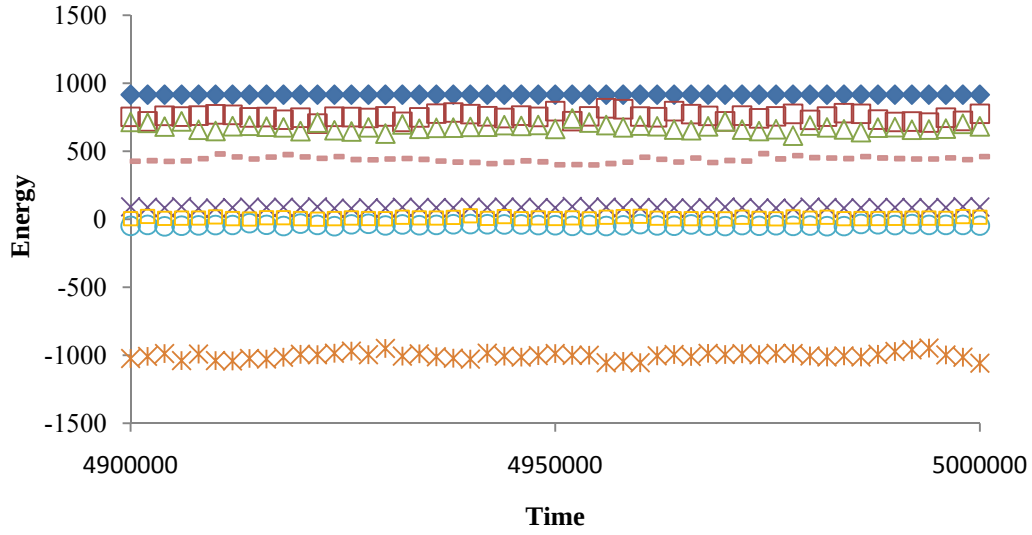

c)

Figure 3.5 Typical energy plot for the cantilever system. a) Plot for the full simulation time. b) Plot for the first 100,000 iterations to show the early trend. c) Plot for the last 100,000 time steps to show the oscillations of potential and kinetic energy. Total energy (♦), target-probe L-J potential energy (*), target-target L-J potential energy (o), target-microcantilever L-J potential energy (□), central force spring potential (Δ), bond bending spring potential (x), kinetic energy of the target molecules (-),and kinetic energy of the probe and microcantilever molecule (□).

In the early stage of the simulation, the target molecules possess some motion due to the temperature excitation as per the discussion in Section 2.3. These target molecules move around and some of them come near the probe molecules. If the

strength of target-probe interactions is strong enough, the target molecules would bind to the probe molecules resulting in the loss of the target kinetic energy (-), the gain in target-probe L-J potential (negative energy for L-J potential correspond to the increase of bonding between target and probe molecules and represented by *) and the increase in strain energy (Δ for the central force term and x for the bond bending term). In addition, the microcantilever vibrates leading to the change of the kinetic energy (□) because of the motion of the microcantilever molecules.

After the first few thousand iterations, the initial increase/decrease of energy dies down, which indicates equilibrium. This equilibrium is achieved within a similar time duration as the bonding number shown in Figure 3.4. After reaching equilibrium, some energy oscillation still occurs within a small range as shown in Figure 3.5c which could be the result of the exchanging of potential lattice spring energy(Δ) and kinetic energy of the beam(□) during the vibration of the microcantilever. Furthermore, some target molecules form new bonds, while others de-bond thus the total energy for the Lennard-Jones potential between target-probe interactions oscillates as well.

The total energy in Figure 3.5 stays almost constant. Therefore, as expected and required, the total energy of the system can be considered to be conserved. This verifies that the programming, at least for the boundary and energy calculation, might be correct. Moreover, the constant total energy indicates that the simulation is stable. If a large change in energy occurs, it might indicate a program problem.

3.4 Summary

This chapter discusses how the raw data were computed. Three main types of measurements were collected: the position of the molecules, the number of target molecules bonded with the probe molecules, and the energy of the system. On account of our model, the deflection measurement shows a persistent vibration due to the lack of damping. However, since these data were compared with respect to each other, the vibration should not affect the mean deflection. It was observed that the number of the bonding target molecules and the energy show a similar feature of reaching steady values within the first hundred thousand iterations, which indicated that the simulation time is long enough for the system to reach the equilibrium state. All of the data beside the one collected for the snap shots were sampled at the rate of one measurement for every 2,000 iterations. This sampling rate seems to be able to capture the change in molecular properties such as the vibration of the microcantilever, the bonding/debonding of the target molecules, and the oscillation of energy. Therefore, the sampling rate is believed to be sufficient. Furthermore, these raw data were used to verify the computer code. The constant total energy of the system seems to confirm that the program works fine. These data will be used in Chapters 4 and 5 for the analysis of the system with variation in manipulated variables including the Lennad-Jones parameters (Chapter 4) and the probe placements (Chapter 5).

Chapter 4

Effect of Lennard-Jones Parameters

This chapter discusses the results from the simulations having the Lennard-Jones parameters as the manipulating variables, which are $\sigma_{tar\text{-}probe}$, $\varepsilon_{tar\text{-}probe}$, $\sigma_{tar\text{-}tar}$, and $\varepsilon_{tar\text{-}tar}$. Each of the parameters influences the molecular interactions in different manners and, thus, yields different microcantilever deflection.

4.1 $\sigma_{tar\text{-}probe}$

Generally, the Lennard-Jones parameter σ is considered to represent the interaction distance. It determines the equilibrium distance of 1.12σ where the potential reaches its minimum energy state, i.e. no net attractive or repulsive force.

Figure 4.1a shows the plot of the microcantilever deflection vs. $\sigma_{tar\text{-}probe}$ and Figure 4.1b one of the curves in the previous plot with labels for each transition points. Interestingly, all deflection curves have 3 distinct regions:

I. from point A to B
II. from point B to C
III. from point C to D

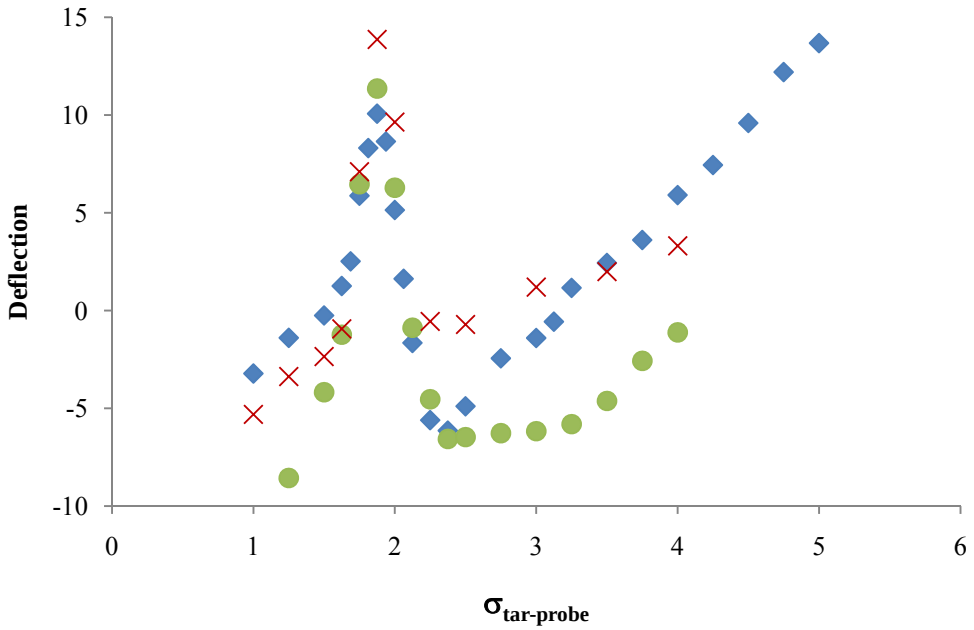

a)

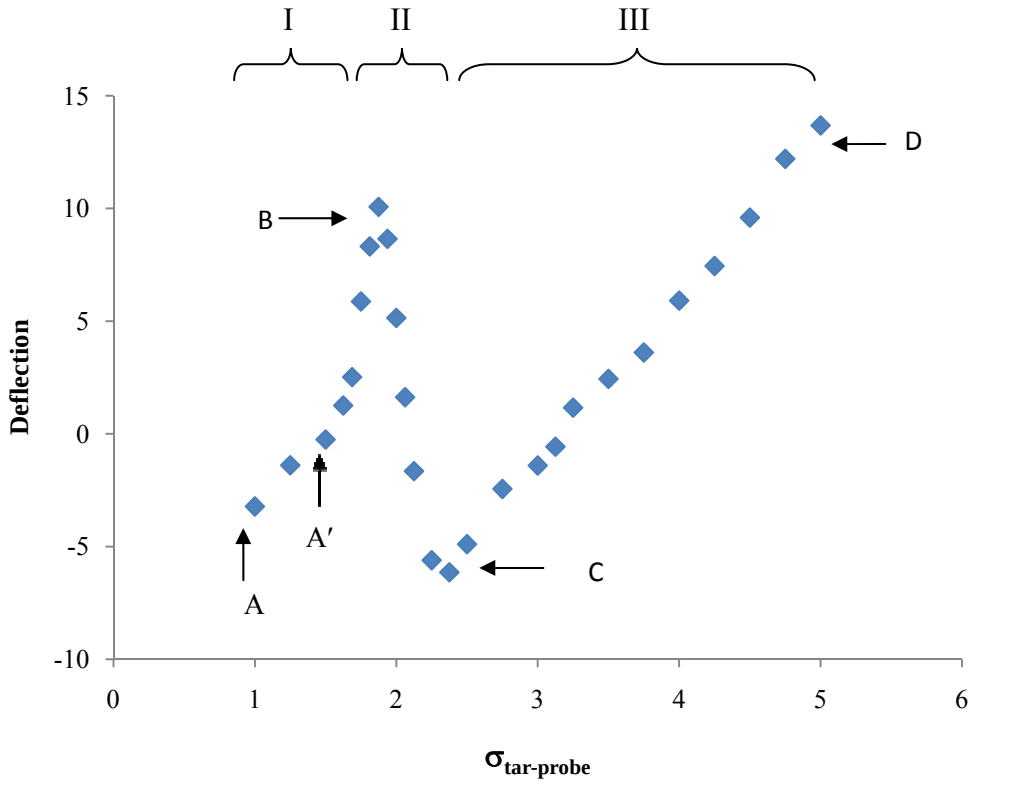

b)

Figure 4.1 Effect of $\sigma_{tar\text{-}probe}$ on the microcantilever deflection. (♦) $\sigma_{tar\text{-}tar} = 1.50$, (×) $\sigma_{tar\text{-}tar} = 1.75$, (•) $\sigma_{tar\text{-}tar} = 2.00$. Plots are generated with $\varepsilon_{tar\text{-}probe} = 15.0$, $\varepsilon_{tar\text{-}tar} = 1.00$, $\varepsilon_{tar\text{-}cantilever} = 0.05$, $\sigma_{tar\text{-}tar} = 1.50$, and $\sigma_{tar\text{-}cantilever} = 1.50$.

At point A, with low $\sigma_{tar\text{-}probe}$, deflection is negative, i.e. bending down. In region I, the deflection curve gradually increases from point A until it reaches point A′. Afterwards, the curve increases at a higher rate up to point B. At point B, the curve declines abruptly and decreases to point C, but increases again in region III. To help understand the relationship between deflection and molecular interactions, plots of bonding number, separation distance, and the bonding energy were generated. Interestingly, those curves also conform to the same trend with similar changes in slope and transition points between different regions that correlate quite well with the deflection curves. Appendix B shows variation involved in calculating one of the data points from different initial conditions. For that specific point, the error seems to be small (less than 10%). Due to the lack of computing power and limited time, variations for other data points were not calculated.

Figure 4.2 shows the plot of the average number of the target molecules that bond with the probe molecules. The number is computed by counting the target molecules that are within the cut-off distance ($2.5\sigma_{tar\text{-}probe}$) from the probe molecules. Details of the calculation are shown in Section 3.2. This number behaves in a similar manner as the number of bonds. Both have a very similar trend, albeit different slope. For example, if one target molecule interacts with 2 probe molecules, then the number of bonding target molecules is 1 while the number of bonds is 2. Thus if the number of bonds is plotted against $\sigma_{tar\text{-}probe}$, its curve will have similar features as Figure 4.2 but with a steeper slope. The discussion will often refer to both numbers but will only show the plot for the number of target molecules that bond with the probe molecules. For Figure 4.2, the slopes, again, fluctuate with relatively high slope in region I, shallow in region II, and high again in region III.

Figure 4.3 shows the plot for the separation distance in the y-direction between neighbouring target molecules. The method of measuring the separation distance in the y-direction is shown in the snap shot of Figure 4.4. The curves have the

similar features of distinctive regions where the separation distance increases in region I, then declines in region II, and finally increases again in region III. Interestingly, this trend resembles closely the shape of the deflection curves shown in Figure 4.1, although the slope in region II is not as steep and the rise of region III has a flatter slope.

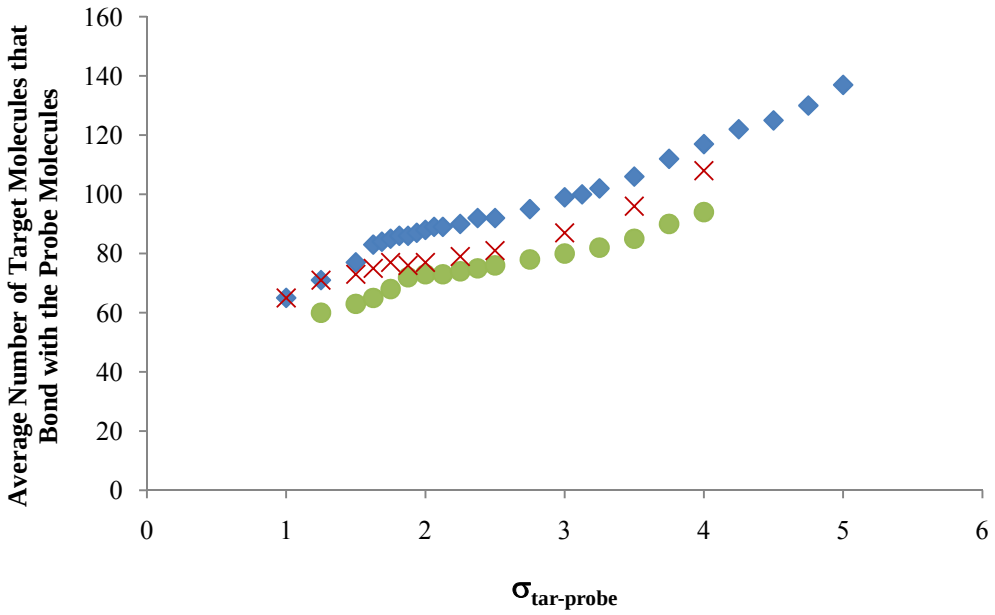

Figure 4.2 Effect of $\sigma_{tar\text{-}probe}$ on the average number of the target molecules that bond with the Probe Molecules. (♦) $\sigma_{tar\text{-}tar} = 1.50$, (×) $\sigma_{tar\text{-}tar} = 1.75$, (●) $\sigma_{tar\text{-}tar} = 2.00$. Plots are generated with $\varepsilon_{tar\text{-}probe} = 15.0$, $\varepsilon_{tar\text{-}tar} = 1.00$, $\varepsilon_{tar\text{-}cantilever} = 0.05$, and $\sigma_{tar\text{-}cantilever} = 1.50$.

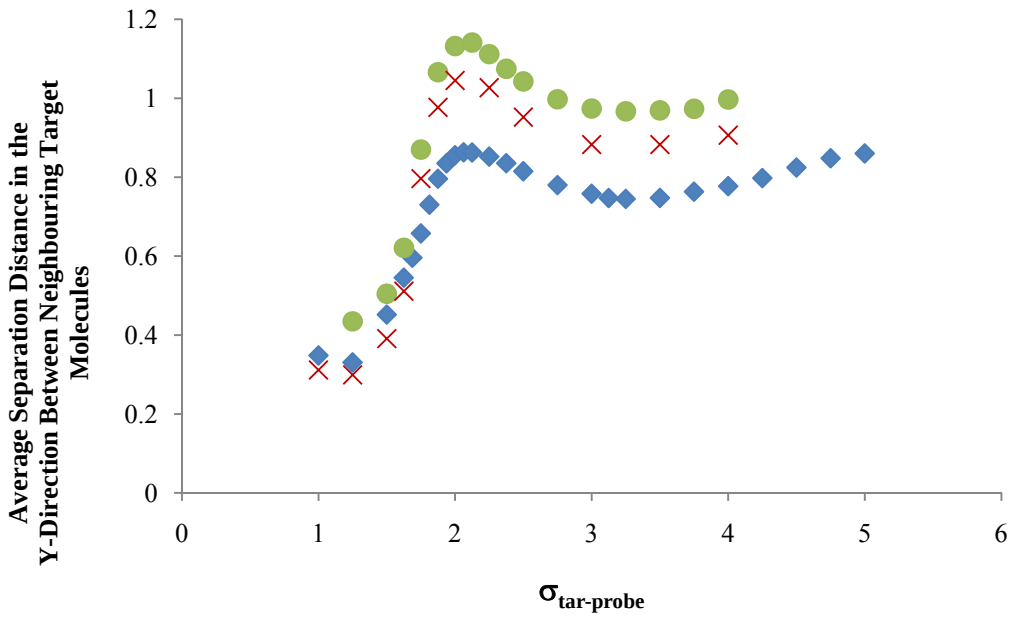

Figure 4.3 Effect of $\sigma_{tar\text{-}probe}$ on the average separation distance in the y-direction between neighbouring target molecules. (♦) $\sigma_{tar\text{-}tar} = 1.50$, (×) $\sigma_{tar\text{-}tar} = 1.75$, (•) $\sigma_{tar\text{-}tar} = 2.00$. Plots are generated with $\varepsilon_{tar\text{-}probe} = 15.0$, $\varepsilon_{tar\text{-}tar} = 1.00$, $\varepsilon_{tar\text{-}cantilever} = 0.05$, and $\sigma_{tar\text{-}cantilever} = 1.50$.

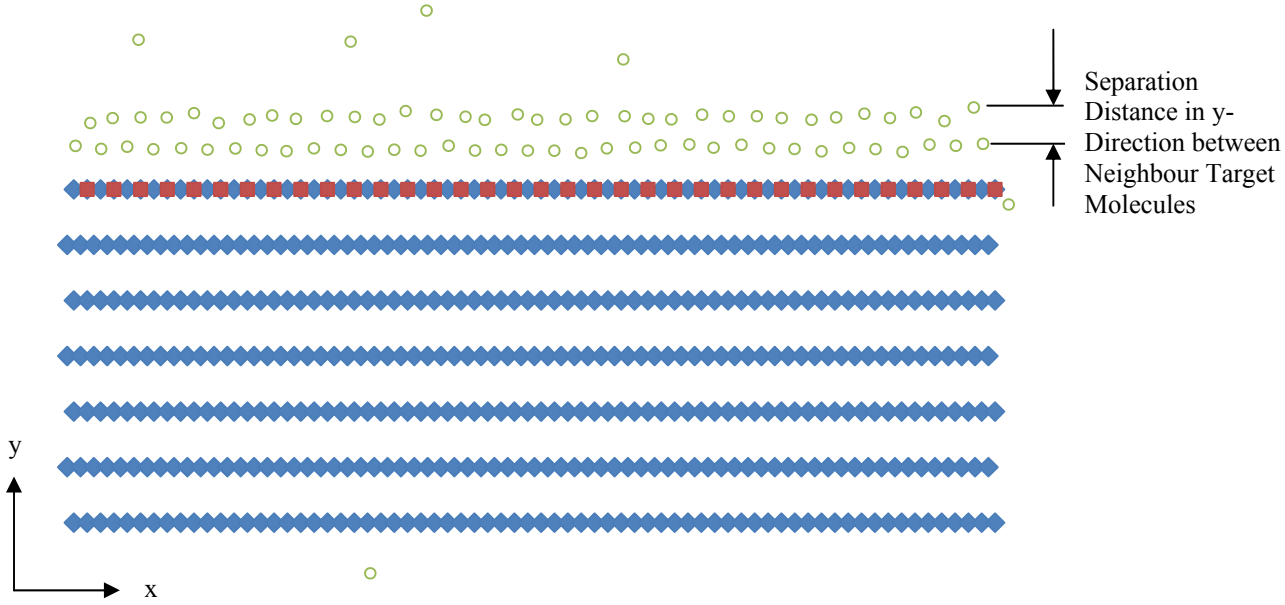

Figure 4.4 Schematic presentation of the microcantilever showing the separation distance in the y-direction which is the distance in the y-direction that separates 2 target molecules that bond with the probe molecules. The blue diamond (♦) represents the microcantilever molecules, red square (■) the probe molecules, and green circle (o) the target molecules. (Noted: the figure is not to scale.)

Figure 4.5 shows the plot for the bonding energy. The bonding energy is the Lennard-Jones potential generated by target-probe interactions. Note that the bonding energy is negative because the Lennard-Jones potential is mainly negative near its equilibrium state. At the beginning, the curves of the bonding energy decline gradually. Then when $\sigma_{tar\text{-}probe}$ reaches 1.50, which is approximately the same location as transition point A′, the decline accelerates and the curves decrease at a rapid rate. This rapid decrease dies down between 2.00 < $\sigma_{tar\text{-}probe}$ < 2.75 but then picks up again at a faster rate afterward.

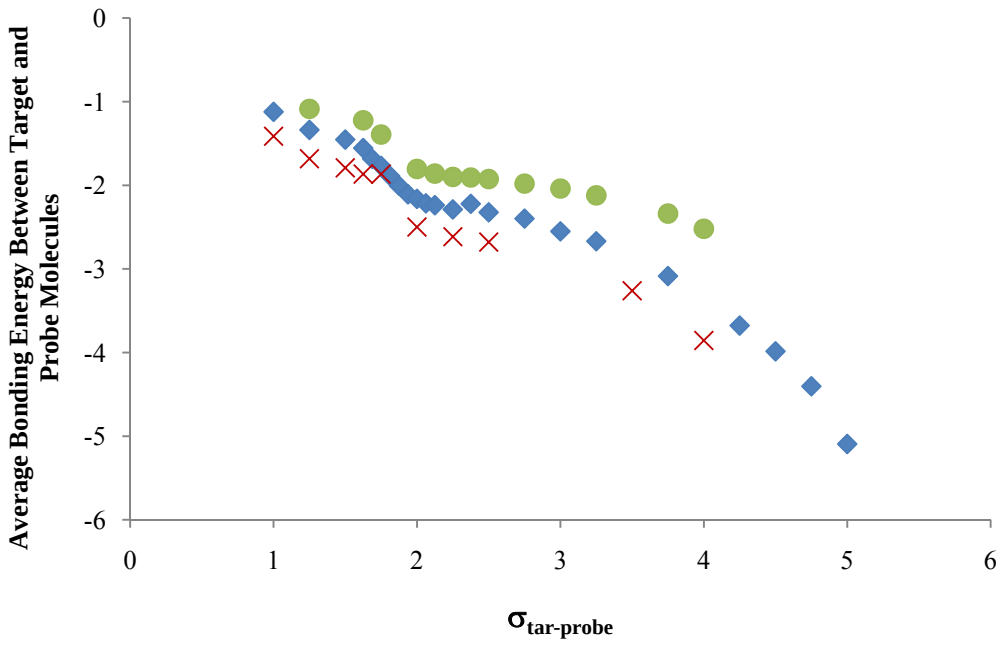

Figure 4.5 Effect of $\sigma_{tar\text{-}probe}$ on the bonding energy between target and probe molecules. (♦) $\sigma_{tar\text{-}tar}$ = 1.50, (×) $\sigma_{tar\text{-}tar}$ = 1.75, (•) $\sigma_{tar\text{-}tar}$ = 2.00. Plots are generated with $\varepsilon_{tar\text{-}probe}$ = 15.0, $\varepsilon_{tar\text{-}tar}$ = 1.00, $\varepsilon_{tar\text{-}cantilever}$ = 0.05, and $\sigma_{tar\text{-}cantilever}$ = 1.50.

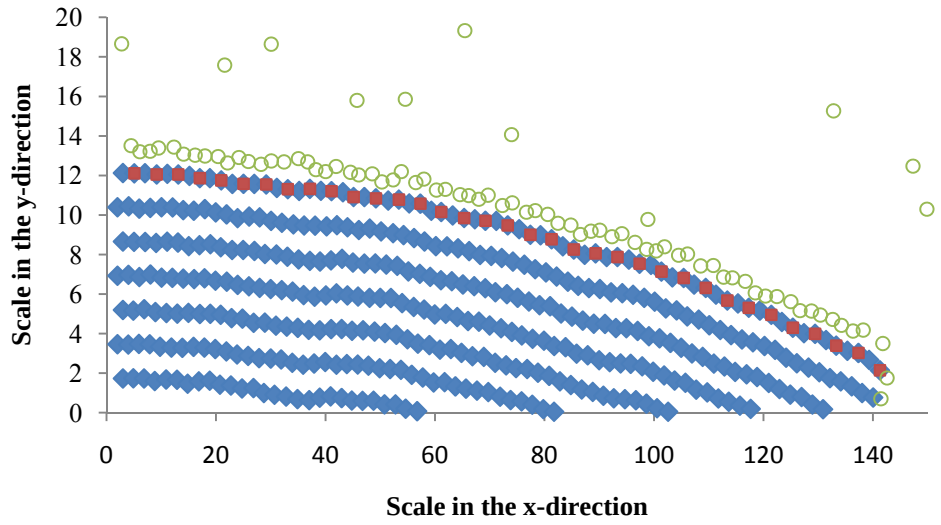

a)

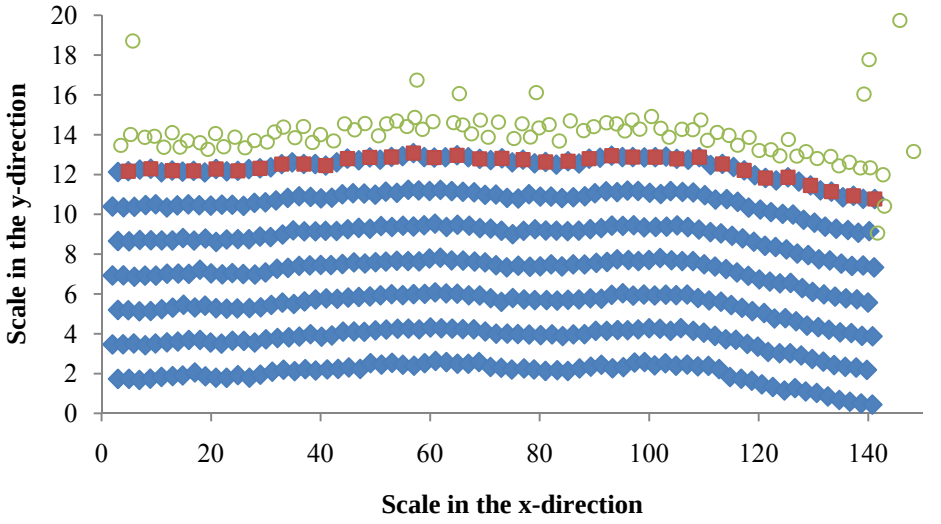

b)

Figure 4.6 Snap shots of the simulation results. (a) microcantilever at transition point A. (b) microcantilever at transition point A′. The blue diamond (♦) represents the microcantilever molecules, red square (■) represents the probe molecules, and green circle (o) represent the target molecules. (Note: plots are not to scale.)

The snap shots in Figure 4.6, which represent transition points A and A' respectively, show that target molecules bond with the probe molecules within an area just above the microcantilever. From the Lennard-Jones potential, it is known that the probe molecules attract the target molecules when the distances between them are approximately $1.12\sigma_{tar\text{-}probe}$ to $2.5\sigma_{tar\text{-}probe}$ (cut-off distance). This forms a 'bonding area' where the target molecules bond to the probe molecules.

Consequently, lower the $\sigma_{tar\text{-}probe}$ value, smaller the distance range of $1.12\sigma_{tar\text{-}probe}$ to $2.5\sigma_{tar\text{-}probe}$. It was observed that at low $\sigma_{tar\text{-}probe}$, the target molecules arrange themselves in the single-layer layout, as observed in Figure 4.6a. One can think about $\sigma_{tar\text{-}tar}$ as the size of the target molecules and $\sigma_{tar\text{-}probe}$ as bonding or interaction distance. At point A, the size of target molecules are 'relatively bigger' than the bonding distance. Therefore, the target molecules can only fit into a single bonding layer. This is probably the reason for the separation in the y-direction of Figure 4.3 being smaller at lower $\sigma_{tar\text{-}probe}$ value. It is believed that, when these target molecules are limited by $\sigma_{tar\text{-}probe}$ to fit into a single layer, the target molecules want to spread more in the x-direction to maintain the target-target equilibrium distance (more on target-target distance in Section 4.3). As a result, the microcantilever bends down, in order to generate more surface area to accommodate the spread in the x-direction. As for the case of point A′, the target molecules can be considered to be relatively smaller than the bonding distance. Hence, the target molecules have more room in the y-direction as suggested by the increasing trend in region I of Figure 4.3. The increase of space in the y-direction allows the target molecules to arrange themselves into a 'zigzag' pattern (see Figure 4.6b) with one layer staggered on top of another, in order to cover as much of the bonding area as possible. This also allows more bonds between target and probe molecules to form, as indicated by the rising curve in region I of Figure 4.2. By arranging themselves in the zigzag pattern with longer separation in the y-direction, the target molecules do not require as much room in the x-direction as before. This results in reduction of the downward deflection.

At point A′ which is approximately at the midway point of region I, the deflection curves in Figure 4.1 increase at a much faster rate. This sharp rise is believed to be caused by the spacing effect of the probe molecules. Originally, the probe molecules were assigned at a distance of 4.0 apart. At value of $\sigma_{tar\text{-}probe}$ below 1.5, a target molecule typically bonds with only one probe molecule as this target molecule is located at a distance greater than $2.5\sigma_{tar\text{-}probe}$ away from the next probe molecule. For example, at $\sigma_{tar\text{-}probe} = 1.00$, a target molecule was often found to be

at a radius of a little greater than 1.00 from one probe molecule. Since the distance from that particular probe molecule to the next probe molecule is 4.00, the original target molecule is often too far away to interact with the next probe molecule. As $\sigma_{tar\text{-}probe}$ increases, the interaction distance increases and when the interaction distance is long enough, it causes the next neighbour probe molecule to exert an attraction force on the target molecule. The increase in interaction is observed from the bonding energy plot of Figure 4.5, which shows the slope of the bonding energy changes at a higher rate after $\sigma_{tar\text{-}probe}$ reaches 1.50. At this point, each of the 2 probe molecules wants to pull the target molecule toward itself. This tends to bend the microcantilever upward to reduce the surface area so that the probe and target molecules move closer to each other, in order to minimize the energy due to the pulling.

At point B of Figure 4.1b, there is an abrupt decrease of the microcantilever deflection. One common element found in any abrupt drop is that it occurs when the $\sigma_{tar\text{-}probe}$ value is just below half the distance between 2 probe molecules. Figure 4.7 shows more results on the abrupt change with variation in the probe distance. Curve (♦) is the same curve shown in Figure 4.1b. This curve and all deflection curves in Figure 4.1 have a probe-to-probe distance of 4.0 and the abrupt drop for those curves occurs at $\sigma_{tar\text{-}probe} \cong 1.9$. Curve (+) has the probe-to-probe distance of 6.0 and the abrupt drop occurs at approximately 2.7.

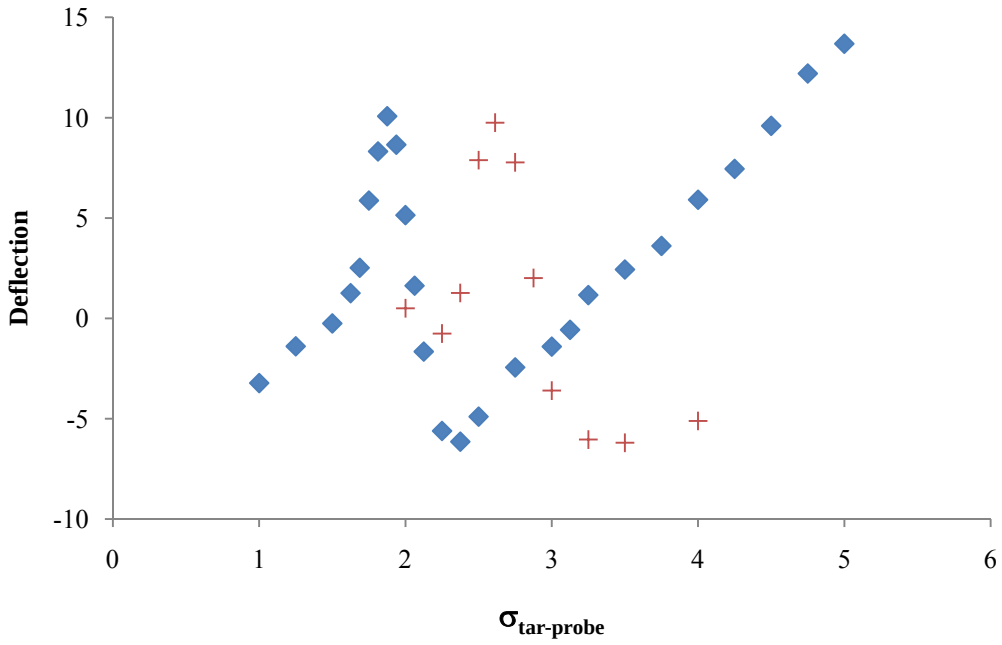

Figure 4.7 Effect of probe spacing with distance between 2 probe molecules at 4.0(♦), and 6.0 (+). Plots are generated with $\sigma_{tar\text{-}tar}$ = 1.50, $\sigma_{tar\text{-}cantilever}$ = 1.50, $\varepsilon_{tar\text{-}probe}$ = 15.0, $\varepsilon_{tar\text{-}tar}$ = 1.00, $\varepsilon_{tar\text{-}cantilever}$ = 0.05, probe coverage percentage of 50% for (♦) and $\sigma_{tar\text{-}tar}$ = 2.00, $\sigma_{tar\text{-}cantilever}$ = 1.875, $\varepsilon_{tar\text{-}probe}$ = 15.0, $\varepsilon_{tar\text{-}tar}$ = 1.00, and $\varepsilon_{tar\text{-}cantilever}$ = 0.05.

At the moment when the thesis is written, the exact reason behind the abrupt change is not clear. To my best knowledge, this phenomenon has not been reported in any previous studies. Since experimental work for the microcantilever sensor were often concentrated on particular system with a known pair of target and probe molecules as well as fixed molecular properties, the abrupt change was not observed. Previous simulation studies were usually performed under the conditions of fixed number of bonding target molecules and sometimes even the locations of target molecules. The current study shows that, by changing the values of $\sigma_{tar\text{-}probe}$ and $\sigma_{tar\text{-}tar,}$ the number of target molecules interacting with the probe molecules and their locations change. Both factors can affect the microcantilever bending. In addition, previous simulation studies focused mainly on the target-target interactions, with little emphasis on the target-probe interactions. Therefore, the previous simulation studies did not reveal the possibility of abrupt decrease of the beam deflection as observed here.

In region III, the microcantilever deflection increases again (see Figure 4.1). It was suspected that the increase in $\sigma_{tar\text{-}probe}$ value allows larger separation distance between bonding target molecules in the y-direction, as observed from the increase of the separation distance in region III of Figure 4.3. The increase of the aforementioned factor might reduce the high repulsive forces that bend the microcantilever downward. Another possibility is that with large $\sigma_{tar\text{-}probe}$ value, one probe molecule could attract many target molecules that bond with the neighbouring probe molecules. For example, with $\sigma_{tar\text{-}probe} = 3.00$, the attractive force can be applied up to the cut-off distance of $2.50 \times 3.00 = 7.50$. Therefore, target molecules within the radius of 7.50 from any probe molecules will interact with those probe molecules. This is quite a long distance compared to the distance between 2 probe molecules of 4.0, which suggests that one target molecules is able to interact with several probe molecules. This behaviour seems to be supported by the rapid increase of bonding energy in region III of Figure 4.5. When multiple probe molecules are competing to pull the same target molecules toward themselves, the microcantilever tends to bend upward.

4.2 $\varepsilon_{tar\text{-}probe}$

Generally, ε determines the strength of the Lennard-Jones potential. Higher the value of ε, deeper the potential well, which, in turn, creates stabler bonds with stronger bonding forces. Hence, the target molecules require very high kinetic energy to escape from the deep potential well and break the bonds.

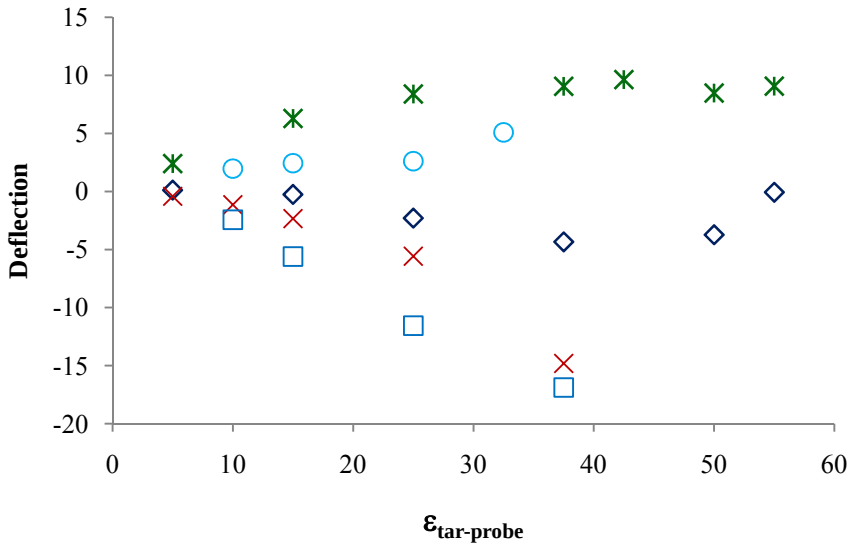

Figure 4.8 Effect of $\varepsilon_{tar\text{-}probe}$ on the microcantilever deflection. (×) $\sigma_{tar\text{-}tar} = 1.25$, $\sigma_{tar\text{-}probe} = 1.25$; (◊) $\sigma_{tar\text{-}tar} = 1.50$, $\sigma_{tar\text{-}probe} = 1.50$; (□) $\sigma_{tar\text{-}tar} = 1.50$, $\sigma_{tar\text{-}probe} = 2.25$; (o) $\sigma_{tar\text{-}tar} = 1.50$, $\sigma_{tar\text{-}probe} = 3.50$; (*) $\sigma_{tar\text{-}tar} = 2.00$, $\sigma_{tar\text{-}probe} = 2.00$. Plots are generated with $\varepsilon_{tar\text{-}tar} = 1.00$, $\varepsilon_{tar\text{-}cantilever} = 0.05$, and $\sigma_{tar\text{-}cantilever} = 1.50$.

Figure 4.8 shows the curve of the microcantilever deflection vs. $\varepsilon_{tar\text{-}probe}$. The figure shows that the magnitude of the deflection increases with the increase of $\varepsilon_{tar\text{-}probe}$, except the curve (*) for $\sigma_{tar\text{-}tar} = 2.00$, $\sigma_{tar\text{-}probe} = 2.00$ that reaches a constant value after $\varepsilon_{tar\text{-}probe} > 25$ and the curve (◊) ($\sigma_{tar\text{-}tar} = 1.50$, $\sigma_{tar\text{-}probe} = 1.50$) that has its last data point against the trend. At very high value of $\varepsilon_{tar\text{-}probe}$ the interaction forces are very strong that may cause instability of the program, i.e. equilibrium not being reached. This is probably the reason why the simulation for the curve (×), (□), and (o) can only be performed up to a certain value of $\varepsilon_{tar\text{-}probe}$, as shown in the figure, in addition to the reason that the last point of curve (◊) is not conformed to the trend. The exception of the curve (*) could be explained through the number of the target molecules that bond with the probe molecules which will be discussed next.

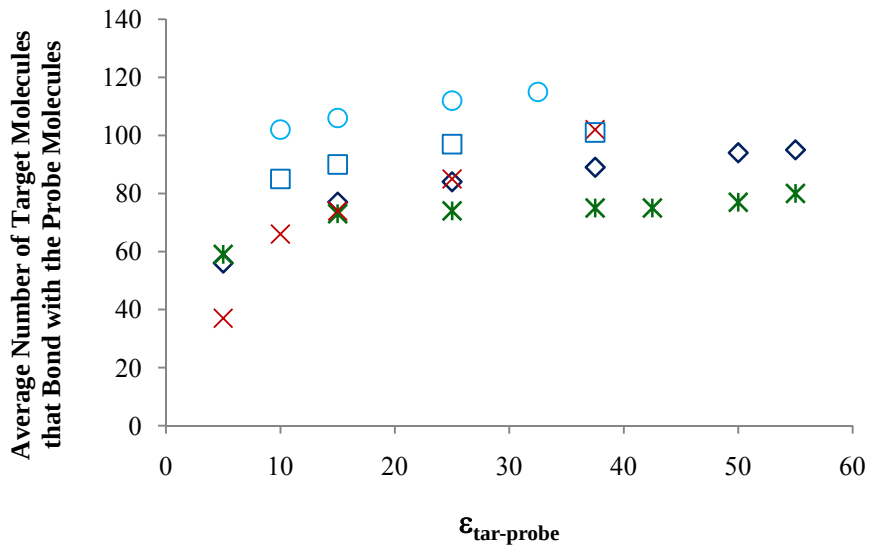

Figure 4.9 Effect of $\varepsilon_{tar\text{-}probe}$ on average number of target molecules that bond with the probe molecules. (×) $\sigma_{tar\text{-}tar} = 1.25$, $\sigma_{tar\text{-}probe} = 1.25$; (◊) $\sigma_{tar\text{-}tar} = 1.50$, $\sigma_{tar\text{-}probe} = 1.50$; (□) $\sigma_{tar\text{-}tar} = 1.50$, $\sigma_{tar\text{-}probe} = 2.25$; (o) $\sigma_{tar\text{-}tar} = 1.50$, $\sigma_{tar\text{-}probe} = 3.50$; (*) $\sigma_{tar\text{-}tar} = 2.00$, $\sigma_{tar\text{-}probe} = 2.00$. Plots are generated with $\varepsilon_{tar\text{-}tar} = 1.00$, $\varepsilon_{tar\text{-}cantilever} = 0.05$, and $\sigma_{tar\text{-}cantilever} = 1.50$.

Figure 4.9 shows that the number of the target molecules that bond with the probe molecules increases with $\varepsilon_{tar\text{-}probe}$. At low $\varepsilon_{tar\text{-}probe,}$ the bonding strength is weak. If the target velocities are high enough (thus high enough kinetic energy), those target molecules can break the bonds. This behaviour is further confirmed through the snap shot shown in Figure 4.10a, which is a plot for $\varepsilon_{tar\text{-}probe} = 5.0$, representing the curve × in Figures 4.8, 4.9, and 4.11. The snap shot shows many vacant spaces on the microcantilever surface. With higher $\varepsilon_{tar\text{-}probe}$, the bonds are stronger, thus preventing the target molecules from breaking the bonds. The snap shot in Figure 4.10b for $\varepsilon_{tar\text{-}probe} = 25.0$ shows more target molecules bonding to the probe molecules. In this case, the target molecules appear to fill out the entire bonding area. Therefore, their molecular interactions should be much higher because there are more bonds and the target molecules are closer to each other than in the previous situation, leading to an increase in magnitude of the microcantilever deflection.

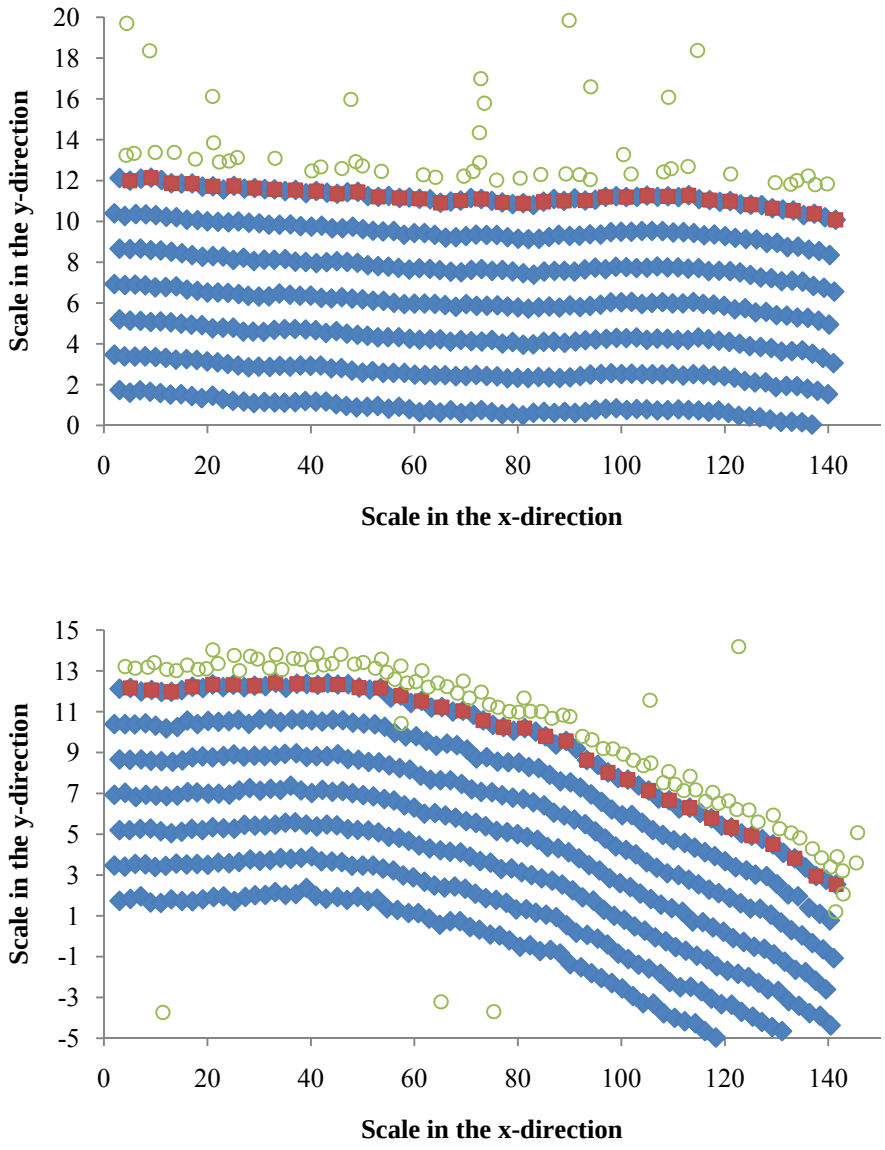

Figure 4.10 Snap shots of microcantilever represented by × in Figures 4.8, 4.9, and 4.11. a) $\varepsilon_{tar\text{-}probe}$ = 5.0. b) $\varepsilon_{tar\text{-}probe}$ 25.0. Plots are generated with $\sigma_{tar\text{-}tar}$ = 1.25, $\sigma_{tar\text{-}probe}$ = 1.25, $\sigma_{tar\text{-}cantilever}$ = 1.50, $\varepsilon_{tar\text{-}tar}$ = 1.00, and $\varepsilon_{tar\text{-}cantilever}$ = 0.05.

It is observed that increase of the bonding number eventually levels off in Figure 4.9. Note that the attractive bonding interactions only exist between $1.12\sigma_{tar\text{-}probe}$ and $2.5\sigma_{tar\text{-}probe}$ and can only accommodate a certain number of target molecules. After the bonding area is saturated, even with very high $\varepsilon_{tar\text{-}probe}$, those target molecules outside the bonding area are not able to interact with the probe

molecules, thus the number of bonds remains constant. This is probably the reason for the exception of the deflection curve (∗) in Figure 4.8, which reaches a steady value. For the curve (∗), its bonding number seems to reach the steady value sooner and remains almost constant compared to other curves in Figure 4.9, which indicates that the target molecules saturate the bonding area very early for the curve(∗), leading to nearly constant molecular interactions and microcantilever deflection (see Figure 4.8) for further increase of $\varepsilon_{tar\text{-}probe}$.

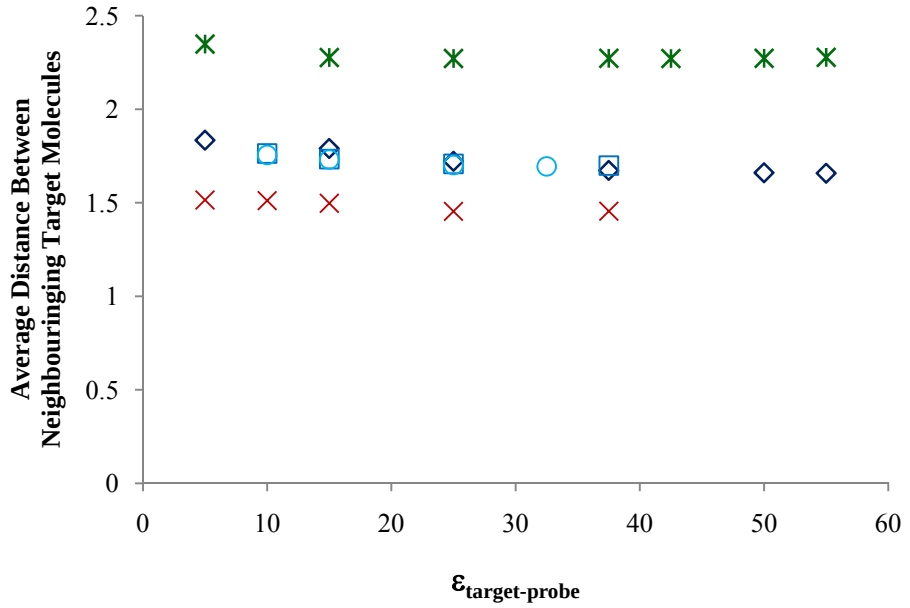

Figure 4.11 Effect of $\varepsilon_{tar\text{-}probe}$ on the average distance between neighbouring target molecules (×) $\sigma_{tar\text{-}tar} = 1.25$, $\sigma_{tar\text{-}probe} = 1.25$; (◊) $\sigma_{tar\text{-}tar} = 1.50$, $\sigma_{tar\text{-}probe} = 1.50$; (□) $\sigma_{tar\text{-}tar} = 1.50$, $\sigma_{tar\text{-}probe} = 2.25$; (o) $\sigma_{tar\text{-}tar} = 1.50$, $\sigma_{tar\text{-}probe} = 3.50$; (∗) $\sigma_{tar\text{-}tar} = 2.00$, $\sigma_{tar\text{-}probe} = 2.00$ Plots are generated with $\varepsilon_{tar\text{-}tar} = 1.00$, $\varepsilon_{tar\text{-}cantilever} = 0.05$, and $\sigma_{tar\text{-}cantilever} = 1.50$.

Figure 4.11 shows the average distance between target molecules that bond with the probe molecules. The average distance remains quite constant, except for the first few data points that have higher average distance than the rest. The snap shot in Figure 4.10a shows that, at low value of $\varepsilon_{tar\text{-}probe}$, only a few bonds form resulting in longer distances between the bonding target molecules. When the bonding area is saturated, distances between target molecules remain constant. This leads to another interesting observation that the curves with the same $\sigma_{tar\text{-}tar}$

have almost the same average distance. For example, the curves for ◊, □, and o- all with the value of $\sigma_{tar\text{-}tar}$ at 1.50- have the same average distance at approximately 1.7, which is roughly equivalent to the equilibrium distance for the Lennard-Jones potential at $1.12\sigma_{tar\text{-}tar}$. This suggests that the distances between 2 target molecules are related to $\sigma_{tar\text{-}tar}$. Further analysis on the effect of $\sigma_{tar\text{-}tar}$ will be discussed next.

4.3 $\sigma_{tar\text{-}tar}$

Figure 4.12 shows the effect of $\sigma_{tar\text{-}tar}$ on the microcantilever deflection. Generally, the trend indicates decrease of the deflection with the increase of $\sigma_{tar\text{-}tar}$. However, most curves in Figure 4.12 do not decrease monotonically with a few data points showing some increase compared to the previous ones. These non-conformities could be the result of the program uncertainty (see Appendix B) or perhaps the number of bonding target molecules, which is another topic to be discussed later in this section. One can think of $\sigma_{tar\text{-}tar}$ as the size of the molecules. The bonding area determined by $\sigma_{tar\text{-}probe}$ stays relatively unchanged at the distance between $1.12\sigma_{tar\text{-}probe}$ and $2.5\sigma_{tar\text{-}probe}$. Given this constant bonding area and the increase of the target size with $\sigma_{tar\text{-}tar}$, the tendency of the system is to bend the microcantilever down to increase its surface area in order to accommodate size increase of target molecules. In addition to this effect, increase of $\sigma_{tar\text{-}tar}$ can also cause reduction of the number of bonded target molecules, thus reducing the interaction strength and the magnitude of the deflection. The reduction in the bonding number is presented in Figure 4.13.

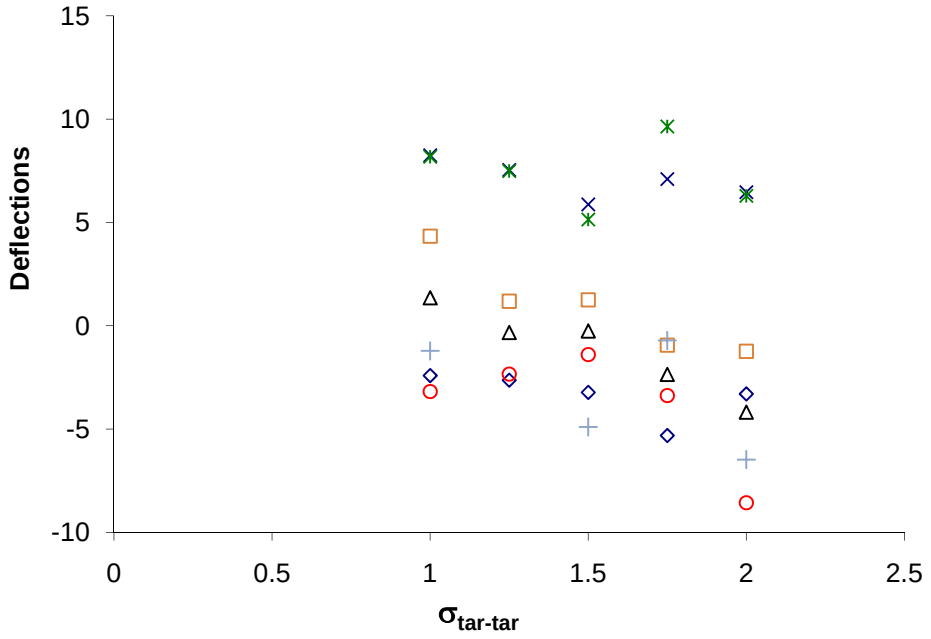

Figure 4.12 Effect of $\sigma_{tar\text{-}tar}$ on microcantilever deflection. (◊) $\sigma_{tar\text{-}probe} = 1.00$, (o) $\sigma_{tar\text{-}probe} = 1.25$, (Δ) $\sigma_{tar\text{-}probe} = 1.50$, (□) $\sigma_{tar\text{-}probe} = 1.63$ (×) $\sigma_{tar\text{-}probe} = 1.75$, (*) $\sigma_{tar\text{-}probe} = 2.00$, and (+) $\sigma_{tar\text{-}probe} = 2.50$. Plots are generated with $\varepsilon_{tar\text{-}probe} = 15.0$, $\varepsilon_{tar\text{-}tar} = 1.00$, $\varepsilon_{tar\text{-}cantilever} = 0.05$, and $\sigma_{tar\text{-}cantilever} = 1.50$.

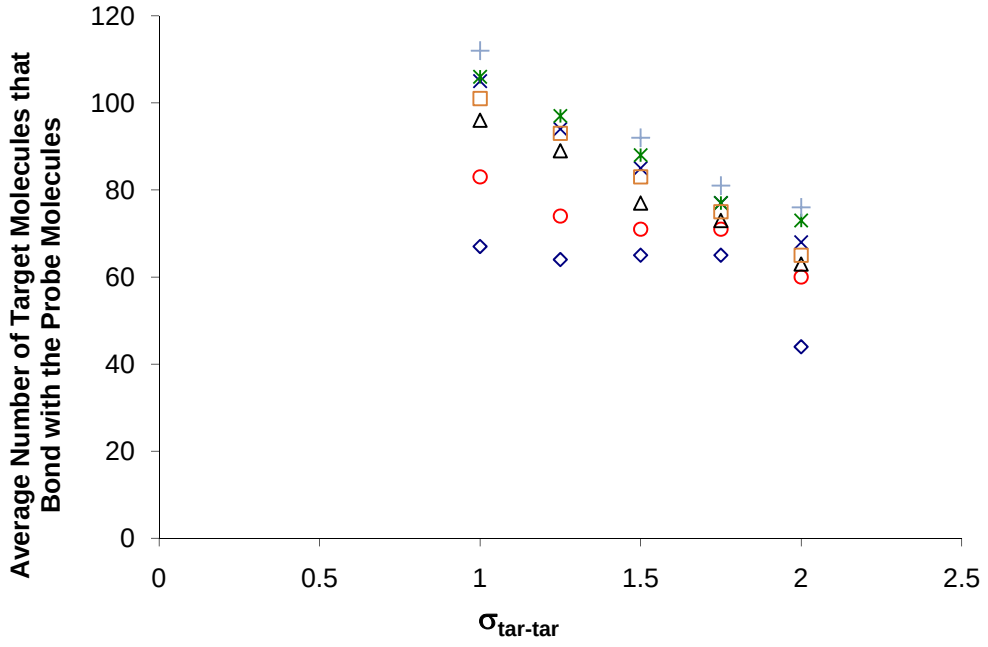

Figure 4.13 Effect of $\sigma_{tar\text{-}tar}$ on the average number of target molecules that bond with the probe molecules. (◊) $\sigma_{tar\text{-}probe} = 1.00$, (o) $\sigma_{tar\text{-}probe} = 1.25$, (Δ) $\sigma_{tar\text{-}probe} = 1.50$, (□) $\sigma_{tar\text{-}probe} = 1.63$ (×) $\sigma_{tar\text{-}probe} = 1.75$, (*) $\sigma_{tar\text{-}probe} = 2.00$, and (+) $\sigma_{tar\text{-}probe} = 2.50$. Plots are generated with $\varepsilon_{tar\text{-}probe} = 15.0$, $\varepsilon_{tar\text{-}tar} = 1.00$, $\varepsilon_{tar\text{-}cantilever} = 0.05$, and $\sigma_{tar\text{-}cantilever} = 1.50$.

Figure 4.13 shows the plots for number of bonding target molecules vs. $\sigma_{tar\text{-}tar}$. Overall, the bonding number decreases as $\sigma_{tar\text{-}tar}$ increases. Again for the constant $\sigma_{tar\text{-}probe}$, the bonding area remains at the same size. Hence, if the size of the target molecules is bigger, fewer of them can be fitted into the bonding area. Some of the curves in Figure 4.13 do not decrease monotonically. For example, the curves for $\sigma_{tar\text{-}probe} = 1.00$ (◊) and $\sigma_{tar\text{-}probe} = 1.25$ (o) stay nearly at the same value for $\sigma_{tar\text{-}tar}$ between 1.25 and 1.75. This might be because even though the target molecules are bigger, their interactions are still not high enough to overcome the stronger bonding force of target–probe interactions because $\varepsilon_{tar\text{-}probe}$ is much larger than $\varepsilon_{tar\text{-}tar}$.

It appears that $\sigma_{tar\text{-}tar}$ has 2 opposite effects on the microcantilever deflection. First, $\sigma_{tar\text{-}tar}$ increases the size of the target molecules, which tends to bend the microcantilever down. However, its second effect is that $\sigma_{tar\text{-}tar}$ reduces the number of bonds. With fewer bonds, the interactions become weaker and the magnitude of the deflection is reduced. It is the combination of the two factors that influences the deflection of the microcantilever. This could also be the reason why the deflection curves in Figure 4.12 do not have a monotonic trend. For example, the deflection curve of $\sigma_{tar\text{-}probe} = 1.00$ (◊) declines between $1.00 < \sigma_{tar\text{-}tar} < 1.75$. Within this domain, the number of bonding target molecules remains quite steady at the value around 70 (see Figure 4.13). With the bonding number constant and the size of the target molecules increases as $\sigma_{tar\text{-}tar}$ increases, the microcantilever bends down. Then at $\sigma_{tar\text{-}tar} = 2.00$, the number of bonding target molecules decrease to about 40 molecules. With fewer bonds, the molecular interactions are weaker, yielding lower deflection magnitude.

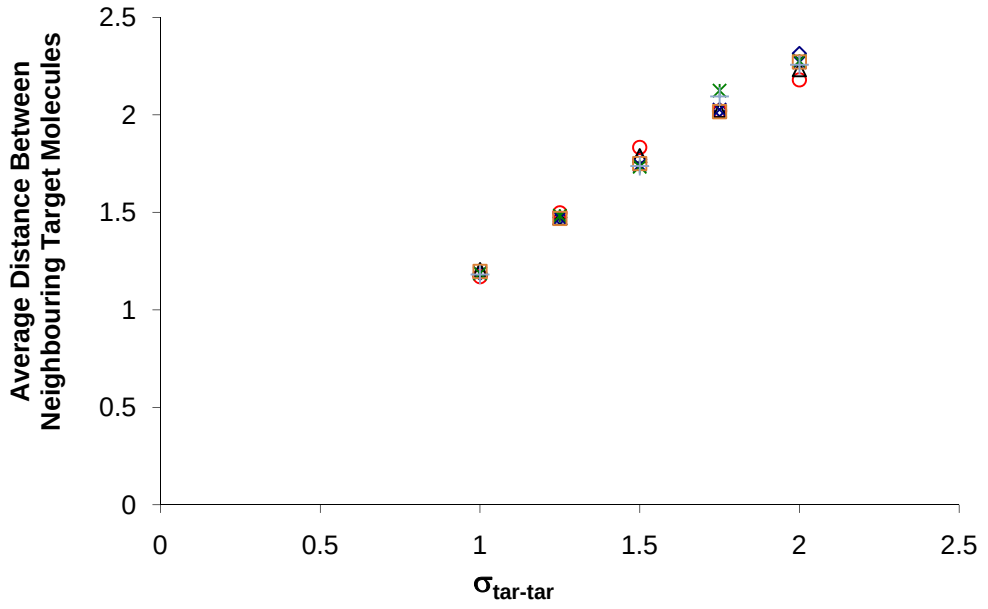

Figure 4.14 Effect of $\sigma_{tar-tar}$ on the average distance between neighbouring target molecules. (◊) $\sigma_{tar-probe} = 1.00$, (o) $\sigma_{tar-probe} = 1.25$, (Δ) $\sigma_{tar-probe} = 1.50$, (□) $\sigma_{tar-probe} = 1.63$ (×) $\sigma_{tar-probe} = 1.75$, (*) $\sigma_{tar-probe} = 2.00$, and (+) $\sigma_{tar-probe} = 2.50$. Plots are generated with $\varepsilon_{tar-probe} = 15.0$, $\varepsilon_{tar-tar} = 1.00$, $\varepsilon_{tar-cantilever} = 0.05$, and $\sigma_{tar-cantilever} = 1.50$.

Another interesting effect of $\sigma_{tar-tar}$ is its relationship with the distance between bonding target molecules. It was noted earlier in Section 4.2 that the average distance between the target molecules varies quite closely with $\sigma_{tar-tar}$. Figure 4.14 shows the plot of this average distance vs. $\sigma_{tar-tar}$. All data points for the same $\sigma_{tar-tar}$ conform to the same value and increase linearly with $\sigma_{tar-tar}$. This behaviour strongly suggests that $\sigma_{tar-tar}$ is a major factor in determining the target-target distance and moreover the target molecules seem to prefer to be separated from each other at the equilibrium distance of $1.12\sigma_{tar-tar}$.

4.4 $\varepsilon_{tar\text{-}tar}$

Generally, $\varepsilon_{tar\text{-}tar}$ has a minor effect on the microcantilever deflection compared to other Lennard-Jones parameters. Figure 4.15 shows the plots of the deflection vs. $\varepsilon_{tar\text{-}tar}$. According to the curves, it appears that the deflection does not deviate much with the change of $\varepsilon_{tar\text{-}tar}$. Most curves seem to have constant deflection except for some minor deviation at very low $\varepsilon_{tar\text{-}tar}$. It is possible that, at very low value of $\varepsilon_{tar\text{-}tar}$, the target-target interactions are very weak compared to the much stronger target-probe interactions, thus the latter interactions dominate the molecular interactions causing the change of deflection.

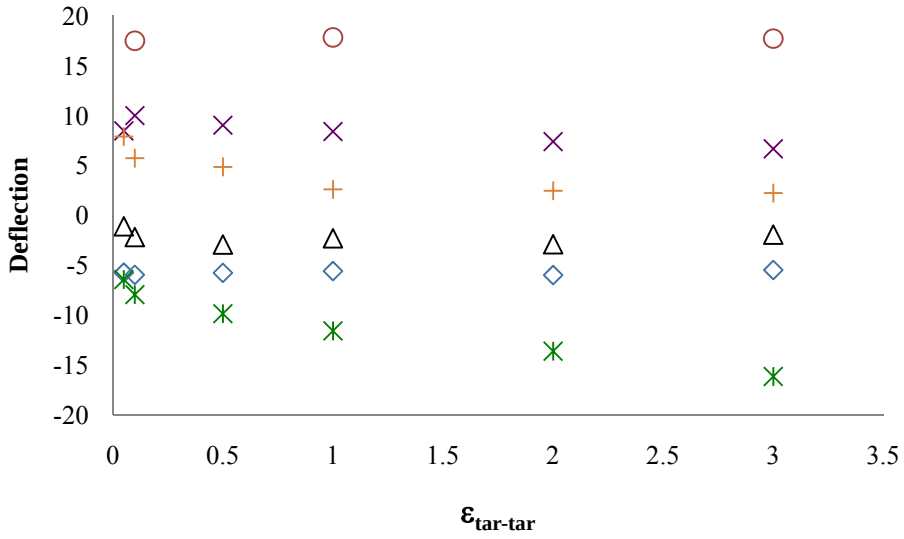

Figure 4.15 Effect of $\varepsilon_{tar\text{-}tar}$ on the microcantilever deflection. (◊) $\sigma_{tar\text{-}probe} = 1.25$, $\sigma_{tar\text{-}tar} = 1.25$; (o) $\sigma_{tar\text{-}probe} = 1.75$, $\sigma_{tar\text{-}tar} = 1.25$; (Δ) $\sigma_{tar\text{-}probe} = 1.50$, $\sigma_{tar\text{-}tar} = 1.50$; (×) $\sigma_{tar\text{-}probe} = 2.00$, $\sigma_{tar\text{-}tar} = 2.00$; (*) $\sigma_{tar\text{-}probe} = 2.25$, $\sigma_{tar\text{-}tar} = 1.50$; and (+) $\sigma_{tar\text{-}probe} = 3.50$, $\sigma_{tar\text{-}tar} = 1.50$. Plots are generated with $\varepsilon_{tar\text{-}probe} = 25.0$, $\varepsilon_{tar\text{-}cantilever} = 0.05$, and $\sigma_{tar\text{-}cantilever} = 1.50$.

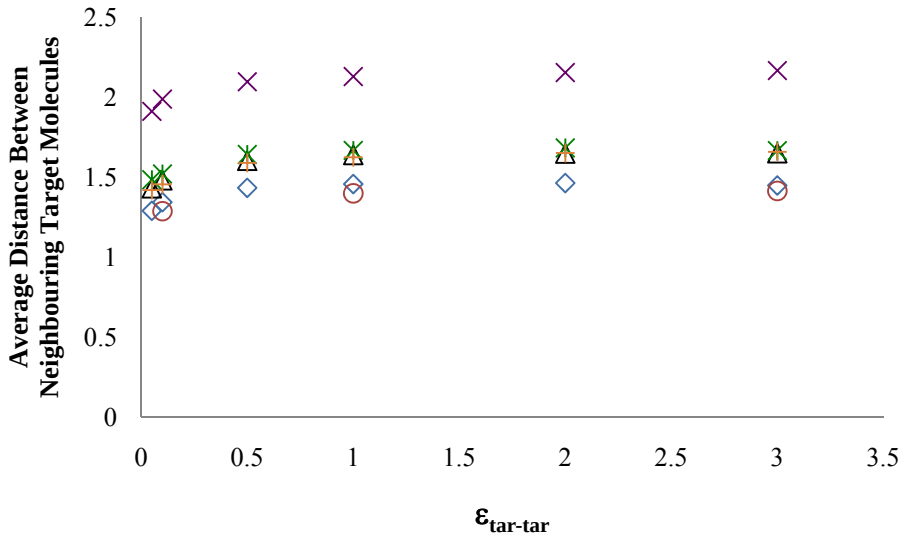

Figure 4.16 Effect of $\varepsilon_{tar\text{-}tar}$ on the average distance between neighbouring target molecules. (◊) $\sigma_{tar\text{-}probe} = 1.25$, $\sigma_{tar\text{-}tar} = 1.25$; (o) $\sigma_{tar\text{-}probe} = 1.75$, $\sigma_{tar\text{-}tar} = 1.25$; (Δ) $\sigma_{tar\text{-}probe} = 1.50$, $\sigma_{tar\text{-}tar} = 1.50$; (×) $\sigma_{tar\text{-}probe} = 2.00$, $\sigma_{tar\text{-}tar} = 2.00$; (*) $\sigma_{tar\text{-}probe} = 2.25$, $\sigma_{tar\text{-}tar} = 1.50$; and (+) $\sigma_{tar\text{-}probe} = 3.50$, $\sigma_{tar\text{-}tar} = 1.50$. Plots are generated with $\varepsilon_{tar\text{-}probe} = 25.0$, $\varepsilon_{tar\text{-}cantilever} = 0.05$, and $\sigma_{tar\text{-}cantilever} = 1.50$.

Figure 4.16 shows the effect of $\varepsilon_{tar\text{-}tar}$ on the average distance between neighbouring target molecules. The two leftmost data points have lower values than the rest, which probably suggest that the target-target bonds have been compressed by the stronger target-probe interactions. Beside those 2 data points, the rest of the curves stay nearly at the same value regardless of $\varepsilon_{tar\text{-}tar}$. Another interesting observation is that the curves with the same $\sigma_{tar\text{-}tar}$ have the same average target-target distance. For example the data points for curves (Δ), (*), and (+) – all with $\sigma_{tar\text{-}tar}$ at 1.50- have the same average distance. This further confirms the relationship between $\sigma_{tar\text{-}tar}$ and target-target distance observed throughout this chapter.

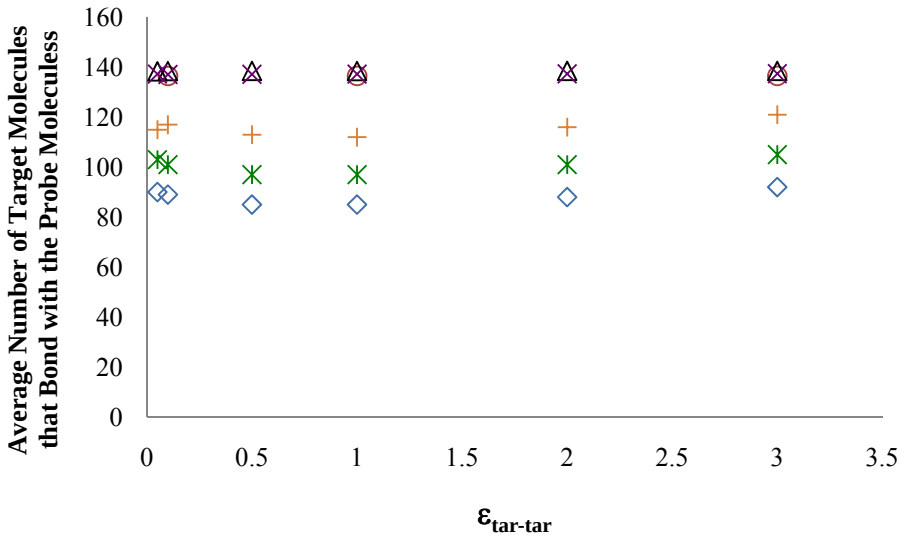

Figure 4.17 Effect of $\varepsilon_{tar\text{-}tar}$ on the average number of target molecules that bond with the probe molecules. (◊) $\sigma_{tar\text{-}probe} = 1.25$, $\sigma_{tar\text{-}tar} = 1.25$; (o) $\sigma_{tar\text{-}probe} = 1.75$, $\sigma_{tar\text{-}tar} = 1.25$; (Δ) $\sigma_{tar\text{-}probe} = 1.50$, $\sigma_{tar\text{-}tar} = 1.50$; (×) $\sigma_{tar\text{-}probe} = 2.00$, $\sigma_{tar\text{-}tar} = 2.00$; (*) $\sigma_{tar\text{-}probe} = 2.25$, $\sigma_{tar\text{-}tar} = 1.50$; and (+) $\sigma_{tar\text{-}probe} = 3.50$, $\sigma_{tar\text{-}tar} = 1.50$. Plots are generated with $\varepsilon_{tar\text{-}probe} = 25.0$, $\varepsilon_{tar\text{-}cantilever} = 0.05$, and $\sigma_{tar\text{-}cantilever} = 1.50$.

Figure 4.17 shows the plot of the average number of target molecules that bond with the probe molecules vs. $\varepsilon_{tar\text{-}tar}$. Similar to the previous two plots for $\varepsilon_{tar\text{-}tar}$, the average bonding number does not change much. As observed throughout this chapter, the distances between target molecules are roughly equivalent to the equilibrium distance of $1.12\sigma_{tar\text{-}tar}$. At this distance, no matter what value $\varepsilon_{tar\text{-}tar}$ is, the force between two target molecules remains zero. This could be the reason that $\varepsilon_{tar\text{-}tar}$ has less effect than the other Lennard-Jones parameter.

4.5 Summary

This chapter shows the effect of Lennard-Jones parameters on the molecular interactions and microcantilever deflection. It was observed that each parameter affects the system in a different way. $\sigma_{tar\text{-}probe}$ appears to determine the bonding area. The size of this area in comparison with the size of the target molecules can influence the microcantilever deflection. $\varepsilon_{tar\text{-}probe}$ dictates the bonding strength between target and probe molecules and tends to increase the magnitude of the deflection. $\sigma_{tar\text{-}tar}$ seems to effect the distance between two target molecules or, in other words, the size of target molecules. This tends to create two opposite effects on the microcantilever deflection. As the target size increases, the microcantilever would bend down. However, at the same time, the number of bonds is reduced, thus lowering the interaction strength and the magnitude of the deflection. $\varepsilon_{tar\text{-}tar}$ was found to have minimal effect on the system because target molecules prefer to be at equilibrium distance away from each other, resulting in zero force for the target-target interaction. Furthermore, the spacing of the probe molecules appears to influence the deflection as well. Overall, it seems that combination of all Lennar-Jones parameters and the probe spacing determines the direction and magnitude of the microcantilever deflection.

Chapter 5

Effect of Probe Locations

In this chapter, the effects of the probe locations were studied. Two sets of tests were performed. The objective of the first set is to find out the response of the microcantilever deflection to the change of number of probe molecules that are uniformly distributed on the microcantilever surface. In the second set, two probe configurations were used to compare their interaction with a very low number of target molecules. One microcantilever will have the probe molecules cover its entire top surface while the other for half of its length. Effect of both configurations will be compared to identify the one that yield higher sensitivity.

5.1 Effect of Percentage of Microcantilever Surface with Probe Molecules

In this study, the top surface of the microcantilever was covered uniformly 25%, 33%, 50%, and 100% by the probe molecules. As mentioned in Section 2.3, the probe molecules are the special microcantilever molecules at certain interval along the top surface of the microcantilever that undergo the target-probe interactions. For 25% probe coverage, one in four microcantilever molecules along the top surface was assigned to be the probe molecule and subjected to the target-probe interaction. On the other hand, at 100%, all molecules along the top surface become the probe molecules. Note that in this simulation, the interactions

between probe molecules were assumed to be zero. The probe-probe interactions could possibly affect the system since the distances between probe molecules were changed along with the probe percentage. In the experiments, it was observed that some microcantilever bends after the probe layer is applied. However, as mentioned in Chapter 2, we are mainly interested in the interactions after target molecules are introduced into the system. Thus in this work, the probe-probe interactions are ignored.

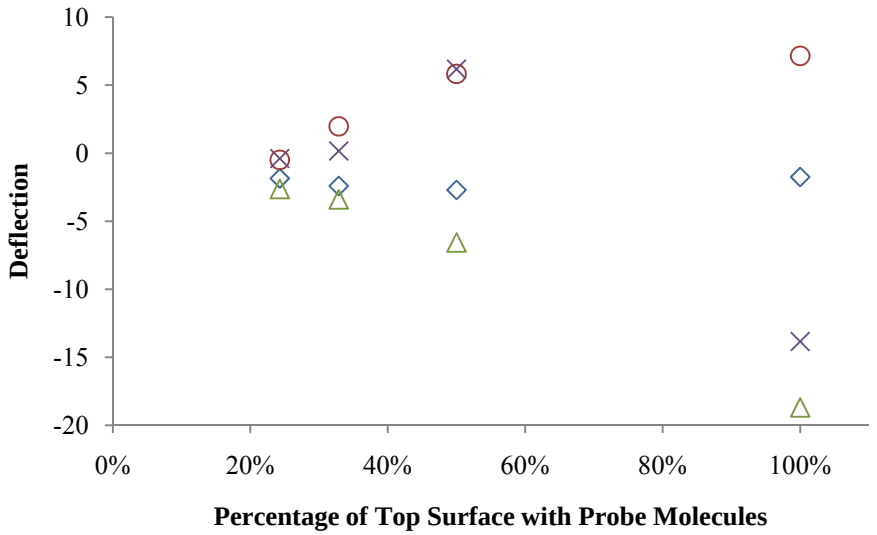

Figure 5.1 Effect of probe percentage on the microcantilever deflection. (◊) $\sigma_{tar\text{-}probe} = 1.00$, $\sigma_{tar\text{-}tar} = 1.50$; (o) $\sigma_{tar\text{-}probe} = 2.00$, $\sigma_{tar\text{-}tar} = 1.50$; (Δ) $\sigma_{tar\text{-}probe} = 1.25$, $\sigma_{tar\text{-}tar} = 2.00$; and (×) $\sigma_{tar\text{-}probe} = 2.00$, $\sigma_{tar\text{-}tar} = 2.00$. Plots are generated with $\varepsilon_{tar\text{-}probe} = 15.0$, $\varepsilon_{tar\text{-}tar} = 1.00$, $\varepsilon_{tar\text{-}can} = 0.05$, and $\sigma_{tar\text{-}can} = 1.50$

Figure 5.1 shows the effect of the probe coverage percentage on the microcantilever deflection. In general, the deflection magnitude increases with the probe percentage. However, direction and trend of the curves for particular pairs of $\sigma_{tar\text{-}probe}$ and $\sigma_{tar\text{-}tar}$ are different. For example, for curve (×), deflection increases as coverage increases to 50%, then drops to negative at 100%. Other curves have monotonically increasing or decreasing trends. These deviations in deflection trends are probably a result of the variation in values of $\sigma_{tar\text{-}probe}$, $\sigma_{tar\text{-}tar}$,

and the spacing between the probe molecules. The aforementioned factors influence the molecular interactions and the arrangements of target molecules, in terms of their separation distances in the y-direction as well as the number of bonding target molecules, both of which could greatly influence the microcantilever deflection.

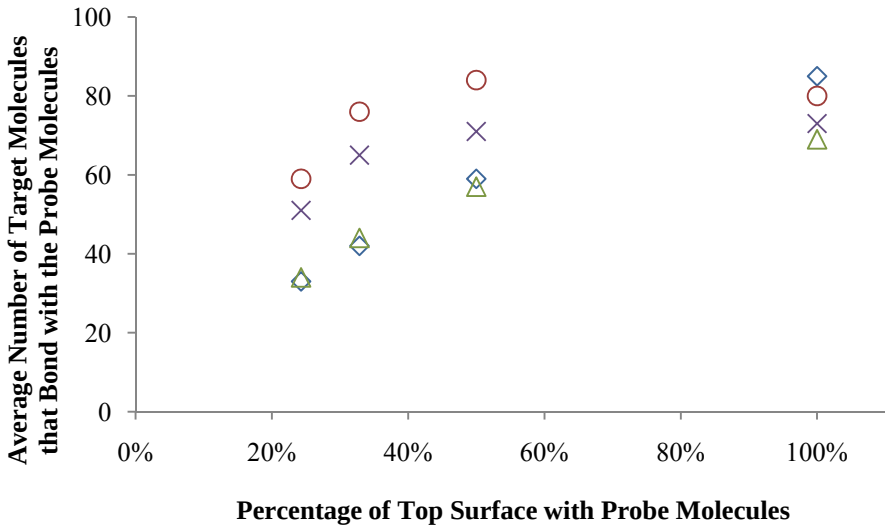

Figure 5.2 Effect of probe percentage on the average number of target molecules that bond with the probe molecules. (◊) $\sigma_{tar\text{-}probe} = 1.00$, $\sigma_{tar\text{-}tar} = 1.50$; (o) $\sigma_{tar\text{-}probe} = 2.00$, $\sigma_{tar\text{-}tar} = 1.50$; (Δ) $\sigma_{tar\text{-}probe} = 1.25$, $\sigma_{tar\text{-}tar} = 2.00$; and (×) $\sigma_{tar\text{-}probe} = 2.00$, $\sigma_{tar\text{-}tar} = 2.00$. Plots are generated with $\varepsilon_{tar\text{-}probe} = 15.0$, $\varepsilon_{tar\text{-}tar} = 1.00$, $\varepsilon_{tar\text{-}can} = 0.05$, and $\sigma_{tar\text{-}can} = 1.50$

Figure 5.2 shows that the number of the bonding target molecules increases as the coverage percentage increases from 25% to 50%, then remains relatively constant between 50% and 100%. To illustrate the bonding arrangements, Figure 5.3 shows the snap shots of curve (Δ) in Figures 5.1, 5.2, and 5.4 (i.e., $\sigma_{tar\text{-}probe} = 1.25$, $\sigma_{tar\text{-}tar} = 2.00$). This pattern of local bonding between target and probe molecules was observed in all results at low probe percentage.

According to Figure 5.2, at low probe coverage of 25%, the number of target molecules is small, as further depicted by the snap shot in Figure 5.3a. Because

there are only a few probe molecules in the system, the probe molecules are located quite far apart from each other. From the snap shot, it was observed that the target molecules only stay within a close proximity to the probe molecules, leaving vacant area in between. The target and probe molecules in one area are often at a great distance from those in the next area. Therefore, it should be reasonable to assume that the molecular interactions primarily exist between local target molecules and probe molecules. Consequently, the molecular interactions should be weaker, which supports the finding of low deflection for the 25% coverage observed in Figure 5.1.

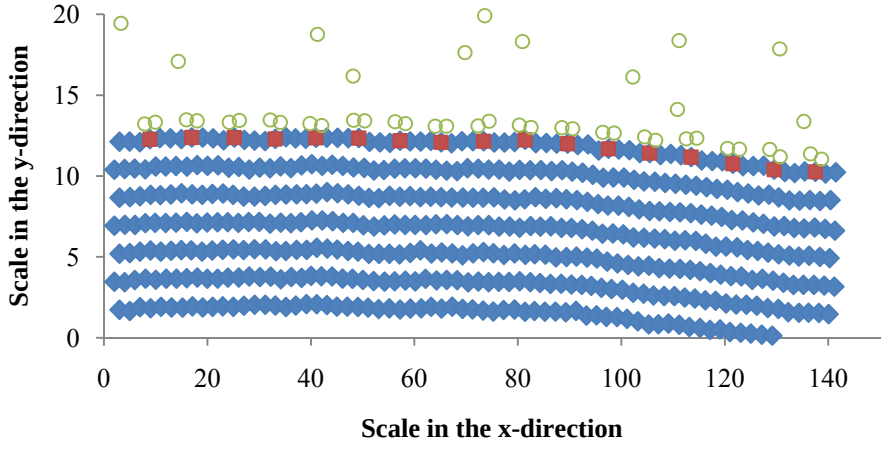

a)

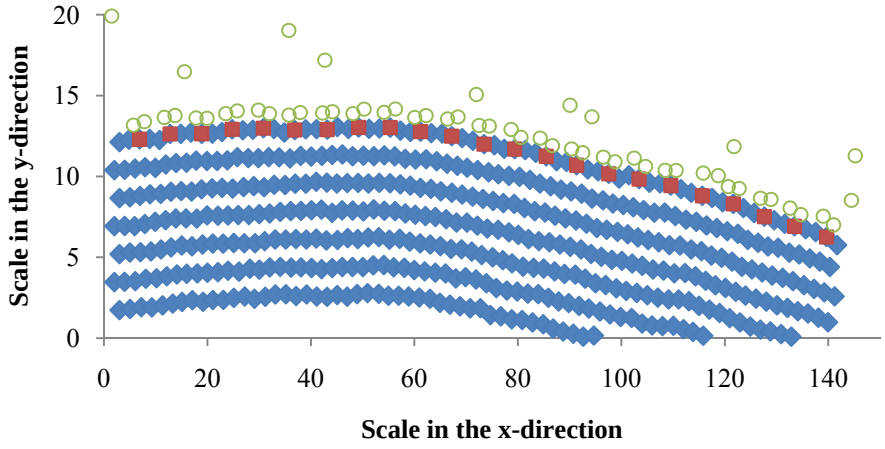

b)

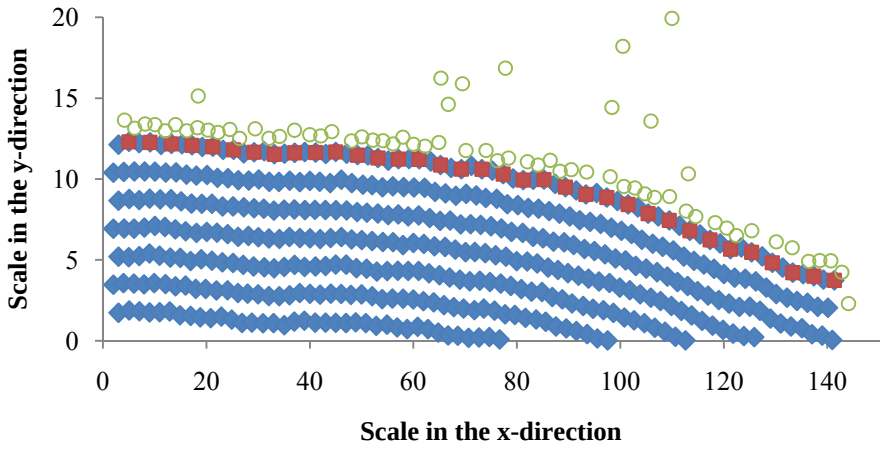

c)

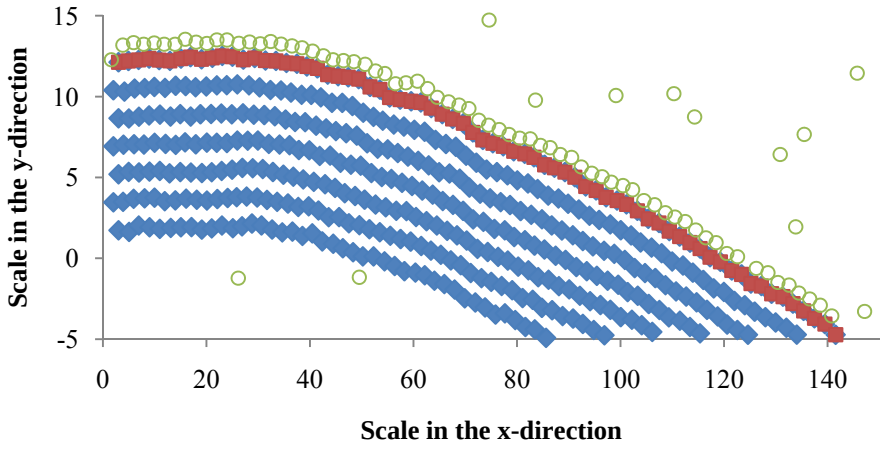

d)

Figure 5.3 Snap shots of the microcantilever with probe coverage at 25%, 33%, 50%, and 100% (for Figures 5.3a, 5.3b, 5.3c, and 5.3d respectively). The green circle (o) represents the target molecules, blue diamond (♦) the microcantilever beam molecules and red square (■) the probe molecules. Plots are generated with $\sigma_{tar\text{-}probe} = 1.25$, $\sigma_{tar\text{-}tar} = 2.00$, $\sigma_{tar\text{-}can} = 1.50$, $\varepsilon_{tar\text{-}probe} = 15.0$, $\varepsilon_{tar\text{-}tar} = 1.00$, and $\varepsilon_{tar\text{-}can} = 0.05$

With the probe percentage increases to 33%, more bonds are formed. The snap shot in Figure 5.3b shows that at this point, the bonding pattern still shows the target molecules within a small area around each probe molecule and empty spaces in between. However, the empty space in between is smaller than at 25% coverage, and there are more bonds. Both factors should lead to an increase in the overall molecular interactions, which, in turn, raises the magnitude of deflection.

With probe molecules covering 50% of the surface, the target molecules seem to fill out the area above the microcantilever (see Figure 5.3c). From the snap shot, it appears that the pattern of local bonding with unoccupied spaces in between, as observed at 25% and 33% percentages, disappears. Instead, a new pattern of a long line of target molecules filling out the entire top surface emerges. In addition, the target molecules are in closer proximity to each other, suggesting that target and probe molecules can interact more with each other, unlike the mainly local interactions at lower probe percentage. Consequently, the molecular interactions should increase, leading to increase of the microcantilever deflection.

Figure 5.2 indicates that the number of target molecules at 50% and 100% appears to be equal. This behaviour is further observed from the snap shots in Figures 5.3c and 5.3d. With 50% coverage, the target molecules appear to already saturate the bonding area. Even though there are more probe molecules for the 100% coverage, the fixed bonding area could not accommodate more new target molecules. Thus, the number of bonded target molecules stays nearly constant. Again by having the target molecules filling out its bonding area, the magnitude of the microcantilever deflection is much higher than that with probe percentage of 25% or 33%.

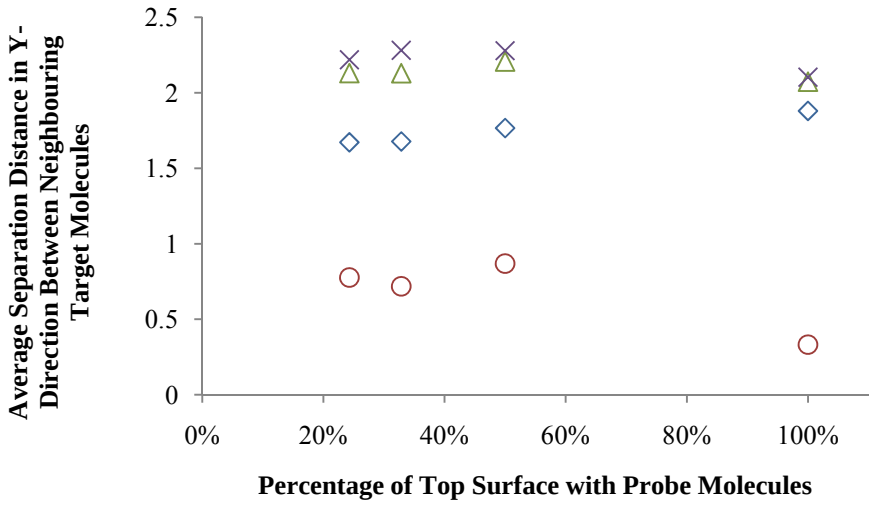

Figure 5.4 Effect of probe coverage on the average separation distance in the y-direction between neighbour target molecules. (◊) $\sigma_{tar\text{-}probe} = 1.00$, $\sigma_{tar\text{-}tar} = 1.50$; (o) $\sigma_{tar\text{-}probe} = 2.00$, $\sigma_{tar\text{-}tar} = 1.50$; (Δ) $\sigma_{tar\text{-}probe} = 1.25$, $\sigma_{tar\text{-}tar} = 2.00$; and (×) $\sigma_{tar\text{-}probe} = 2.00$, $\sigma_{tar\text{-}tar} = 2.00$. Plots are generated with $\varepsilon_{tar\text{-}probe} = 15.0$, $\varepsilon_{tar\text{-}tar} = 1.00$, $\varepsilon_{tar\text{-}can} = 0.05$, $\sigma_{tar\text{-}can} = 1.50$

Figure 5.4 shows the plot of the separation distances between target molecules in the y-direction vs. the probe percentage. In most cases, the separation distance in the y-direction decrease, with the increase of probe percentage from 50% to 100%, except for the curve (◊), which shows slight increase. Note that at probe percentage of 20% or 30%, the target-target interactions are weak as mentioned above. Hence, the separation in the y-direction should have weak effect on them. The decrease in separation distance in the y-direction is best described through the snap shots of Figures 5.3c and 5.3d. In Figure 5.3c (50% coverage) the target molecules appear to be staggered in a zigzag pattern. At 100% coverage (see Figure 5.3d), the addition of the probe molecules seems to force the staggered target molecules into one layer, thus reducing the separation distance. In the Chapter 4, it was observed that when the target molecules are forced into one layer, they require more room in the x-direction. As a result, the microcantilever bends down to increase the surface area.

Another interesting behaviour is that the change in the probe coverage percentage changes the distance between 2 probe molecules. As discussed in Chapter 4, the spacing between probe molecules could affect the molecular interactions. At lower probe coverage, the probe molecules are separated at greater distances, thus the target molecules are only able to interact locally with one probe molecule. In the other extreme case with 100% probe coverage, target molecules are in closer proximity to many probe molecules; thus, one target molecule might interact with many probe molecules. This multiple bonding could affect the microcantilever deflection in a different way, which might be related to the deviation of the microcantilever deflection trends shown in Figure 5.1.

Overall, deflection curves for certain pairs of $\sigma_{tar\text{-}probe}$ and $\sigma_{tar\text{-}tar}$ show different trends when plotted against the probe percentage. As discussed in this section and the previous chapter, many factors are involved in determining the direction and magnitude of the bending, such as the number of bonding target molecules, the target-target separation distance, and the spacing of the probe molecules. The complex nature of the molecular interactions creates a distinctive trend for each curve. In particular, this section demonstrates that close proximity of target and probe molecules might be essential in increasing interactions as seen by the increase of deflection as the probe percentage increases. The high percentage of probe coverage tends to generate greater microcantilever deflection.

5.2 Microcantilever Sensitivity as a Function of Probe Configurations

This section studies the microcantilever in a system with low concentration of target molecules. The number of target molecules inside the system was reduced to 20, 30, 40, and 50 as opposed to 277 molecules for the simulations described in Chapter 4 and Section 5.1. Two types of probe configurations were used. One microcantilever has the probe coverage at 100% for its entire length and the other with the probe coverage also at 100% but only for half of its length. The purpose

of this test is to find out which probe configuration yields a greater deflection at low target molecule concentrations.

Note that there are two methods of changing the concentration. One is to adjust the number of target molecules inside the system while keeping the volume constant and the other by changing the volume (in our case the boundary area). Our simulation was found to be sensitive to the change of number of molecules. However, it does not response as much to the change in volume. The change in volume mostly influences the time for the system to reach the equilibrium (i.e., the steady state for bonding number and energy) because for a larger volume, the target molecules have to travel a longer distance before they reach the probe molecules. Regardless of the volume used, after the target molecules saturate the bonding area, the molecular interactions as well as the deflection remain approximately the same. In this section, the reference of concentration refers to the change in number of target molecules.

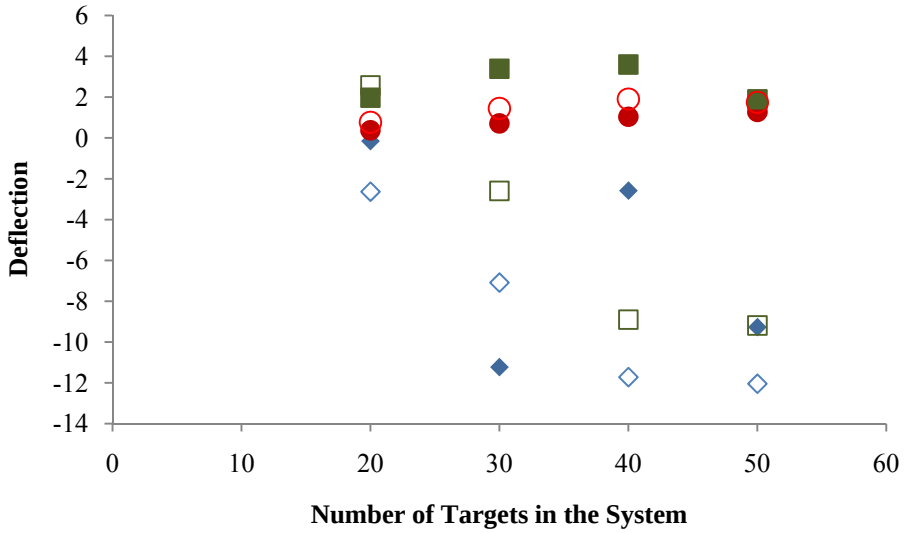

Figure 5.5 Comparison of the effect of the microcantilever with probe coverage of half of its length (unfilled symbols) and the entire length (filled symbols) on the microcantilever deflection. (◊) $\sigma_{tar\text{-}probe} = 1.25$, $\sigma_{tar\text{-}tar} = 2.00$, half-length coverage; (♦) $\sigma_{tar\text{-}probe} = 1.25$, $\sigma_{tar\text{-}tar} = 2.00$, full-length coverage; (o) $\sigma_{tar\text{-}probe} = 1.25$, $\sigma_{tar\text{-}tar} = 1.50$, half-length coverage; (•) $\sigma_{tar\text{-}probe} = 1.25$, $\sigma_{tar\text{-}tar} = 1.50$, full-length coverage; (□) $\sigma_{tar\text{-}probe} = 2.00$, $\sigma_{tar\text{-}tar} = 2.00$, half-length coverage; (■) $\sigma_{tar\text{-}probe} = 2.00$, $\sigma_{tar\text{-}tar} = 2.00$, full-length coverage. Plots are generated with $\varepsilon_{tar\text{-}probe} = 15.0$, $\varepsilon_{tar\text{-}tar} = 1.00$, $\varepsilon_{tar\text{-}can} = 0.05$, and $\sigma_{tar\text{-}can} = 1.50$

Figure 5.5 shows the deflection results with the solid symbols representing the full-length coverage microcantilever and the open symbols the half-length configuration. The deflection magnitude tends to increase with the number of target molecules inside the system. With small number of target molecules inside the system, there are hardly any target molecules to form the bonds, thus the deflection values are small for all curves of different Lennard-Jones parameters. Depending on the values of $\sigma_{tar\text{-}probe}$ and $\sigma_{tar\text{-}tar}$, some half-length coverage microcantilevers have a greater deflection than those with full-length coverage, particularly when the number of target molecules is between 40 and 50. Curve (□) has a decreasing trend while its counterpart (■) remains relatively unchanged. Note that at the concentration of 40 and 50 molecules, the magnitude of deflection for curve (□) is higher than for curve (■). Curves (o) and (•) appear to have slightly increasing trend with curve (o) having slightly higher deflection values over the entire plot. Curve (♦) seems to exhibit a large fluctuation. This may be attributed to the fact that the interaction distance between target molecules ($\sigma_{tar\text{-}tar}$ = 2.00) are much larger compared to the interaction distance between target and probe molecules ($\sigma_{tar\text{-}probe}$ = 1.25). The bonding of these large target molecules inside a very short bonding distance is not very stable, subsequently generating significant uncertainty. Again, at the value of 40 to 50 target molecules inside the system, curve (◊) has higher deflection than curve (♦).

Another interesting observation is that for half-length coverage (open symbols), the microcantilever deflection remains roughly at the same value between the domain of 40-50 target molecules inside the system, which correlates closely with the bonding number of target molecules to be discussed next.

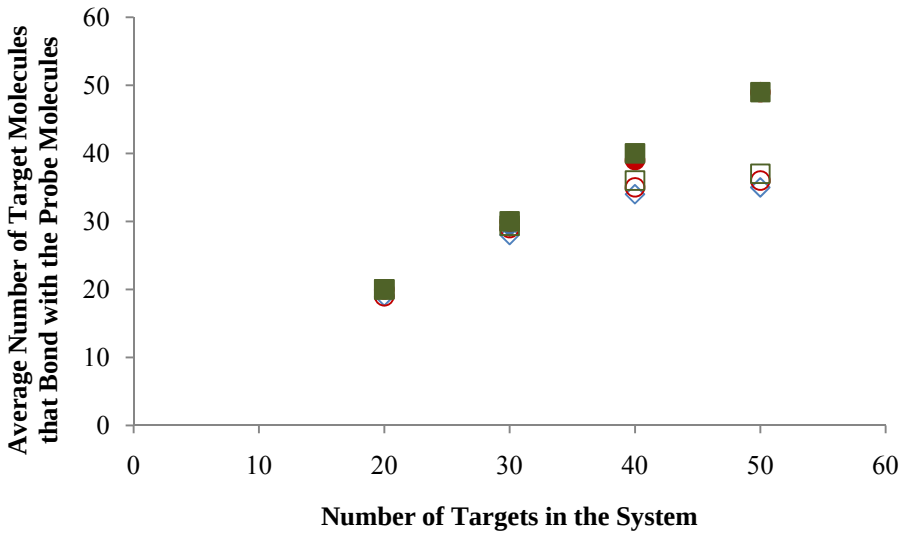

Figure 5.6 Comparison of the effect of the microcantilever with probe coverage of half of its length (unfilled symbols) and the entire length (filled symbols) on the number of target molecules that bond with the probe molecules. (◊) $\sigma_{tar\text{-}probe}$ = 1.25, $\sigma_{tar\text{-}tar}$ = 2.00, coverage half the length; (◊) $\sigma_{tar\text{-}probe}$ = 1.25, $\sigma_{tar\text{-}tar}$ = 2.00, half-length coverage; (♦) $\sigma_{tar\text{-}probe}$ = 1.25, $\sigma_{tar\text{-}tar}$ = 2.00, full-length coverage; (o) $\sigma_{tar\text{-}probe}$ = 1.25, $\sigma_{tar\text{-}tar}$ = 1.50, half-length coverage; (•) $\sigma_{tar\text{-}probe}$ = 1.25, $\sigma_{tar\text{-}tar}$ = 1.50, full-length coverage; (□) $\sigma_{tar\text{-}probe}$ = 2.00, $\sigma_{tar\text{-}tar}$ = 2.00, half-length coverage; (■) $\sigma_{tar\text{-}probe}$ = 2.00, $\sigma_{tar\text{-}tar}$ = 2.00, full-length coverage. Plots are generated with $\varepsilon_{tar\text{-}probe}$ = 15.0, $\varepsilon_{tar\text{-}tar}$ = 1.00, $\varepsilon_{tar\text{-}can}$ = 0.05, and $\sigma_{tar\text{-}can}$ = 1.50

Figure 5.6 shows a plot for the number of bonding target molecules vs. the number of target molecules inside the system. As expected, a higher number of target molecules in the system leads to a higher number of target molecules bonding to the probe molecules. When there were 20-30 target molecules in the system all of them bond to the probe molecules. However, this trend seems to alter when there are 40 target molecules in the system. At this point, the plots for the half-length and full-length differ from each other. The number of bonding target molecules for the half-length coverage remains at 35 molecules while the curves for the full-length coverage continue to increase at the one-to-one ratio.

Snap shots of the microcantilever exposed to different numbers of target molecules are presented in Figures 5.7-5.10 for the microcantilever with $\sigma_{tar\text{-}probe}$ = 2.00 and $\sigma_{tar\text{-}tar}$ = 2.00 (same systems as described by □ and ■ in Figures 5.5-5.6). Note that the snap shots are drawn from a specific $\sigma_{tar\text{-}probe}$ and $\sigma_{tar\text{-}tar}$ pair.

Different $\sigma_{tar\text{-}probe}$ and $\sigma_{tar\text{-}tar}$ values could affect deflection differently. However, the general arrangement of target molecules at various concentrations shows similar behaviours as observed from the snap shots.

With the number of the target molecules inside the system at 20 molecules, the snap shots in Figure 5.7 show that there are many unoccupied spaces for both half-length and full-length coverage cases because there are not enough target molecules to bond with the available probe molecules. As a result, the distance from one target molecule to its neighbour is quite large. Being separated at a great distance, the target molecules are unable to effectively interact with each other. Only interactions from a few target-probe bonds exist. Therefore, the overall molecular interactions should be weak, leading to a small deflection for both microcantilever configurations.

With more target molecules inside the system, more bonds can be formed as observed through the increase of the number of target molecules on the top microcantilever surface in Figure 5.8. At 30 target molecules inside the system, the target molecules seem to fill up most of the bonding area of the half-length coverage microcantilever, while there are still a considerable number of vacant sites for the full-length one. With more target molecules and shorter interaction distances, the molecular interactions should be stronger, thus producing greater deflection than the system with 20 target molecules.

At 40 and 50 molecules (see Figures 5.9 and 5.10), the target molecules seem to saturate the bonding area of the half-length coverage while it appears to be some unoccupied area on the microcantilever with the full-length configuration. The required number of bonding target molecules to saturate the bonding area for half-length configuration appears to be around 35 molecules, which is supported by the finding in Figure 5.6 (with the number of bonding target molecules reaching steady value at 35 molecules). Since the bonding area is saturated and the target molecules are closer to each other, the molecular interactions for the half-length

coverage are much stronger, leading to a greater deflection. For the full-length coverage, there are vacant sites. Thus, the molecular interactions for the full-length configuration microcantilever might not be as strong as the half-length one.

Overall, the results show that at a small number of target molecules inside the system, there are not enough target molecules to saturate the bonding area. Therefore, some of the full-length coverage microcantilevers do not give as large a deflection compared to their half-length counterparts. The microcantilever deflection depends greatly on the molecular interactions and how the target molecules saturate the bonding area. Greater the level of the saturation, higher the molecular interaction, and thus greater the microcantilever deflection.

5.3 Summary

This chapter shows that locations of probe molecules on the microcantilever surface can affect the molecular interactions and thus the sensitivity of the microcantilever deflection. It was found that the percentage of probe molecules on the microcantilever can influence the molecular interactions. At low probe coverage, target molecules that bond to the probe molecules are found to be quite far apart from each other, and thus their interactions are weak. Overall it appears that the higher percentage of probe molecules on top of the microcantilever yields a greater deflection. In addition, this chapter shows that small probe coverage area might work quite well in the system with very few target molecules. The small probe coverage area requires only a few target molecules to saturate its bonding area. By filling out the bonding area, the target and probe molecules create relatively strong molecular interactions to increase the deflection. Therefore the design of the microcantilever sensor should incorporate a way to optimize the molecular interaction, i.e., the saturation of the bonding area in order to increase sensitivity of the sensor.

Half-Length Coverage

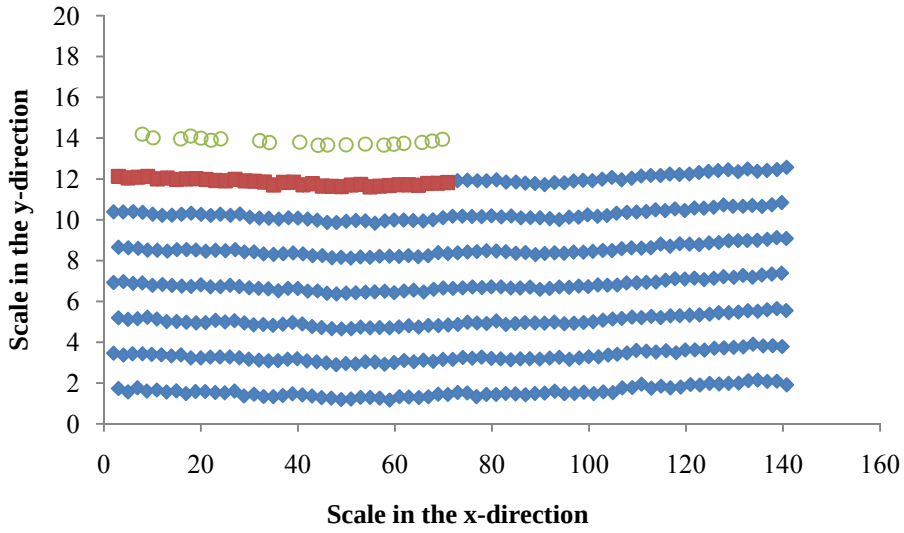

Full-Length Coverage

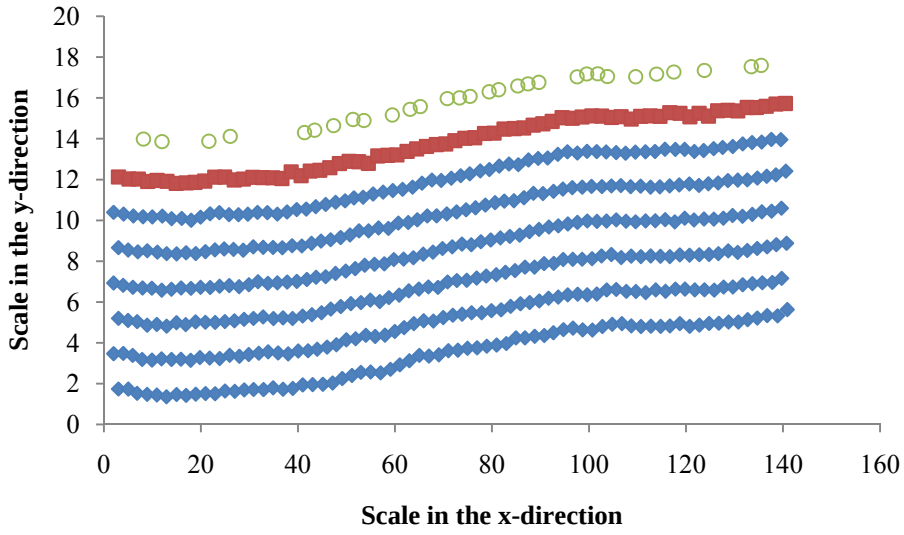

Figure 5.7 Snap shots for a system with 20 target molecules. The green circle (o) represents the target molecules, blue diamond (♦) the microcantilever beam molecules, and red square (■) the probe molecules. Simulations are at $\varepsilon_{tar\text{-}probe} = 15.0$, $\varepsilon_{tar\text{-}tar} = 1.0$, $\varepsilon_{tar\text{-}can} = 0.05$, $\sigma_{tar\text{-}probe} = 2.00$, $\sigma_{tar\text{-}tar} = 2.00$, and $\sigma_{tar\text{-}can} = 1.50$. (Note: plots are not to scale.)

Half-Length Coverage

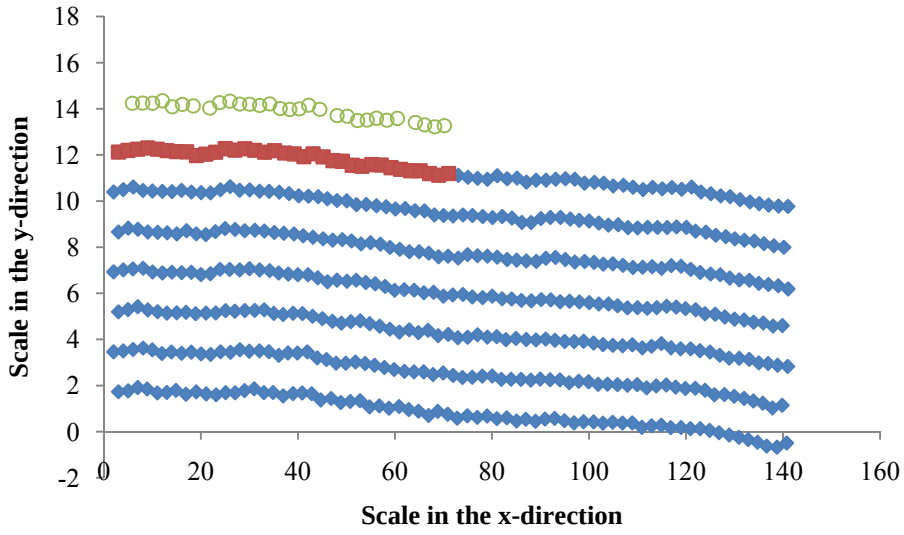

Full-Length Coverage

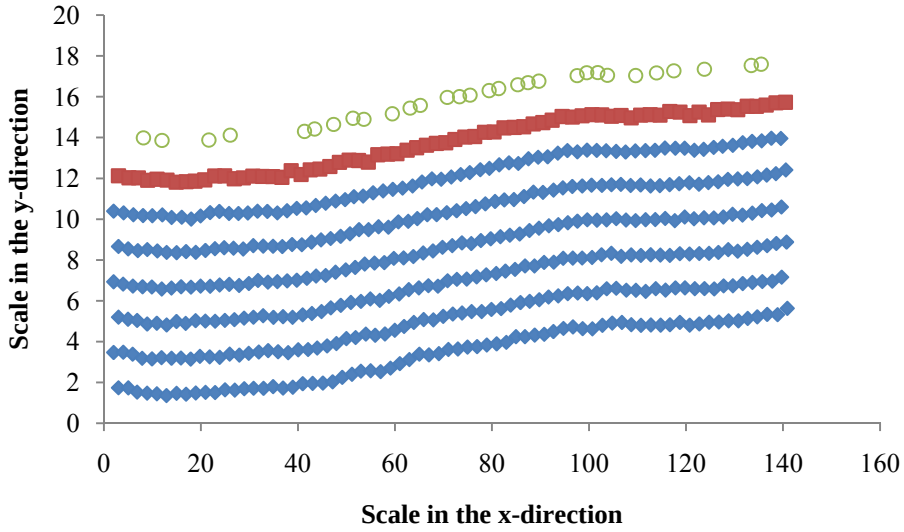

Figure 5.8 Snap shots for a system with 30 target molecules. The green circle (o) represents the target molecules, blue diamond (♦) the microcantilever beam molecules, and red square (■) the probe molecules. Simulations are at $\varepsilon_{tar\text{-}probe}$ = 15.0, $\varepsilon_{tar\text{-}tar}$ = 1.0, $\varepsilon_{tar\text{-}can}$ = 0.05, $\sigma_{tar\text{-}probe}$ = 2.00, $\sigma_{tar\text{-}tar}$ = 2.00, and $\sigma_{tar\text{-}can}$ = 1.50. (Note: plots are not to scale.)

Half-Length Coverage

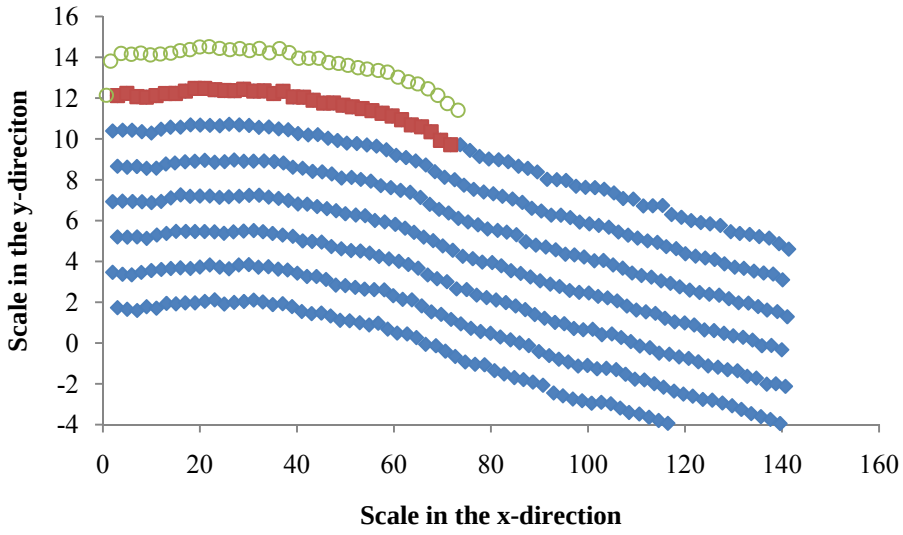

Full-Length Coverage

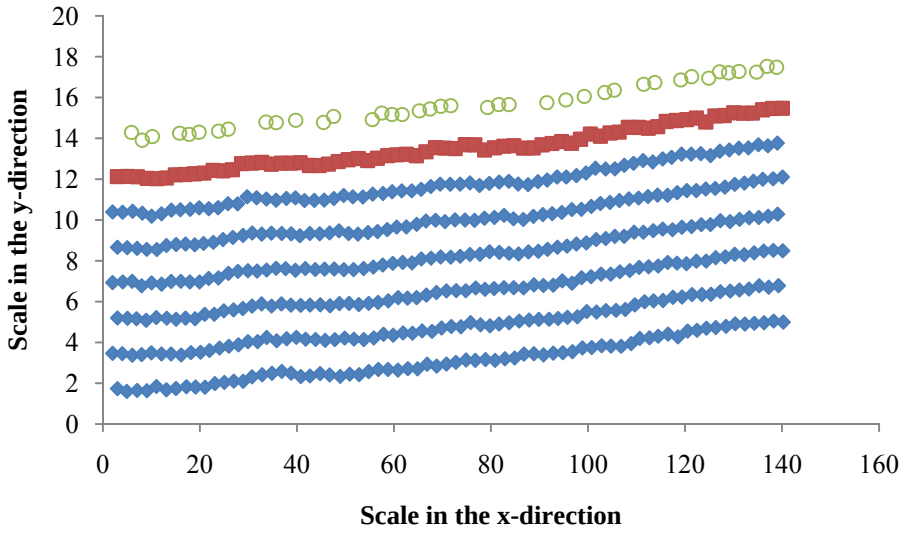

Figure 5.9 Snap shots for a system with 40 target molecules. The green circle (o) represents the target molecules, blue diamond (♦) the microcantilever beam molecules, and red square (■) the probe molecules. Simulations are at $\varepsilon_{tar\text{-}probe} = 15.0$, $\varepsilon_{tar\text{-}tar} = 1.0$, $\varepsilon_{tar\text{-}can} = 0.05$, $\sigma_{tar\text{-}probe} = 2.00$, $\sigma_{tar\text{-}tar} = 2.00$, and $\sigma_{tar\text{-}can} = 1.50$. (Note: plots are not to scale.)

Half-Length Coverage

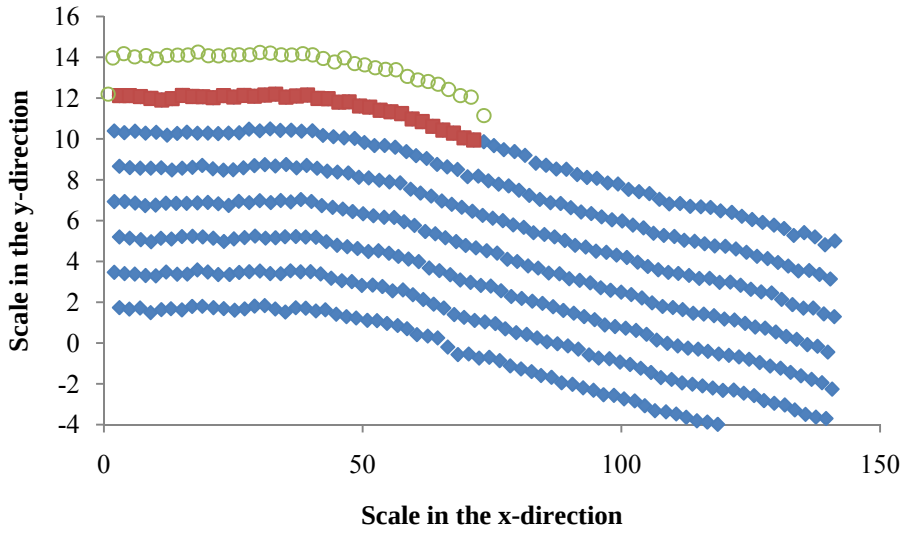

Full-Length Coverage

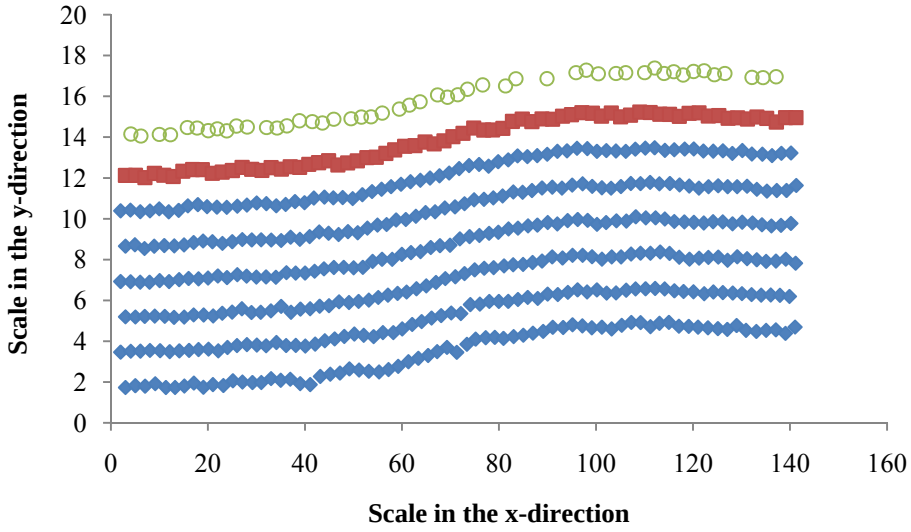

Figure 5.10 Snap shots for a system with 50 target molecules. The green circle (o) represents the target molecules, blue diamond (♦) the microcantilever beam molecules, and red square (■) the probe molecules. Simulations are at $\varepsilon_{tar\text{-}probe} = 15.0$, $\varepsilon_{tar\text{-}tar} = 1.0$, $\varepsilon_{tar\text{-}can} = 0.05$, $\sigma_{tar\text{-}probe} = 2.00$, $\sigma_{tar\text{-}tar} = 2.00$, and $\sigma_{tar\text{-}can} = 1.50$. (Note: plots are not to scale.)

Chapter 6

Conclusions

In this research, molecular dynamics simulation was used to study the microcantilever sensor. The objective is to examine the effect of the molecular interactions as well as the probe locations on the microcantilever deflection.

The molecular interactions for target and probe molecules were modeled by the Lennard-Jones potentials. The results show that many factors influence the microcantilever deflection.

Observations were made that target molecules bond with probe molecules within a ‘bonding area’. When the bonding area is not saturated, there are fewer bonds. In addition, locations of those bonded molecules are far apart from each other. When the target molecules saturate the bonding area, distances among the bonded target molecules are reduced, resulting in greater interactions. Hence, it is likely that the higher saturation level will produce a greater microcantilever deflection.

When the bonding area is saturated, its size, determined by the distance between $1.12\sigma_{tar\text{-}probe}$ and $2.5\sigma_{tar\text{-}probe}$, relative to the size of the target molecules, determined by $\sigma_{tar\text{-}tar}$, seem to be a factor that influences the direction and magnitude of the deflection. If the target molecules are relatively big compared to the bonding area, the results show that target molecules can only be fitted into one layer. When the target molecules are forced into a single layer with very little

separation in the y-direction, they tend to spread more in the x-direction. This seems to cause downward bending of the microcantilever to generate more surface area. On the other hand, if the target molecules are relatively small compared to the bonding area, they will have more room in the y-direction. Often in this case, the target molecules arrange themselves in a zigzag pattern with one layer staggered on top of the other to cover as much of the bonding area as possible. As a result, the target molecules require less room in the x-direction, thus reducing the microcantilever's tendency to bend down.

Another interesting observation is the variation of the probe-to-probe spacing. At short probe-to-probe distances, target molecules are able to interact with multiple probe molecules. It was suspected that the manner, in which two or more probe molecules interact with the same target molecule, can cause the upward deflection of the microcantilever, in order to reduce the target-probe distance, hence lowering the target-probe attraction energy.

Another factor studied is $\varepsilon_{tar\text{-}probe}$, which was used to model the strength of the target-probe interactions. At low $\varepsilon_{tar\text{-}probe}$, the interactions between the target and probe molecules are weak. If the target molecules have enough kinetic energy, they can easily break the bonds. On the other hand, with stronger target-probe interactions, more bonds are formed, thus increasing number of target molecules in the bonding area and causing greater microcantilever deflection.

In addition, the results suggest that the target-target distances are influenced by $\sigma_{tar\text{-}tar}$. Generally, target molecules were found at around the distances equivalent to 1.12 $\sigma_{tar\text{-}tar}$, which is the distance at which the Lennard-Jones potentials are minimal.

The results also show that $\varepsilon_{tar\text{-}tar}$ has less effect than the other Lennard-Jones parameters. $\varepsilon_{tar\text{-}tar}$ was used to model the strength of the target-target interactions. Since target molecules assume positions at around equilibrium distances from each other, their interaction forces remain nearly zero, which could be a possible reason for $\varepsilon_{tar\text{-}tar}$ to have very little effect.

The research also looked into the effect of the probe locations. It was found that manipulation of the probe locations (either by changing the percentage of the probe molecules on the top surface or the placement of the probe molecules, i.e. grouping the probe molecules into one area) can influence the microcantilever deflection.

The results show that deflection tends to increase with increasing probe coverage percentage. When the probe molecules are too far apart, such as the case of low probe coverage percentage, target molecules bond locally within the area near the probe sites. Due to a long distance between the sites, the molecules from one site are not able to interact with those from the other site. This generates weaker interactions than the system with higher probe coverage percentage where the molecules are closer to each other.

Another study was conducted for a system with only a few target molecules. In this case, 2 microcantilever configurations were used: one with uniform probe coverage of 100% for its entire length and the other with 100% coverage but only up to half of its length. It was found that, in some cases, the half-length configuration gives a greater deflection. It appears that, in a low concentration environment, the full-length configuration does not have enough target molecules to saturate its large bonding area, leaving many vacant sites that lower the interaction strengths.

This study has shown that many factors influence the microcantilever deflection. Understanding of these interactions can be used to improve the sensor design.

Bibliography

Allen, M. P., & Tildesley, D. J. (2007). *Computer Simulation of Liquids.* Toronto: Oxford University Press.

Arbabi, S., & Sahimi, M. (1990). Test of universality for three-dimentional models of mechanical breakdown in disorderd solids. *Physical Review B, 21* (1), 772-775.

Ashurst, W. T., & Hoover, W. G. (1976). Microscopic fracture studies in the two-dimensional triangular lattice. *Physical Review B, 14* (4), 1465-1473.

Baller, M. K., Lang, H. P., Fritz, J., Berber, C., Gimzewski, J. K., Drechsler, U., et al. (2000). A cantilever array-based artificial nose. *Ultramicroscopy, 82*, 1-9.

Beale, P. D., & Srolovitz, D. J. (1988). Elastic fracture in random materials. *Physical Review B, 37* (10), 5500-5507.

Berger, R., Gerber, C., Lang, H. P., & Gimzewski, J. K. (1997). Micromechanics: A toolbox for femtoscale science: "Towards a laboratory on a tip". *Microelectronic Engineering, 35*, 373-379.

Born, M., & Huang, K. (1966). *Dynamical Theory of Crystal Lattices.* Toronto: Oxford University Press.

Buxton, G. A., Verberg, R., Jasnow, D., & Balazs, A. C. (2005). Newtonian fluid meets an elastic solid: Coupling lattice Boltzmann and lattice-spring models. *Physical Review E, 71*, 056707.

Chen, G. Y., Thundat, T., Wachter, E. A., & Warmack, R. J. (1995). Adsorption-induced surface stress and its effects on resonance frequency of microcantilevers. *Journal of Applied Physics, 77* (8), 3618-3622.

Cunningham, M. J., Jenkins, D. F., & Khalid, M. A. (1997). Cantilever vibration control by electrostatic actuation for magnetic force microscopy. *Sensors and Actuators A, 63*, 125-128.

Curin, W. A., & Scher, H. (1990). Brittle fracture in disordered materials: A spring network model. *Journal of Materials Research, 5* (3), 535-553.

Dareing, D. W., & Thundat, T. (2005). Simulation of adsorption-induced stress of a microcantilever sensor. *Journal of Applied Physics, 97*, 043526.

Daw, M. S., & Baskes, M. I. (1984). Embedded-atom method: Derivation and application to impurities, surfaces, and other defects in metals. *Physical Review B, 29* (12), 6443-6453.

Drelich, J., White, C. L., & Xu, Z. (2008). Laboratory tests on mercury emission monitoring with resonating gold-coated silicon cantilevers. *Environmental Science & Technology*, *42* (6), 2072-2078.

Feng, S., & Sen, P. N. (1984). Percolation on elastic networks: New exponent and threshold. *Physical Review Letters, 52* (3), 216-219.

Feng, S., Sen, P. N., Halperin, B. I., & Lobb, C. J. (1984). Percolation on two-dimensional elastic networks with rotationally invariant bond-bending forces. *Physical Review B, 30* (9), 5386-5389.

Fritz, J., Baller, M. K., Lang, H. P., Rothuizen, H., Vettiger, P., Meyer, E., et al. (2000). Translating biomolecular recognition into nanomechanics. *Science, 288*, 316-318.

Garcia-Molina, R., Guinea, F., & Louis, E. (1988). Percolation in isotropic elastic media. *Physical Review Letters, 60* (2), 124-127.

Haile, J. M. (1992). *Molecular Dynamics Simulation Elementary Methods.* Toronto: A Wiley-Interscience Publication.

Han, W., Lindsay, S. M., & Jing, T. (1996). A magnetically driven oscillating probe microscope for operation in liquids. *Applied Physics Letters, 69* (26), 4111-4113.

Hassold, G. N., & Srolovitz, D. J. (1989). Brittle fracture in materials with random defects. *Physical Review B, 39* (13), 9273-9281.

Hill, T. L. (1986). *An Introduction to Statistical Thermo-dynamics.* New York: Dover Publications.

Kantor, Y., & Webman, I. (1984). Elastic properties of random percolating systems. *Physical Review Letters, 52* (21), 1891-1894.

Klein, C. A. (2000). How accurate are Stoney's equation and recent modifications. *Journal of Applied Physics, 88* (9), 5487-5489.

Ladd, A. J., & Kinney, J. H. (1997). Elastic constants of cellular structures. *Physica A, 240*, 349-360.

Lang, H. P., berger, R., Andreoli, C., Brugger, J., Despont, M., Vettiger, P., et al. (1998). Sequential position readout from arrays of micromechanical cantilever sensors. *Applied Physics Letters, 72* (3), 383-385.

Madet, S. S. (2007). *Essentials of biology.* Toronto: McGraw-Hill.

Maitland, G. C., Rigby, M., Smith, E. B., & Wakeham, W. A. (1981). *Intermolecular Forces Their Origin and Determination.* Toronto: Oxford University Press.

McKendry, R., Zhang, J., Arntz, Y., Strunz, T., Hegner, M., Lang, H. P., et al. (2002). Multiple label-free biodetection and quantitative DNA-binding assays on a nanomechanical cantilever array. *Proceedings of the National Academy of Sciences of the United States of America, 99* (15), 9783-9788.

Monetter, L., & Anderson, M. P. (1994). Elastic and fracture properties of the two-dimensional triangular and square lattices. *Modelling and Simulation in Materials Science and Engineering, 2* (1), 53-66.

Moulin, A. M., O'Shea, S. J., & Welland, M. E. (2000). Microcantilever-based biosensors. *Ultramicroscopy, 82*, 23-31.

O'Shea, S. J., Welland, M. E., Brunt, T. A., Ramadan, A. R., & Rayment, T. (1996). Atomic force microscopy stress sensors for studies in liquids. *Journal of Vacuum Science & Technology. B, 14* (2), 1383-1385.

Passian, A., Muralidharan, G., Kouchekian, S., Mehta, A., Cherian, S., Ferrell, T. L., et al. (2002). Dynamics of self-driven microcantilevers. *Journal of Applied Physics, 91* (7), 4693-4700.

Stoney, G. G. (1909). The tension of metallic films deosited by electrolysis. *Proceedings of the Royal Society of London. A*, 172-175.

Su, M., Li, S., & Dravid, V. P. (2003). Microcantilever resonance-based DNA detection with nanoparticle probes. *Applied Physics Letters, 82* (20), 3562-3564.

Thundat, T., Oden, P. I., & Warmack, R. J. (1997). Microcantilever Sensors. *Microscale Thermophysical Engineering, 1*, 185-199.

Thundat, T., Pinnaduwage, L., & Lareau, R. (2004). Explosive vapour detection using micromechanical sensors. In J. W. Gardner, & J. Yinon, *Electronic Noses & Sensors for the Detection of Explosives* (pp. 249-266). Netherlands: Kluwer Academic.

Thundat, T., Wachter, E. A., Sharp, S. L., & Warmack, R. J. (1995). Detection of mercury vapor using resonating microcantilevers. *Applied Physics Letters, 66* (13), 1695-1697.

Vidic, A., Then, D., & Ziegler, C. (2003). A new cantilever system for gas and liquid sensing. *Ultramicroscopy, 97*, 407-416.

Wu, g., Datar, R. H., Hansen, K. M., Thundat, T., Cote, R. J., & Majumdar, A. (2001). Bioassay of prostate-specific antigen (PSA) using microcantilevers. *Nature Biotechnology, 19*, 856-860.

Wu, G., Ji, H., Hansen, K., Thundat, T., Datar, R., Cote, R., et al. (2001). Origin of nanomechanical cantilever motion generated from biomolecular interactions. *Proceedings of the National Academy of Sciences of the United States of Americas, 98* (4), 1560-1564.

Wu, H. A., Sun, Z. H., & Wang, X. X. (2007). Molecular mechanics modelling and simulation of the adsorption-induced surface stress in micro-nano-cantilever sensors. *Journal of Physics: Conference Series, 61*, 1266-1270.

Yu, h., Huang, Q.-A., & Liu, X.-X. (2009). Modeling of H_2O adsorption-induced curvature of a metal/silicon nanocantilever. *Applied Surface Science*, summitted.

Yue, M., Lin, H., Dedrick, D. E., Satyanarayana, S., Majumdar, A., Bedekar, A. S., et al. (2004). A 2-D microcantilever array for multiplexed biomolecular analysis. *Journal of Microelectromechanical Systems, 13* (2), 290-299.

Yue, M., Majumdar, A., & Thundat, T. (2006). Cantilever arrays: A universal platform for multiplexed label-free bioassays. In R. Bashir, & S. Wereley (Eds.), *BioMEMS and Biomedical Nanotechnology: Volume IV: Biomolecular Sensing, Processing and Analysis*, (pp. 21-33). Springer.

Zhao, Q., Zhu, Q., Shih, Q. Y., & Shih, W.-H. (2006). Array adsorbent-coated lead zirconate titanate (PZT)/stainless steel cantilevers for dimethyl methylphosphonate (DMMP) detection. *Sensors and Actuators B, 117*, 74-79.

Zumdahl, S. S. (1995). *Chemical Principles.* Toronto: D. C. Heath and Company.

Appendix A: Simulation Values and Units

All computation properties in this simulation are calculated from the Lennard-Jones potentials (Equation 2.8) and the equations of motion (Equation 2.14). Lennard-Jones potentials are a function of σ and ε and the equations of motion a function of mass m_i. Hence, all computation properties can be expressed in terms of σ, ε, and m_i. These three parameters are considered to be the units of the simulation values and typically referred to as the fundamental units. The fundamental units can be used to relate the computation values (represent by*) to the actual value as:

Temperature:	$T^* = k_B T/\varepsilon$	(A.1)[1]
Energy:	$E^* = E/\varepsilon$	(A.2)[1]
Force:	$F^* = F\sigma/\varepsilon$	(A.3)[1]
Spring Constant:	$k^* = k\sigma^2/\varepsilon$	(A.4)
Torsional Spring Constant:	$c^* = c/\varepsilon$	(A.5)
Time:	$t^* = \left(\frac{\varepsilon}{m_i\sigma^2}\right)^{1/2} t$	(A.6)[1]

Even though, the simulation values can be scaled to the actual values using equations above, our simulation expresses the simulation values as a function of the fundamental units with no values assigned to σ, ε, and m_i. As mentioned in

[1] Equations from Allen and Tildesley (2007)

Chapter 2, the purpose of this research is to compare general trends of the effect of molecular interactions on the deflection. Since the simulation was not intended to calculate the actual deflection; the usage of real units was not considered.

The main purpose of the equations in this appendix is in the assignment of some simulation properties. For example, the value of the initial temperature is obtained from scaling the actual room temperature of 300 K by a ratio of k_b/ε (Equation A.1). Another example is that the velocity in Equation 2.15 is expressed in term of the Boltzmann's constant which is 1.38×10^{-23} J/K. With Equation A.1, the velocity can be expressed as:

$$< v_x^2 > = < v_y^2 > = \frac{k_B T}{m_i} = \frac{k_b}{m_i}\frac{\varepsilon T^*}{k_b} = \frac{\varepsilon T^*}{m_i} \quad (A.7)$$

By expressing the actual value in the fundamental units, the simulation can remain in terms of σ, ε, and m_i.

Appendix B: Uncertainty due to Initial Locations of Target Molecules

Uncertainty of the simulation can arise from the accumulation of the truncation errors as well as the computer round-off errors. For molecular dynamics simulation, one common method of finding the uncertainty is to determine the repeatability of the results, by giving different initial set-ups for the locations of molecules. Due to the time restriction (because each data points in Chapter 4 and 5 requires several simulations to calculate its uncertainty), this study only determines the uncertainty for one system with the Lennard-Jones parameters: $\sigma_{tar\text{-}probe}$ = 2.00, $\sigma_{tar\text{-}tar}$ = 2.00, $\sigma_{tar\text{-}can}$ = 1.50, $\varepsilon_{tar\text{-}probe}$ = 15.0, $\varepsilon_{tar\text{-}tar}$ = 1.00, and $\varepsilon_{tar\text{-}can}$ = 0.05.

Table B.1 Simulation uncertainty for system with $\sigma_{tar\text{-}probe}$ = 2.00, $\sigma_{tar\text{-}tar}$ = 2.00, $\sigma_{tar\text{-}can}$ = 1.50, $\varepsilon_{tar\text{-}probe}$ = 15.0, $\varepsilon_{tar\text{-}tar}$ = 1.00, and $\varepsilon_{tar\text{-}can}$ = 0.05.

Test	Deflection	Number of Bonding Target Molecules	Average Separation Distance Distance	Average Separation Distance in the y-direction
1	5.847	70.94	2.280	1.128
2	5.878	70.94	2.280	1.130
3	5.989	71.55	2.278	1.127
4	6.029	70.77	2.280	1.128
5	6.111	71.12	2.279	1.127
6	6.209	70.80	2.279	1.127
7	6.240	70.78	2.279	1.127
8	6.284	72.53	2.277	1.132
9	6.353	72.01	2.277	1.129
Mean	6.115	71.22	2.279	1.128
Standard Deviation	0.173	0.61	0.001	0.002

Each test has different initial conditions with starting distance between target molecules ranging from $2\sigma_{tar\text{-}tar}$ to more than $10\sigma_{tar\text{-}tar}$. As shown in Table B.1, the uncertainty for the simulation values is small.